Advanced characterisation of industrially important coal-based carbon materials

Sima-Ella, Edwige

Award date:
2005

Awarding institution:
University of Bath

Advanced Characterisation of Industrially Important Coal-based Carbon Materials

Edwige Sima-Ella

A thesis submitted for the degree of Doctor of Philosophy

University of Bath

Department of Chemical Engineering

November 2005

Copyright

ProQuest LLC
789 East Eisenhower Parkway
P.O. Box 1346
Ann Arbor, MI 48106-1346

Abstract

The aim of this work is to develop a simplified, though rigorously based thermogravimetric analysis (TGA) method to estimate the intrinsic reactivity parameters (activation energy E, and pre-exponential factor A) for the oxidation in air of engineering carbonaceous materials derived from coal. Using TGA methods, the oxidation reaction of the coal chars was found to be best modelled by a first order global kinetics within the chemical control regime. A modified Coats-Redfern method was developed for analysing thermogravimetric data obtained at constant heating rate. Hence a reactivity equation was produced to estimate the intrinsic reactivity parameters of these chars at various rate of heating. A novel statistical criterion was subsequently devised to determine the heating rate at which optimum values of the activation energy and the pre-exponential factor were obtained. This is a valuable development, for in conventional non-isothermal TGA, while it is accepted that kinetic parameters vary with heating rate, there is no formal method for selecting one rate over another. An optimum-heating rate was observed between 25 and 35 °C min^{-1} for the different types of chars, suggesting that this optimum-heating rate is an instrumental factor. The resulting reactivity parameters were found to be in good agreement with those derived from using time-consuming isothermal analyses and two well-known isoconversional methods (Kissinger and Ozawa-Flynn-Wall). These results were further compared with those presented in the literature for similar materials. They all showed good agreement. By using these reactivity data, a novel sample controlled thermal analysis (SCTA) technique was developed, which enables both reactivity parameters to be evaluated. This method is referred to as step-ramp analysis, and represents an improvement over existing SCTA methods. However, step-ramp analysis is more complex than the novel constant rate heating technique, as it requires continuous monitoring of the weight loss. It was concluded therefore that the new constant heating rate TGA technique is a highly accurate and simple tool for characterising the oxidation reactivity of coal chars in air.

Acknowledgements

This project was undertaken with the financial support received from the British Coal Utilisation Research Association (BCURA, Contract B56). The author would also like to express her thanks to the following people: my supervisor, Dr Tim Mays, whose continuous guidance, support, and advice are gratefully acknowledged; Mr Brian Smith (Mitsui Babcock Energy Ltd), for coordinating this work with industry and for his interest in this project; the Department of Chemical Engineering at the University of Bath for the provision of facilities and technical assistance. Thanks are also due to all my friends at the University of Bath, for their friendship throughout, especially to Ben. To Father Bill McLoughlin, for his support and prayers. Finally, special thanks are due to my parents Ada Pauline and Moïse Sima-Ella, and to my family for their continuous encouragement.

Contents

Nomenclature

Abbreviation	Full name
ASA	Active surface area
BET	Brunauer-Emmet-Teller
CRTA	Constant rate thermal analysis
daf	Dry ash free
DR	Dubinin-Radushkevitch
dTG	Derivative thermogravimetric signal
FSIA	Forced stepwise isothermal analysis
HTT	Heat treatment temperature
RMS	Root mean square
SCTA	Sample controlled thermal analysis
SEM	Scanning electron microscopy
SIA	Stepwise isothermal analysis
TG	Thermogravimetric signal
TGA	Thermogravimetric analysis

Symbols	Definition
A	Pre-exponential factor
E	Activation energy
Ea	Apparent activation energy
Eo	Characteristic energy in the DR equation
G°	Standard Gibbs energy
H°	Standard enthalpy
K°	Equilibrium constant
k	Intrinsic rate constant
L	Avogadro's number (6.023×10^{23} mol $^{-1}$)
m	Characteristic shape constant
n	Reaction order
P	Total pressure
p	Relative pressure of adsorptive gas
p°	Saturated vapour pressure
R	Molar gas constant = 8.314 J mol^{-1} K^{-1}
S	Surface area
S°	Standard entropy
T	Absolute temperature
t	Time
V	Amount of adsorbed gas per unit mass of solid
V°	Molar volume of gas = 22.414 dm^3 mol^{-1}

Vm	Monolayer adsorption capacity
Vo	Micropore volume capacity
W	Weight of char or coal

Greek Symbols	Definition
α	Fractional conversion of the char = 1-W/Wo
β	Heating rate
Δ	Difference of state
θ	Affinity constant
λ	Molecular cross-sectional area
σ	Root mean square error
ψ	Random pore model structural parameter

Subscripts	Definition
Calc	Calculated value
Exp	Experimental data
f	Final conditions
i	Instantaneous
Max	Maximum value
o	Initial conditions
p	Peak or maximum reaction rate conditions
r	Range

List of Figures

Page

List of Tables

Chapter 1

Introduction

1.1 Importance of Coal Characterisation

The reserve to production ratio of coal is in excess of two hundred years, compared to oil (< 50 years) and natural gas (< 70 years) (BP statistical review of world energy 2005). In addition, the index price for coal is significantly lower. It is therefore not surprising that coal remains an important energy source, especially in the United Kingdom (UK), where it accounts for 33% of the total fuel available in electricity production against natural gas (40%) and nuclear energy (19%) (DTI UK energy in brief july 2005). The major uses of coal in the UK include pulverised fuel combustion (PF) in electricity generation (83%), and also in coking and pulverised coal injection (PCI) in blast furnaces for the iron and steel-making industry (12%). Coal is also used as a heat supply and steam raising in other industries such as the cement and paper industries. It is clear that coal remains a vital energy source and raw material in UK industries.

Power generation industries, in particular, are faced with recurrent problems such as slagging, fouling and corrosion of the tube furnaces. These predicaments arise from the ash, which melts at high temperature and deposits onto the tube before reacting with the alloy. Furthermore, coal industries are subjected to continuous legislative pressure on emissions with respect to NOx, SOx and CO_2 in particular (LCPD 2001/80/EC; Kyoto Protocol 2002/358/EC). It is therefore important for

these industries to have adequate characterisation data for coal, in order to determine its physical and chemical properties. These properties may be used to compare and select between different types of coals. More importantly, the chemical properties such as amount of fixed carbon and minerals, and the physical properties such as porosity or particle size, can give an indication of the performance of a coal in service. Hence, characterisation data are important in understanding and predicting the performance of a particular coal (or coal blend) in applications such as PF combustion or in PCI in blast furnaces. One key property of the coal is the intrinsic reactivity of the carbon contained in the coal. This is a measure of the rate of reaction taking place at the surface of the carbon, and not being affected by diffusion of the gas. Carpenter and Skorupska (1993) commented on the detrimental effects of inadequate characterisation of char reactivity on coal combustion systems. Other researchers such as Arenillas *et al.*(1999) have shown that the intrinsic reactivity of the char may be used as an indicator to predict NOx emissions. The incentives for this work are perhaps best described by the research and training development needs in pulverised fuel combustion, advanced by the European Commission (20/09/05):

"...Develop/improve science-based coal characterisation techniques to predict performance of unknown coals in existing/new plants, particularly with regard to combustion, NOx emission, slagging, fouling and corrosion characteristics with a view to increasing fuel flexibility..."

The intrinsic reactivity of the char plays a crucial role in understanding coal combustion processes, as it describes the dynamics of the process. Accurate kinetic parameters are increasingly being sought for computational fluid dynamics (CFD) modelling of combustion processes. The combination of CFD models with reactivity data offers a unique insight into the mechanisms occurring within large pulverised-fuel combustion systems. Williams *et al.* (2002), have recently demonstrated that CFD models can successfully predict burnout time and temperature within small-scale test facilities, given adequate intrinsic kinetic data. Indeed, the intrinsic reactivity of the char is currently being used as a predictive tool in full-scale power station boiler design (Mitsui Babcock Energy Ltd, 2005).

Furthermore, intrinsic kinetic data may be used for setting the operating conditions and for fuel utilisation efficiency in industrial applications, as recently pointed out by Ulloa *et al.* (2005).

Reactivity data of various coal chars in air is extensively discussed in the literature (Smith 1982; Smoot and Smith 1985). However, many researchers have considered the overall reactivity as opposed to the intrinsic char reactivity (Field 1969; Herbig and Jess 2002; Feng *et al.* 2003). The main reason behind this approach is that intrinsic kinetic data are not easily measurable as they relate to the structure of the material. In spite of this, Smith (1978) estimated the oxidative intrinsic reactivity of various types of chars by measuring their structural properties such as characteristic particle size, specific surface and pore diameter. More recently, Chan *et al.* (1999) performed a similar analysis. This approach, however, is somewhat tedious and time-consuming. For this reason, Russell *et al.* (1998) have suggested the use of thermogravimetric analysis, where direct intrinsic kinetic data can be measured by performing experiments at low temperature (< 1000 °C).

In the furnace of a thermogravimetric analyser, the weight of an oxidising char is continuously recorded whilst it is being subjected to a controlled temperature atmosphere. These experiments have widely been applied to coal char analyses, as discussed in section 2.6. The basic approach is to study the kinetics of the reaction isothermally: the mathematical analysis is straightforward but the experimental time is long. This method is not useful in understanding the oxidation process at a fundamental level. Conventional thermogravimetry involves non-isothermal experiments, by applying a constant rate of heating. In this way, the reaction takes place over a wider range of temperature, and a better correlation may be derived between experiments in a laboratory and real applications (Brown 2001). These types of experiments, however, suffer from two inherent problems. Firstly, the mathematical analysis is complicated by the change of temperature with time, which introduces a new variable. Secondly, the rate of heating induces thermal effects, so that the estimated kinetic data vary with

the selected rate of heating (Serageldin and Pan 1982). Hence, the constant rate of heating method becomes seriously unreliable.

Because of this uncertainty in the determination of kinetic parameters from a single heating rate experiment, modern thermal analyses have encouraged the use of isoconversional methods (Vyazovkin and Lesnikovich 1989; Vyazovkin and Sbirrazzuoli 2003; Zhou *et al.* 2003). These methods combine multiple heating rate experiments in order to minimise the thermal effects occurring from a single rate of heating. Nonetheless, these techniques can be time-consuming as more than three experiments are required. In addition, modern thermal analyses are moving towards the use of temperature programmes, which simplify the kinetic analysis. These recent techniques are referred to as sample controlled thermal analysis, where the reaction rate is controlled by variation in the temperature programme. Although these techniques have presented several advantages over the constant rate of heating approach, kinetic reactivity data are not easily measurable with these techniques (Sorensen 1992; Gotor *et al.* 1998). As a result, it is not surprising that sample controlled thermal analysis methods have still not been used in coal char characterisation, where determination of the intrinsic reactivity parameters is essential.

Hence, there is scope in this work to develop a new thermogravimetric analysis technique, which is simpler and more reliable than existing techniques. Furthermore, there is also a potential to develop a sample controlled thermal analysis technique, which facilitate the determination of the kinetic parameters. These opportunities are best described by Ortega (2002) who said:

> *"The dream of many workers involved in thermal analysis is: to obtain thermogravimetric curves independent of experimental conditions; to have more reproducible results; to obtain reliable kinetic parameters; to overcome the problems of complex reactions."*

1.2 Scope of the Thesis

The present investigation is concerned with extensive experimental studies in the development and application of a novel thermogravimetric analysis method for characterising the intrinsic reactivity of carbons in or derived from coals. It should be noted at this stage that oxidation conditions, in this proposed work, are not intended to simulate the operating environment in either PF combustion or in a blast furnace raceway. Indeed specialised apparatus are required to reproduce these conditions (rapid heating rate at $10^4 - 10^6$ °C s^{-1} for temperatures up to 2000 °C). Instead, the idea of this work is to produce intrinsic reactivity data, which can only be evaluated at laboratory-scale at lower temperatures (< 1000 °C min^{-1}) and slow heating rates (< 50 °C min^{-1}).

1.3 Structure of the Thesis

This thesis has been divided into eight chapters including this one. Chapter 2 provides background information on related and published research on thermogravimetric techniques. The chemical and physical properties of coal are reviewed, which raise interest and concern in kinetics studies. This chapter closes with a clear statement of the aims and objectives of this work. Chapter 3 discusses the analytical methods for modelling the char oxidation process. Fundamental rate-equations for gas-solid systems during constant heating rate are reviewed, and a simple mathematical analysis is developed for deriving the intrinsic reactivity parameters of the char during oxidation. Chapter 4 deals with the experimental procedures required for implementing this novel kinetic analysis using thermogravimetric techniques. In this chapter, the thermogravimetric analyser instrument is presented together with the methods used to prepare the coal chars, and assess their structural properties. Chapter 5 presents the experimental results from this novel constant rate heating TGA method. In Chapter 6, the validity of this novel technique is discussed by comparing the results with those from established techniques. In addition, the sensitivity of the proposed kinetic analysis is tested by verifying the different assumptions

postulated in Chapter 3, when deriving the kinetic model analysis. This chapter also discusses the main advantages of the novel kinetic analysis for thermogravimetric experiments. Chapter 7 is concerned with applying sample controlled thermal analysis to coal chars studies, since these techniques are perhaps the current thinking and likely future of thermal analysis techniques. Their difficulty in estimating the kinetic parameters is discussed, and an alternative approach is implemented, which tries to capture the accuracy of the analysis in a simpler manner. This thesis concludes with chapter eight, which gathers the main conclusions from this work, and outlines recommendations for future research work.

1.4 Dissemination

The outcome from this work has been disseminated at progress meetings with the sponsors of the project (BCURA), taking place every six months, and at national and international conferences, as listed below. This work has also been communicated in peer-reviewed journals (Sima-Ella *et al.* 2005; Sima-Ella and Mays 2005a) and conference proceedings (Sima-Ella and Mays 2005b). This conference paper is included in Appendix A as a summary of the proposed work. Opportunities for patenting the novel thermogravimetric analysis technique are also being considered.

1. 5th European Conference on Coal and its Applications, Edinburgh, UK: September 6-8, 2004. Abstract and Poster Presentation

2. 13th International Congress on Thermal Analysis and Calorimetry, Sardinia, Italy: September 12-19, 2004. Abstract and Poster Presentation

3. 7th World Congress on Chemical Engineering, Glasgow, UK: July 10-14, 2005. Refereed Paper and Poster Presentation.

Chapter 2

Background

2.1 Introduction

The complexity of coal makes it difficult to always understand and predict how processes such as combustion or oxidation develop. Although coal conversion technologies have received a great consideration over the century, it is still difficult to exactly model the combustion process. In fact, the reaction mechanism is not fully understood, and this is important in deriving the kinetics of the process. Experimental conditions used in assessing the reactivity of the char are not always clearly specified or they are inadequately controlled. It is not surprising that contradictory models of char oxidation are often discussed in the literature.

The work presented in this chapter aims at providing a critical literature review into the fundamental aspects of coal characteristics and modelling of the oxidation reaction. This chapter is divided into eight sections. The first section deals with the complexity of coal by presenting its chemical and physical structure. The second and third sections define the intrinsic reactivity of the char and the various factors affecting its evaluation. In the fourth section, experimental techniques for assessing char reactivity are reviewed, and a particular emphasis on thermogravimetric techniques is detailed in the fifth section. The sixth and seventh sections are concerned with the modelling side of the coal char oxidation

reaction. A detailed literature review is provided on the fundamental carbon-oxygen reaction, and the various kinetic models that may apply in modelling this chemical reaction. The final section of this chapter outlines the aims and objectives of this project.

2.2 Coal Characteristics

2.2.1 Different Types of Coal

It has been established that coal originated from plant substances preserved from complete decay in waterlogged regions (Wen and Stanley Lee 1979). This wide variety of plants accumulated over million of years, going through several reactions under prevailing conditions of pressure and temperature. This metamorphism process is known as the coalification process, which resulted in different types of coal. These different types of coals are generally categorised as: lignite; subbituminous; bituminous and; anthracite (Van Krevelen 1993). As a brownish-black coal, lignite is the geological youngest coal, with the lowest carbon content (25-35%), large moisture content, and obvious woody material structure. Lignite coals make up the largest portion of world coal reserves, being mostly used for power generation. Subbituminous coals are dull and soft black coal, which tend to crumble when exposed. They have lower moisture content but higher heating value than lignite coals. In general, subbituminous coals have the lowest sulphur content compared to the other types of coals, making them more attractive to use in power generation. As an intermediate grade of coal, bituminous coals are black with bright shining lustre. They are widely used in electricity generation and steel industry, but also as a heat supply for industrial processes such as the cement and paper industries. Anthracite coals are the hardest type consisting of nearly pure carbon, with the highest heating value. Anthracite coals have the highest carbon content and heating value with lowest moisture and ash content. Their primary use is usually associated with domestic heating and the metallurgical industry.

2.2.2 Chemical and Physical Structure

Coal is an organic sedimentary rock, with complex physical and chemical properties, which has extensively been studied in the literature (Speight 1983; Van Krevelen 1993). The main chemical structure of the coal comprises organic and inorganic compounds. The organic matrix consists mainly of polymers of carbon, hydrogen, and oxygen with small amounts of sulphur and nitrogen. There, the atoms are bonded together to form various organic structures such as aliphatic chains. Although the definitive molecular structure of the coal is not known with any degree of certainty, it is generally found that coal is highly aromatic; hence, the coal structure contains predominantly condensed polycyclic aromatic rings, and has a high degree of condensation. The inorganic materials in coal, on the other hand, consist of essentially of clays, silicates, oxides, sulphates and carbonates. These minerals vary from one coal to the other, so that a normally trace mineral is found in larger quantities in certain geographical regions.

An understanding of the physical structure of coal requires petrographic studies: macroscopic and microscopic appearance of coal. The macroscopic structure consists of complex aggregates of discrete microscopic entities, known as macerals. These macerals represent the different plant tissues from which the coal originated. They have distinctive reflectance and fluorescence properties, which are used to distinguish between the various types of coal macerals. There are three major maceral groups: vinitrite, liptinite, and inertinite. Vitrinite is derived from cell walls, essentially, and is relatively oxygen rich. Lipnite, however, arises from algae and resin materials, so that it is a hydrogen-rich maceral type. Inertinite coal is characterised by a cellular structure and originated from plant tissue that had oxidised, so that they are carbon rich maceral and somewhat inert during coal carbonisation processes. (Lester and Cloke 1999; Magasiner *et al.* 2002).

2.2.3 Classification Systems

Various classification systems exist based on the chemical, physical or mechanical properties of the coal (Van Krevelen 1993). There are essentially three ways of categorising coals according to their grade, type, and rank. The most useful and widely applied classification scheme is most probably classification by rank (Wen *et al.* 1979; Carpenter 1988). Classification of coals by type, refer to the organic debris from which the coal is formed or to their macerals composition; whereas, coal grade classification identifies the coal by the amount of ash yield and sulphur content following complete oxidation of the organic fraction.

Coal rank classification system of coals is based on the degree of metamorphism. In general, coal rank increases as the amount of fixed carbon increases and decreases with the amount of moisture and volatile matter. Over the years, many classification systems have been proposed for coal. These include, the North American standard (ASTM D 388 1966, revised 1984) mainly used in coal market. This system is straightforward and simple to use. A copy of the ASTM coal classification is presented in Table 2.2.1. Other coal rank classifications include the NCB used in the United Kingdom (His Majesty's Stationary Office 1946), the Australian (Standard Association of Australia 1987) and the international systems (United Nations Publications 1988).

2.2.4 Characterisation Methods

(i) Proximate Analysis

Proximate analysis evaluates the overall composition of the coal in terms of the amount of moisture, volatile matter, ash and fixed carbon contents. In some cases, the calorific value and tar yield are also measured. Standard procedures include the British Standard (BS 1016-104 1998) and the North American Standard (ASTM D 3172-75 1989). In either case, a small amount of sample is heated to approximately 900 °C in an oxygen-free atmosphere, so that all oxygen,

hydrogen, nitrogen and sulphur are released as volatile matter. The fixed carbon is the amount of residual char after devolatilisation. Moisture content is determined by difference in mass of the sample before and after heating up to 95 to 105 °C. Ash content is determined by oxidising the residual char.

(ii) Ultimate Analysis

Ultimate analysis measures the elemental composition of the coal and is carried out on coal samples when further information is required. Standard procedures have been established such as the British Standard (BS 1016-106 1996) and the North American Standard (ASTM D 3176-79 1989). In general, carbon and hydrogen are measured by heating an air dried sample in a stream of oxygen and collecting the amount of CO_2 and H_2O produced in absorption trains. Nitrogen is converted to ammonium sulphate in concentrated sulphuric acid. The amount of ammonia released is then determined by titration against sulphuric acid to deduce the nitrogen content. Determination of sulphur content is usually carried out by reacting the sample with an Eschka mixture, which contains sodium carbonate. The sulphur compounds are then converted to sulphates, which is then acidified and precipitated to barium sulphate, which is then dried, ignited and weighted. The oxygen content, on the other hand, is usually performed by difference from the other elements from 100%.

(iii) Other Analyses

Other characterisation methods involve a set of technological or petrographic assays, to measure the behaviour of coals upon heating, and the macerals composition of the coal. Technological assays include measurements of: heat capacity; calorific value; free swelling index (increase in volume); plastic and agglutinating properties. Petrographic tests are based on the reflectance of the vitrinite contained in the coal. Under visible light, the light absorbance of the vitrinite is measured at various wavelengths. A detailed experimental procedure is covered by the North American Standard (ASTM D 2798 1999).

Table 2.2.1: ASTM classification of coal by rank (ASTM D 388 1966, revised 1984)

Class	Group	Fixed carbon Limits, (% daf)	Volatile Matter Limits, (% daf)	Calorific Value Limits, (Btu/lb, daf)
I. Anthracite	1. Meta-anthracite	>98	<2	
	2. Anthracite	92-98	2-8	
	3. Semianthracite [a]	86-92	8-14	
II. Bituminous	1. Low-volatile bituminous coal (lvb)	78-86	14-22	
	2. Med.Volatile bituminous coal	69-78	22-31	
	3. High volatile A bituminous coal (hva)	<69	>31	>14,000 [b]
	4. High volatile B bituminous coal (hvb)			14,000 [b]
	5. High volatile C bituminous coal (hvc)			13,000
III. Subbituminous	1. Subbituminous A coal			13,000
	2. Subbituminous B coal			11,000
	3. Subbituminous C coal			9,500
IV. Lignite	1. Lignite A			8,300
	2. Lignite B			<6,300

[a] If agglomerating, classify as Low volatile bituminous B

[b] Coals with more than 69% fixed shall be classified according to fixed carbon, regardless of calorific value.

2.3 Intrinsic Reactivity

2.3.1 Reaction Rates

Char oxidation is a typical heterogeneous gas-solid reaction system: interaction of particles with a moving gas stream. These systems are usually defined in terms of surface area, and modelled on four basic steps (Levenspiel 1972; Fogler 1999):

(i) External diffusion of reactant from bulk gas to the outer of the solid

(ii) Internal diffusion of reactant gas into solid particle

(iii) Adsorption of reactant gas at an active site of the solid particle

(iv) Intrinsic reaction at the site and desorption of products

The adsorption and chemical reaction process usually overlap each other, so that the overall process only involves the diffusion and chemical reactions. Hence, the overall reaction rate relates to the reactant gas consumption; whereas, the intrinsic reaction rate relates to the instantaneous char consumption. The intrinsic reaction rate $d\alpha/dt$ is usually expressed as (Brown *et al.* 1980; Fogler 1999):

Eq. 2.3-1
$$\frac{d\alpha}{dt} = k\, g(\alpha)$$

Where k is the intrinsic reactivity constant, $g(\alpha)$ is a function describing the extent of reaction, and α is the fractional weight conversion of the carbon.

2.3.2 The Arrhenius Equation

The intrinsic reactivity constant k is generally assumed to have an Arrhenius form, depending on the absolute temperature T as:

Eq. 2.3-2
$$k = A\exp\left(-E/RT\right)$$

Where A is the pre-exponential factor or frequency factor, E is known as the activation energy, and R is the molar gas constant equal to 8.314 J °C $^{-1}$mol $^{-1}$. In 1889, Arrhenius successfully applied this empirical equation to a vast number of

reactions, so that equation (2.3-2) is commonly referred to as the Arrhenius equation (Laidler 1984). Although other empirical correlations have been proposed, the Arrhenius equation is probably the simplest and the most applicable (Brown 1997). It may be noted, however, that the Arrhenius equation is based on the Van't Hoff isotherm for the dependence of the equilibrium constant K^o on temperature:

Eq. 2.3-3

$$\frac{d \ln K^o}{d\left(1/T\right)} = -\frac{\Delta H^o}{R}$$

Where ΔH^o is the standard enthalpy change of the chemical reaction. This energy represents the difference of all the energy absorbed in bond-breaking and all the energy released in bond making. By analogy, the intrinsic rate constant k depends on the temperature and an energy factor. The rate constant, however, is based on the principles of collisions. In other words, the reacting molecules must collide for a reaction to take place. Firstly, these molecules must possess a minimum kinetic energy. This condition relates to the activation energy. Secondly, the reacting molecules must have the appropriate orientation for the reaction to occur. This second condition relates to the pre-exponential factor. It emerges that, although there are numerous collisions, not all collisions are successful. The number of successful collisions is therefore described by the intrinsic rate constant $k = A \exp(-E/RT)$ (Laidler *et al.* 2003).

2.3.3 Activation Energy

As previously described, the activation energy relates to a potential energy possessed by the reacting molecules. For this reason, Vyazovkin (2001a) argued that activation energy is the key parameter in determining the reactivity of a chemical process. From the transition-state theory, it is believed that a chemical reaction proceeds through a potential energy surface, as illustrated in Figure 2.3.1. This potential energy usually passes through a maximum, where an activated complex is formed. This maximum energy corresponds to the activation energy required for the bonds to stretch and break before forming any products (Eyring

1935 cited in Laidler *et al.* (2003)). The average bond dissociation energies for some chemical bonds present in coal chars are shown in Table 2.3.1. The activation energy is, therefore, an important factor in the study of chemical reactions. As described by Galwey (2003a), it is an invariable quantity identified with a rate-controlling process and characteristic of a particular reaction. Thus, whenever variable activation energy values are proposed, it is highly possible that the analysis methods are inadequate. In addition, it is very likely that measurements of the reaction rate, and therefore activation energy, have been affected by the experimental conditions. The sensitivity of the experimental conditions on the activation energy value, have been stressed by many researchers (Vyazovkin 2001a; Galwey 2003b). The effects of these procedural variables, such as the particle size and the heating rate of the reactant are discussed in section 2.4.

2.3.4 The Pre-exponential Factor

As previously mentioned, the pre-exponential factor relates to the orientation of the colliding molecules. For this reason, the pre-exponential factor may describe some properties of the molecules such as volume and mean velocity. As Laidler *et al.* (2003) pointed out, the Van't Hoff equation may be rewritten in terms of the Gibbs-free energy ΔG^o, which represents the energy barrier that the reaction must overcome in order to proceed:

Eq. 2.3-4
$$\frac{d \ln K^o}{d\left(1/T\right)} = -\frac{\Delta G^o}{R}$$

Gibbs-free energy is defined as $\Delta G^o = \Delta H^o - T\Delta S^o$, and equation (2.3-4) becomes:

Eq. 2.3-5
$$K^o = \exp\left(\Delta S^o/R\right)\exp\left(-\Delta H^o/RT\right)$$

By analogy with the Arrhenius equation, the pre-exponential factor is related to the entropy change ΔS^o of the reaction. As a thermodynamic property, entropy defines the microscopic state in terms of the position and the momentum of each atom, which is in agreement with the concept of the pre-exponential factor.

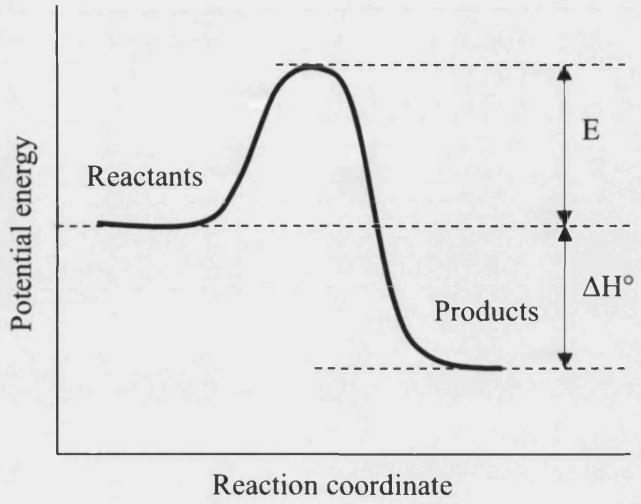

Figure 2.3.1: Potential energy profile for an exothermic reaction: where E is the activation energy and ΔH° is the standard enthalpy of the reaction.

Table 2.3.1: Bond dissociation energies at 25 °C of selected chemical bonds found in coal (Atkins and de Paula 2002)

Bond	Dissociation energy (kJ mol $^{-1}$)
C – O	360
C – C	368
O – H	428
H – H	432
C – H	435
O = O	497
C = C (aromatic)	519
N = O	623
C = C	720
C = O	1076

2.4 Factors Affecting Char Reactivity

2.4.1 Structural Properties

(i) Surface area and porosity

Since the reaction takes place on the surface of the char, the intrinsic reactivity is related to the internal surface area of the char and the surface distribution of reactive groups. During char oxidation, an increase in reactivity is caused by an increase in the active surface area (ASA) due to pore growth, essentially (Karr Jr. 1978). For this reason, many researchers have used the changes in surface area as an index for evaluating the intrinsic reactivity of the char during oxidation (Wayne 1991; Lu *et al.* 2002). In addition, Alvarez *et al.* (1995), observed that char reactivity increased with increasing microporous and active surface area, during the oxidation in air of various coal chars. More recently, Arenillas *et al.* (2003; 2004a) reached a similar conclusion by studying the reactivity in oxygen of five carbonaceous materials. The development of pore structure has also been used as an index for evaluating char reactivity. Liu *et al.* (2000), observed that changes in pore structure led to significant variation in reaction rate, during the oxidation in air and CO_2 of bituminous chars. As pointed out by, Feng and Bhatia (2003a) pore volume appears to increase rapidly at first before slowing down again with carbon conversion. Similar observations have recently been published by Chen *et al.* (2004), whilst studying the oxidation behaviour of chars in air.

(ii) Rank of parent coal

Perusal of coal oxidation studies have demonstrated that char reactivity in air, CO_2, or steam decreases with increasing rank of the parent coal. Recent investigations include the work of de la Puente *et al.* (2000) and also Haykiri-Acma *et al.* (2002) who measured the reactivity of five coals of different rank in air and found that high-rank coal chars were less reactive than low-rank coal chars.

(iii) Maceral composition

The maceral composition of a coal is also believed to have a strong influence on char reactivity (Hampartsoumian *et al.* 1998). However, a direct relationships has not yet been found between the reactivity of the char and maceral content or vitrinite reflectance (Lester *et al.* 1999). Alonso *et al.* (2001a) have been able to show that vitrinite-rich chars have a higher reactivity in air than inertinite-rich chars. In addition, Tang *et al.* (2005) have recently established that char reactivity in oxygen decreases with the rank of coal for vitrinite-rich coals; whereas, for inertinite-rich coals, char reactivity depends on the inertinite content rather than the rank of the parent coal.

(iv) Inorganic impurities

Presence of mineral matter in the coal appears to also affect the reactivity of the resulting char. These minerals may in fact act as catalyst during the oxidation reaction, and hence they lower the apparent activation energy of the process. Past and recent studies have demonstrated the catalytic effects of some minerals and alkali metals such as Li_2CO_3 (Linares *et al.* (1977) cited in (Karr Jr. 1978)) (Serageldin 1984; Gopalakrishnan and Bartholomew 1996).

2.4.2 Experimental Conditions

Evaluation of char reactivity is strongly affected by the experimental conditions. Conditions such as char preparation have a significant effect on the structure of the char, and hence on the resulting reactivity of this char. Chan *et al.* (1999), studied the reactivity in air of three bituminous coals prepared at various heat treatment temperatures (HTT). They found that the reactivity of the resulting char decreased as the HTT increased. Zolin *et al.* (2002) suggested a similar pattern when they studied the effect of HTT of chars, and their subsequent reactivity in oxygen. Another aspect of char preparation is the effect of the heating rate used during the carbonisation process. It appears that the use of very high heating rates lead to a considerable increase in subsequent char reactivity (Ashu *et al.* (1976)

cited in Karr Jr.(1978)). On the other hand, an increase in carbonisation pressure has shown to lead to a decrease in char reactivity (Gadiou *et al.* 2002). Other important experimental conditions include reactant pressure, sample weight and particle size. Banin *et al.* (1997) observed that oxygen partial pressure have significant effects on char reactivity. More recently, Hecker *et al.* (2003) have shown that the value of the kinetic parameters decrease with decreasing O_2 partial pressure, in a total pressure range of 1 to 32 atm. The initial sample weight of the char has also demonstrated some effects on the determination of char reactivity. Salvador *et al.* (2003) have found that as the sample size decreases the measured char reactivity increases. They concluded that mass transfer limitations were in operation at the larger sample size. In a similar manner, Alvarez *et al.* (1995) have demonstrated that the measured char reactivity increases with decreasing particle size. They found that the larger particles induced a mass transfer resistance. It appears from these findings that in the chemical control regime (Zone I), both the sample weight and particle size do not influence the reactivity of the char. Other experimental factors have also been found to affect the kinetics of char oxidation. These factors include the heating rate, geometry of sample holder, or convection currents (Wendlandt 1964; Hatakeyama and Zhenhai 1998). The most influential factor is probably the heating rate since it relates directly to the kinetic analysis.

2.4.3 Heating Rate

The effects of experimental conditions on kinetic studies has long been recognised with the heating rate as the most important variable (Mackenzie 1970). It has generally been found that the heating rate influences the temperature gradient inside the sample, so that the ignition, peak and final reaction temperatures are shifted to higher values as the heating rate is increased. In this way, the measured char reactivity appears to increase with increasing heating rate. Several studies illustrating these observations have been discussed by Wendlandt (1964). Zsáko *et al.* (1971), for instance, found that the rate of heating had a considerable influence on the decomposition scheme of a bromine compound. The shape of the

decomposition profile (i.e. thermogravimetric curve) depended largely on this procedural variable, so that the resulting kinetic reactivity parameters varied with the heating rate. For this reason, Serageldin *et al.* (1982) suggested that such analyses, which are dependent on heating rate, are inadequate as they lead to erroneous reactivity values. They suggested that the rate of heating affects the thermal inertia of the sample and diffusion rate of the gaseous products. Others have suggested that the heating rate influences the phase transition of polymers, so that the chemical reaction may be preceded by a melting phase at low heating rate, and superheating at high heating rates (Hatakeyama *et al.* 1998). Because of these resulting uncertainties in the measured reactivity, Ichihara (1994) and also much earlier on Wendlandt (1964), indicated that there certainly exists an optimum-heating rate at which these thermal interferences may be minimised or eliminated so that accurate reactivity parameters may be obtained.

The effects of heating rate on the thermal properties of the coal have not received a great consideration in the literature. Investigators such as Sampath *et al.* (1998) have linked the effect of heating rate with structural changes of a material during the reaction process. They showed that slow heating rate conditions induce an increase in the heat capacity and thermal conductivity of the coal during devolatilisation. They concluded that bond breaking and structural changes had provoked an increase in the vibration modes of the coal structure. At higher heating rates, however, there were no changes, indicating that the coal structure was frozen at first and a finite time was required for the structure to relax and respond to the thermal input. In a recent study, Pinheiro *et al.* (2002) observed that as the heating rate increases, different self-heating effects take place during the oxidation of explosive materials. The decomposition reaction appeared to take place below its melting point temperature for low heating rates (1 – 5 °C min^{-1}); whereas, the oxidation reaction occurred beyond the melting point temperature, at the higher heating rates (15 – 25 °C min^{-1}). These results show that the rate of heating affects the phase transition of a material in a complex manner. It is highly possible, therefore, that a specific f heating rate modifies the overall reaction mechanism.

2.5 Intrinsic Char Reactivity from Experiments

2.5.1 Calorimetric Analysis

These tests consist of measuring the heat released during the chemical reaction, which then serves as a reactivity index. This method is empirical and provides no information on the kinetic reactivity parameters. It is not surprising, therefore, that it has not received great consideration in thermal analysis, although Mahajan (1977, cited in Karr Jr. (1978)) used this technique to compare the reactivity of various coals during pyrolysis and hydrogenation.

2.5.2 Gas Analysis

In gas analysis techniques the chemical reaction occurs in an engineered reactor. The product gases are subsequently measured and analysed by gas chromatography, mass spectrometry or infrared techniques. The amount of carbon gasified is therefore deduced at different time intervals from a material balance. Several researchers have measured char reactivities by gas analysis using either fixed or fluidised bed reactors (Krishnaswamy *et al.* 1996b; Luo *et al.* 2001; Kajitani *et al.* 2002; Lu *et al.* 2002). Although fluidised beds provide a more efficient heat and mass transfer, diffusion of the gaseous reactants and/or products through the bed usually limit the chemical process. Hence, the computed kinetic analysis corresponds to the overall reactivity as opposed to the intrinsic reactivity.

2.5.3 Weighing Techniques

(i) Standard Tests

There exist three standard tests on how to measure the reactivity of coke: British standards on coke reactivity (BS 4262 1984; BS 1016-108.6 1992) and a North American standard (ASTM D 5341 1999). These tests are fairly similar, dealing with burning a coke sample in a furnace, and then measuring its weight before and

after the reaction. Reactivity is given as the ratio of weight loss of sample during the reaction over the initial sample weight. This method is empirical and does not provide any estimate on the reactivity parameters: activation energy E and the pre-exponential factor A.

(i) Thermogravimetric Analysis (TGA)

Thermogravimetric analysers measure the weight changes of a char sample during the chemical reaction, whilst the sample is subjected to a controlled temperature atmosphere. The reaction may proceed isothermally or non-isothermally. TGA is convenient to obtain intrinsic reactivity, since it is possible to proceed at low temperatures and low reactant gas flow rates. It is not surprising that these techniques have widely been applied for characterisation of intrinsic reactivity of coal chars (Gibbins and Williamson 1993). In fact, gas analysis techniques are more suitable for overall reaction rate measurements, whereas thermogravimetric analysis are better for direct measurements of intrinsic reactivity (Russell *et al.* 1998).

2.6 Thermogravimetric Analysis Techniques

2.6.1 Isothermal

Isothermal analyses are the oldest types of experiments carried out to measure the reactivity of a chemical process. These experiments may be undertaken in a thermogravimetric analyser, by maintaining the temperature constant. The mathematical analysis for the derivation of kinetic data is straightforward (Brown 2001). However, the char might take up to 3 h to reach 50-wt% conversion. At the same time, an isothermal reaction is unable to show the decomposition of different materials occurring at temperatures different from the selected isothermal temperature. Furthermore, at least three independent isothermal temperature experiments are required for the kinetic analysis. The use of different samples for a single analysis generates an additional error. It is clear that

isothermal analyses are long and laborious, and therefore they are not so attractive. Owing to their analytical simplicity, many researchers are still applying this technique (Lizzio *et al.* 1988; Alvarez *et al.* 1995; Gale *et al.* 1996; Sorensen *et al.* 1996; Senneca *et al.* 1997; Salatino *et al.* 1998; Zolin *et al.* 1998; Chan *et al.* 1999). More recently, Kajitani *et al.* (2003), Arenillas *et al.* (2004a) and also Slaoui *et al.* (2004) have evaluated the reactivity in air of chars using isothermal TGA techniques.

2.6.2 Constant Heating Rate

More conventionally, the temperature in the thermogravimetric analyser is raised linearly with time: constant heating rate. In this temperature mode it is possible to study the chemical process over a wide temperature range. However, the mathematical analysis for deriving the kinetic parameters is complicated. This involves the temperature integral of the Arrhenius equation. This kinetic analysis is discussed in more detail in the next chapter. The main advantages of constant heating rate TGA compare to isothermal experiments lie in the possibility of studying the reaction in one single experimental run, and also achieving complete char conversion in a shorter period of time. In light of this, many researchers have applied this technique to determine the oxidation reactivity of various chars (Shemet *et al.* 1993; Hampartsoumian *et al.* 1998; Lester *et al.* 1999). Later on, Ceylan *et al.* (1999), Alonso *et al.* (2001a) and Peralta *et al.* (2001) also used this single heating rate TGA method to assess the reactivity of chars produced in a novel reactor. In a similar manner, Zolin *et al.* (2002), coupled linear TGA measurements with an entrained flow reactor to study the thermal deactivation of various chars. On the other hand Haykiri-Acma *et al.* (2003b) and Tang *et al.* (2005) have recently used linear TGA for reactivity measurements of different coal rank. All these investigators have performed their experiments at an arbitrary heating rate, following recommendations of Russell *et al.* (1998) or Hatakeyama *et al.* (1998), who suggested a heating rate of 15 °C min^{-1} or 5 – 10 °C min^{-1}. This is not such a reliable technique since the heating rate affects the determination of the intrinsic kinetic parameters. As discussed in 2.4.3, thermal effects are induced

on the sample at the different heating rates, which then influence the chemical reaction in a rather complex manner. In some cases, recrystallisation may occur followed by a melting process at low heating rates, whereas, superheating may take place at higher heating rates. It is possible, however, that there exists an optimum heating rate at which these thermal interferences are minimised or eliminated, and accurate kinetic parameters can be derived. Yet, none of these investigators have verified that their arbitrary heating rate was appropriate for extracting the most accurate estimate for the kinetic parameters.

Although the presented literature is a selective account of the works carried out on reactivity characterisation for coal chars, it is evident that TGA is the conventional technique, established for isothermal and non-isothermal (linear heating rate) conditions. Nonetheless, these two techniques present clear disadvantages. Isothermal TGA methods are simple but time-consuming; whereas, constant heating rate TGA techniques are faster but unreliable. It emerges that there is a need for improving the constant heating rate TGA method, by developing a simpler mathematical analysis and identifying the optimum heating rate, which does not interfere with the kinetic analysis and true intrinsic reactivity parameters are derived.

2.6.3 Sample Controlled Thermogravimetric Analysis

At the present, there is a new range of temperature control techniques arising within thermogravimetric studies. These techniques are emerging as the constant heating rate TGA method is sensitive to the rate of heating with a complex kinetic analysis, and isothermal experiments are laborious (Ortega 2002). These new techniques consist of sample controlled thermal analysis (SCTA) methods, where the heating rate is not predetermined but altered in such a way that feedback from the sample weight is used to control its rate of heating or cooling. In this way, the chemical reaction takes place at its own pace. As described by Gotor *et al.*(1998) and also Sorensen (1999), the main advantages of SCTA methods over constant heating rate are as follows: higher resolution in discriminating among the reaction

kinetic models; consecutive and close-lying reactions are easily separated and; simpler mathematical equations are generated in the kinetic analysis of SCTA methods. They have also suggested that heat and mass transfer effects on the forward reaction are minimised by not applying a constant rate of heating. These advantages have also been pointed out by Criado and Perez-Maqueda (2005), who suggested two main categories of SCTA techniques:

(i) Constant Rate Thermal Analysis (CRTA)

Constant rate thermal analysis (CRTA) techniques were implemented in the early seventies by Paulik *et al.* (1971; 1973). The furnace temperature is controlled in such a way that the reaction rate $d\alpha/dt$ is maintained constant during the course of the chemical reaction. A schematic of a CRTA temperature programme with the corresponding reaction rate profile is given in Figure 2.6.1. The CRTA method developed by Rouquerol (1973) is usually referred to as temperature jump or rate jump analysis. In this case, there is an abrupt change in temperature, which leads to a corresponding jump in the reaction rate. By assuming that the conversion α remains unchanged during the jump, the reaction rate at the two temperatures are compared in order to evaluate the kinetic parameters at this conversion α.

(ii) Stepwise Isothermal Analysis (SIA)

Stepwise isothermal analysis (SIA) technique was introduced in the late seventies by Sorensen (1978; 1992). In this method, the reaction rate oscillates between a maximum and a minimum reaction rate value imposed on the reaction. Once the upper preset limit is reached, the temperature stops increasing and the reaction proceeds isothermally until the reaction rate falls below the lower preset value. At this point, heating is resumed and the reaction proceeds with a linear rise in temperature. It then follows that the overall reaction takes place in a series of isothermal steps. A schematic of the temperature programme together with the resulting reaction rate profile is also presented in Figure 2.6.1. Although both the CRTA and the SIA techniques are probably the most widely used, other temperature control modes have also been discussed in the literature (Ozawa

2000; Brown 2001; Ozawa 2001; Sorensen 2003a). Nonetheless, none of these procedures have been applied to the study of char reactivity (Chen *et al.* 1998; Sorensen 1999, 2003b). In fact, these techniques have not been used to evaluate the kinetic parameters of a chemical process; rather, they are usually applied to determine the reaction mechanism of these processes (Perez-Maqueda *et al.* 1996). Hence there is scope for applying SCTA techniques in the evaluation of kinetic parameters of coal chars oxidation.

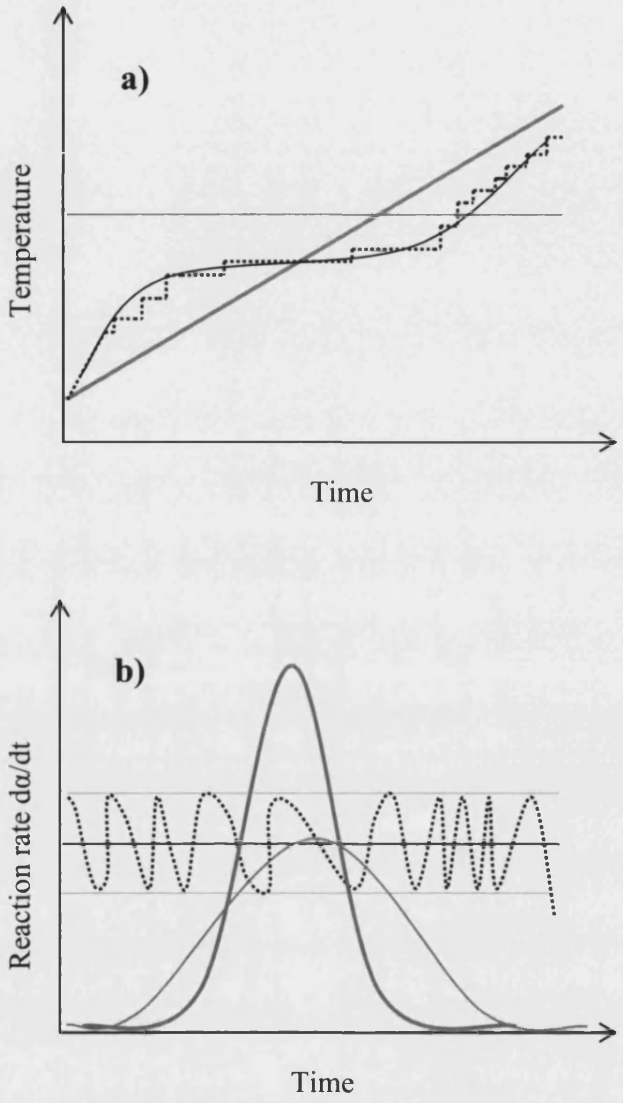

Figure 2.6.1: Trend of temperature and reaction rate (dα/dt) during the thermal decomposition of solid-state reactions, following different temperature control methods: (—) isothermal; (—) constant heating rate; (—) CRTA; (▪▪▪) SIA. Adapted from Gotor *et al.* (Gotor 1998).

2.7 Kinetics of Char Oxidation

2.7.1 Carbon-Molecular Oxygen Reaction

The oxidation of carbon is determined by the nature of the carbon-carbon linkages, and may be characterised as a non-catalysed gas-solid reaction. Several authors have discussed the mechanism of this process in details, yet it is still not completely understood (Itay *et al.* 1989; Van Krevelen 1993; Berkowitz 1994). Most of these works were performed under low temperature conditions (< 200°C), or under very low oxygen partial pressure (< 0.2 atm).

2.7.2 Reaction Mechanism

In the early eighties, Karsner and Perlmutter (1982; 1982a) suggested a three-step reaction mechanism for coal oxidation between 150 °C and 300 °C. This three - steps mechanism has successfully been tested by Ranish *et al.* (1993):

(i) Chemisorption of oxygen complexes at the surface of the char
(ii) Desorption of these oxygen complexes.
(iii) A set of direct burn-off reactions between the char and the oxygen to form gaseous products.

Nonetheless, Itay *et al.* (1989) found that the burn-off reactions did not occur at low temperatures (below 300 °C). In a similar manner, Wang *et al.* (1999) observed that beyond 300 °C these direct burn-off reactions are the main reactions taking place. According to Feng *et al.* (2000) the gasification of carbon in the chemical regime has now been accepted to follow this three-steps mechanism.

The chemisorption process is believed to generate unstable and stable complexes (Lizzio *et al.* 1988). The stable complexes are supposed to remain attached to the char surface even at high temperatures; whereas, the unstable complexes have a very short residence time on the char surface. Wang *et al.* (2002a) have suggested that CO_2 comes from the decomposition of the carboxyl groups whilst CO is

produced from the decomposition of the carbonyl groups. Thermal decomposition of the stable complexes plays an important role in the formation of gaseous products, therefore. In fact, Ahmed *et al.* (1985) have shown that these complexes may block active sites and inhibit the oxidation reaction, so that this reaction is shortened and the overall reaction rate is slightly increased.

2.7.3 Gaseous Products

It is evident that modelling the coal char oxidation process at temperatures above 300 °C is concerned with the burn-off reactions:

$$C + O_2 \rightarrow CO_2 \qquad (I)$$

$$C + \tfrac{1}{2} O_2 \rightarrow CO \qquad (II)$$

$$CO^* + \tfrac{1}{2} O_2 \rightarrow CO_2 \qquad (III)$$

Where CO* is an unstable complex containing the carbon monoxide molecule. At the present, researchers are still trying to establish whether both CO and CO_2 are primary products of the oxidation, or CO_2 is produced from further oxidation of the carbon monoxide. Hayhurst *et al.* (1998) have reached the conclusion that both CO and CO_2 are primary products of carbon oxidation in air, whilst CO_2 may also result from secondary reactions involving CO, H_2O and OH. They found that reaction (I) is the main reaction for temperatures below 727 °C; whereas, reaction (II) takes place for temperatures between 727 °C and 1127 °C. Above 1127°C, CO was rapidly oxidised to CO_2 in the gas phase following reaction (III). Similar observations have been made in the work of Wang *et al.* (2003a; 2003b; 2003c) for the air oxidation of different coal chars at low temperatures (< 200 °C).

In contrast, Arenillas *et al.* (2003) identified a single reaction rate curve during the air oxidation of bituminous coal char. In other words, they found that both reaction (I) and (II) were taking place at the same time. In a detailed investigation of the oxidation of powder charcoal in 1-v% oxygen, Li and Brown (2001) have also shown that reactions (I) and (II) take place at approximately the same time and temperature interval, between 550 °C and 700 °C, as shown in Figure 2.7.1.

At higher temperatures (> 650 °C), they assigned the significant increase in CO_2 production to secondary reactions. In their analysis, these secondary reactions consist of the decomposition of oxygenated carbon monoxide complex located at the surface of the char particle. This decomposition process subsequently moves to the gas phase, and hence is usually assumed to take place in the gas phase. It is therefore possible to detect the progress of this third reaction on the overall thermogravimetric signal since the reacting oxygenated complexes are located on the surface of the char.

2.7.4 Reaction Zones

The concept of reaction zone is essential in order to understand the difference between intrinsic kinetic data, and overall reactivity. As the burn-off reactions take place, either the diffusion of the reacting gases onto the surface of the char or the kinetics of the reaction may slow down the overall process. Dutta and Wen (1977) observed that char oxidation in air is essentially controlled by the kinetics of the chemical reaction for temperatures between 424 °C and 576 °C. More recently, Hustad *et al.* (1991) showed that during char oxidation, chemical control usually takes place in the temperature range 350 - 750 °C; whereas, the process is essentially controlled by external mass transfer between 800 °C and 1390 °C. Nowadays, it is the method of Walker Jr (1959), which is usually applied to determine the temperature boundaries of the different rate-controlling mechanisms during char oxidation. A schematic of this method is represented in Figure 2.7.2 and is characterised as follows (Smoot and Smith 1985):

(i) *Zone I*: Chemical reaction control region occurs at low temperatures and is limited by the total internal surface area. In this temperature region, the apparent activation energy *Ea* corresponds to the true activation energy of the reaction *E*.

(ii) *Zone II*: Pore diffusion regime, the overall rate is controlled by both the chemical reaction and the internal pore diffusion. The small and rough surface of the pores slows the transport of the reactant gas to the

internal surface of the coal particle. The measured activation energy, in this region, is half the value of the true activation energy.

(iii) *Zone III*: Bulk surface diffusion control region, which occurs at higher temperatures, so that further increase of the temperature has no effect on the kinetics of the reaction. Instead, transport of oxygen through the external gas film around the particle controls the overall reaction process.

It is clear that the calculated reaction rate largely depends on the temperature range in which the material is being oxidised. More recently, Medek *et al.* (2001) and also Hu *et al.*(2001) have used this concept to determine the rate controlling regime at various temperature intervals for the oxidation of coal chars by measuring their activation energy values in air between different temperature ranges.

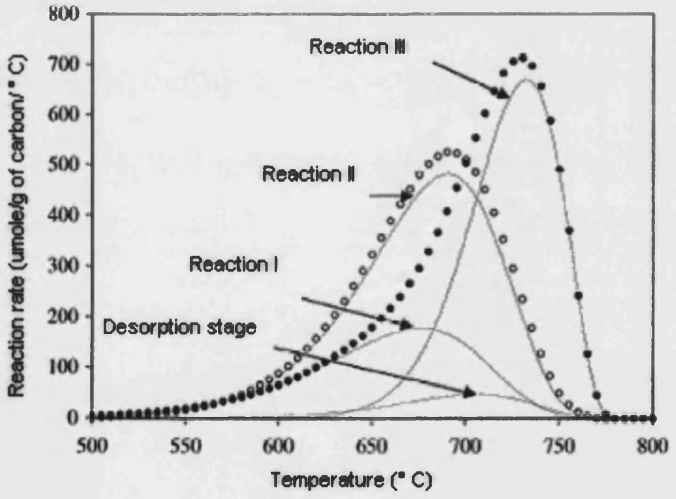

Figure 2.7.1: Experimental evolution rates of CO (○) and CO_2 (●) during temperature programme oxidation, in 0.939-v% O, with heating rate of 10 of powder charcoal. Hairline profiles represent simulated peaks associated with the reactions (adapted from Li and Brown (2001)).

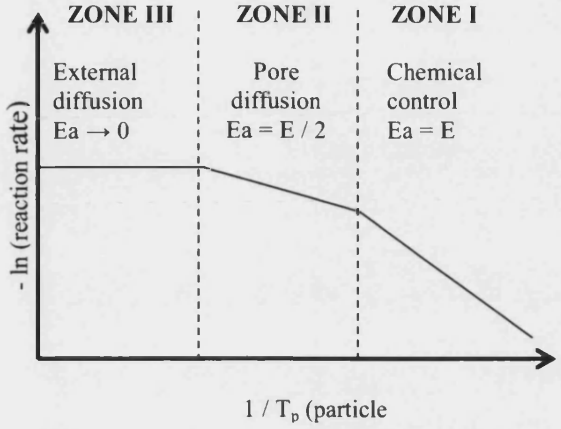

Figure 2.7.2: Rate controlling regimes for heterogeneous char oxidation (Smoot *et al.* 1985). Ea is the apparent activation energy.

2.8 Kinetic Modelling of Gas-Solid Reactions

2.8.1 Kinetic Models

As previously mentioned, the mechanism of coal char oxidation is not simple. The basic process, however, may be described as a gas-solid reaction, and the reaction rate is defined as given in equation (2.3-1):

$$\frac{d\alpha}{dt} = k\, g(\alpha)$$

This mathematical expression incorporates a complex set of physicochemical and thermal phenomena; especially, with structural changes occurring during the reaction. These phenomena are given in some function of the conversion $g(\alpha)$, depending on the reaction mechanism. Several kinetic models have been suggested, to interpret the rate of reaction with or without structural changes

during the oxidation process. The possible kinetic models for char oxidation are summarised in Table 2.8.1 and briefly described below:

(i) *Geometrical based models:* The rate of reaction is based on the changing geometry of the reaction interface. The geometry accounts for the contracting area or volume, and these models generally include the grain or shrinking core model.

(ii) *Diffusion mechanisms based models:* The rate of reaction is determined by a diffusion mechanism through the rough pore of the char. This model is well illustrated by the random pore model described in the next section.

(iii) *Order of reaction based model:* These models are referred to as global kinetics or volumetric reaction models, where the rate of reaction occurs at a nucleus.

Table 2.8.1: Broad classification of solid-state kinetic reaction expression (Brown *et al.* 1980)

	g (α) =1/k d α /dt
1. Acceleratory α - time curves	
Power Law	$n(\alpha)^{(n-1)/n}$
Exponential Law	α
2. Sigmoid α - time curves	
Avrami-Erofe'ev	$m(1-\alpha)(-\ln(1-\alpha))^{(m-1)/m}$
Prout-Tompkins	$\alpha(1-\alpha)$
4. Deceleratory α - time curves	
Geometrical based models	$m(1-\alpha)^{(m-1)/m}$
Diffusion mechanisms based models	
One-dimensional	$1/(2\alpha)$
Two-dimensional	$(-\ln(1-\alpha))^{-1}$
'Order of Reaction' based models	$(1-\alpha)^{n}$

2.8.2 Shrinking Core Model

The shrinking core model is the most fundamental model used in non-catalytic gas-solid reaction. It was first presented by Levenspiel (1972) who assumed that reaction occurs on the external surface of an initially non-porous solid particle. As the reaction proceeds, an ash layer is formed around the unreacted core. Hence, the reaction zone is confined to a sharp interface between the unreacted core and the product. Diffusion of the reactants through the ash layer is therefore limited by its porous structure, so that the rate expression should account for such measurement. In Levenspiel's expression, however, these changes are not represented:

Eq. 2.8-1

$$\frac{d\alpha}{dt} = k\left[3(1-\alpha)^{2/3}\right]$$

Sohn and Szekely (1972) and later on Sampath *et al.* (1975) improved this model by introducing the initial pore volume and external surface area into the rate expression. Sotirchos and Amundson (1984b) have shown that the shrinking core model is, in fact, inadequate if it does not take into account structural changes.

2.8.3 Progressive-Conversion Model

The progressive conversion model was introduced at the same time as the shrinking core model by Levenspiel (1972), and derived for porous solid particles. In this case, the gaseous reactants diffuse freely into the interior of the particle, and the reaction occurs throughout the entire particle, which remains of the same size. The diffusion rate of oxygen is much rapid compare to the kinetics of the reaction, so that the chemical process is kinetically controlled. The reaction rate in this case is represented in terms of internal surface area instead of the external surface as in the shrinking core model, with a similar mathematical expression as in equation (2.8-1). Although this model has not received much consideration in the literature of carbon oxidation, it was recently employed by Krishnaswamy *et al.* (1996a) to describe the low-temperature oxidation of coal.

2.8.4 Random Pore Model

Both the shrinking core and progressive conversion models have limitations and do not always coincide with reality. In fact, reaction may not occur along a sharp interface between the ash layer and the solid particle, nor the gaseous reactant diffuse freely throughout the particle. In a more practical situation, the reaction may take place in an intermediate behaviour between the two approaches (Ishida *et al.* 1971). For this reason, Bhatia and Perlmutter (1980) developed a model, which accounts for stronger influence of the initial structural properties on a porous particle. In this case, the reaction is randomly initiated at the internal surface area of a pore, instead of the outer particle surface. The reaction proceeds by growth of the pore volume, and the rate expression is given as:

Eq. 2.8-2

$$\frac{d\alpha}{dt} = k.(1-\alpha)\sqrt{1-\psi \ln(1-\alpha)}$$

Where ψ is defined as the random pore model structural parameter. This model has proven to successfully predict experimental observations in gas-solid reactions, according to Lu *et al.* (1997). Haji-Sulaiman *et al.* (2002) successfully applied this kinetic model to describe the oxidation of Malaysian coal chars. They found that the model was valid as long as the structural parameter ψ was adjustable. Also, Kajitani *et al.* (2002), found that the random pore model presented a good fit to experimental results for gasification of coal char, with an ideal value of $\psi = 14$.

2.8.5 Global Kinetic

Although sufficiently accurate, the random pore model is rather complex. The presumed structural changes are not sufficiently accounted for, since the structural parameter ψ is constant. These problems have been addressed by Rafsanjani *et al.* (2002) who showed that this model could not simultaneously confirm experimental reaction rates and changes in char surface area. Since the details of these complicated internal structural changes are not completely known, it is better to use a simpler model capable to capture the complexity of the reaction in a

tractable mathematical manner. For this purpose, global kinetic models or volumetric reaction models are commonly used in engineering practices. These models assume that reaction takes place all over the volume of a porous particle rather than at a sharp interface, and the char reaction rate is represented as:

Eq. 2.8-3

$$\frac{d\alpha}{dt} = k(1-\alpha)^n$$

Where n is the order of reaction with respect to carbon conversion. This model has extensively been used in coal char oxidation studies (Zimbardi 2000; He *et al.* 2002).

2.9 Aims and Objectives

The main aim of this project is to develop a new thermogravimetric analysis method to determine the oxidation reactivity of carbons in or derived from coal. This new method is expected to be quicker and more reliable than existing methods for characterising reactivity. This may be useful for characterising, comparing, predicting, and understanding the performance of existing and new coals and coal blends in important industrial processes such as pulverised-fuel combustion and iron and steel-making. The key objectives in achieving the aim are to:

i) *Derive a simple kinetic analysis, which correctly models the oxidation of coal chars in the chemical control regime.*

ii) *Develop an improved constant heating rate thermogravimetric analysis method for obtaining accurate intrinsic reactivity data of char oxidation in air.*

iii) *Develop a simpler sample controlled thermal analysis, which allows for the kinetic parameters to be evaluated.*

Chapter 3

Proposed Model Kinetic Analysis

3.1 Introduction

Since the early development of non-isothermal analysis in the 1960's, determination of the kinetic parameters is the subject of many discussions (Brown 1997; Flynn 1997). The unknown kinetic triplet, consisting of the activation energy E, the pre-exponential factor A and the reaction mechanism $g(\alpha)$, is at the centre of these heated debates (Brown 2001; Galwey 2003b). Several kinetic analysis methods are still being developed, each trying to capture the essence of a reaction mechanism. This attempt is somewhat restricted, as most processes take place in multi-step reactions, so that the whole process cannot be modelled by a simple equation. In addition, the reactivity parameters appear to be strongly dependent on procedural variables. All these effects, however, have not always been taken into consideration, whilst deriving a kinetic analysis.

In this chapter a simple but accurate kinetic analysis is developed to enable determination of the intrinsic reactivity parameters E and A of the oxidation of coal char in air. This novel kinetic analysis approach is presented in three sections. The first section examines the inherent problems of existing analytical methods applied in non-isothermal systems. The second section deals with the implementation of a novel kinetic analysis. The final section presents a methodology for testing the validity of this new method.

3.2 Review of Analytical Methods

3.2.1 Kinetic Analysis of Carbon Oxidation

The intrinsic reaction rate for a gas-solid system was defined in equation (2.3-1) as $d\alpha/dt = k\, g(\alpha)$, where α is the fractional carbon conversion, and $g(\alpha)$ is a kinetic model function described in Table 2.8.1. Since the intrinsic rate constant k is usually defined by the Arrhenius equation (Eq. 2.3-2), the rate equation is then rewritten as:

Eq. 3.2-1
$$\frac{d\alpha}{dt} = g(\alpha) A \exp\left(-E/RT\right)$$

For non-isothermal conditions, the solid sample reacts under a gradual increase in temperature T (usually linearly), $\beta = dT/dt$. The effect of temperature becomes apparent by introducing this new variable as:

Eq. 3.2-2
$$\frac{d\alpha}{dT} = g(\alpha)\frac{A}{\beta}\exp\left(-E/RT\right)$$

Integration of the above, subject to initial conditions $\alpha = 0$ T = 0 yields:

Eq. 3.2-3
$$F(\alpha) = \frac{A}{\beta}\int_{o}^{T}\exp\left(-E/RT\right)dT$$

Eq. 3.2-4
$$F(\alpha) = \int_{0}^{\alpha}\frac{d\alpha}{g(\alpha)}$$

The integral on the right hand side of equation (3.2-3) may be solved by introducing the variable $x = E/RT$ so that:

Eq. 3.2-5
$$\int_{o}^{T}\exp\left(-E/RT\right)dT = \int_{\infty}^{0}\frac{E}{R}\left(-\frac{1}{x^2}\right)e^{-x}\,dx = \frac{E}{R}\int_{x}^{\infty}\frac{e^{-x}}{x^2}dx$$

The temperature integral is now defined as $p(x)$:

Eq. 3.2-6
$$p(x) = \int_{x}^{\infty}\frac{e^{-x}}{x^2}dx$$

And the reactivity model equation (3.2-3) is now given as:

Eq. 3.2-7 $$F(\alpha)=\frac{AE}{\beta R}p(x)$$

The function *p(x)* has no exact analytical solution; however, it may be approximated in various manners. Several approximate functions have been developed and discussed in the literature (Zsáko 1968; Brown *et al.* 1980; Flynn 1997). However, only a selective number of these approximations is mentioned in this work, which are categorised in essentially two ways, arising from:

(i) *Asymptotic expansion series*

The simplest asymptotic series is obtained after integration by parts:

Eq. 3.2-8 $$p(x)=\int_x^\infty \frac{e^{-x}}{x^2}dx=\left[-\frac{e^{-x}}{x^2}+\frac{2e^{-x}}{x^3}-\frac{6e^{-x}}{x^4}+\frac{24e^{-x}}{x^5}+\ldots+(-1)^{n+1}\frac{n!e^{-x}}{x^{n+1}}\right]_x^\infty$$

and $$\lim_{x\to\infty}p(x)=0,$$

Thus, equation (3.2-8) reduces to

Eq. 3.2-9 $$p(x)=\frac{e^{-x}}{x^2}\left(1+\frac{2!}{(-x)}+\frac{3!}{(-x)^2}+\frac{4!}{(-x)^3}+\ldots+\frac{n!}{(-x)^{n-1}}\right)$$

This series may be truncated, giving rise to classical approximate *p(x)* functions, such as the two term approximations of Coats and Redfern (1964):

Eq. 3.2-10 $$p(x)\cong\frac{e^{-x}}{x^2}\left(1-\frac{2}{x}\right)$$

Other more complex asymptotic series, yet more complex, have also been developed (Paterson 1971). Their general formula is of the type:

Eq. 3.2-11 $$p(x)=\frac{\exp(-x)}{x(w+mx)}(h(x))$$

Where *w* and *m* are positive constants independent of *x*, and *h(x)* is the ratio of two polynomials. These series are usually truncated giving rise to traditional *p(x)* functions such as the one derived by (Gorbachev 1975):

Eq. 3.2-12
$$p(x) \cong \frac{e^{-x}}{x^2}\left(\frac{1}{x+2}\right)$$

The most acclaimed *p(x)* functions of this type are probably those of Senum and Yang (1977). They are a ratio of polynomials in *x*. The fourth degree function is given as:

Eq. 3.2-13
$$p(x) \cong \frac{\exp(-x)}{x^2}\left[\frac{x^4+18x^3+86x^2+96x}{x^4+20x^3+120x^2+240x+120}\right]$$

(ii) Approximations by integrated expressions

These types of approximations to the temperature integral *p(x)* are empirical. They are derived from observing that the logarithm of the temperature integral varies with *x* in the following manner:

Eq. 3.2-14
$$\ln p(x) \cong -B - mx - w\ln x$$

Eq. 3.2-15
$$p(x) \cong \frac{\exp(-mx+B)}{x^w}$$

Where *B* is a positive constant independent of *x*, and *m* and *w* are positive constants independent of x. Although, Madhusudanan *et al.* (1986) first postulated this formulation of *ln p(x)* as a function of *x*, Doyle (1962) derived the first approximation in this category:

Eq. 3.2-16
$$p(x) \cong \exp(-1.052x - 5.33)$$

Starink (1996) suggested that for m = 1, the most accurate approximation is probably given with w = 1.95

Eq. 3.2-17
$$p(x) \cong \frac{\exp(-x-0.235)}{x^{1.95}}$$

Later on, he showed that for m ≠ 1 (Starink 2003) the following was more accurate:

Eq. 3.2-18
$$p(x) \cong \frac{\exp(-1.0008x-0.312)}{x^{1.92}}$$

Yet, Tang *et al.* (2003) have argued that the following was also highly accurate:

Eq. 3.2-19
$$p(x) \cong \frac{\exp(-1.0014x - 0.378)}{x^{1.89}}$$

The accuracy of these different approximations is discussed in the next section of this Chapter.

3.2.2 Model-Fitting Methods

Model-fitting methods are based on evaluating equation (3.2-7) by identifying a kinetic model *g(α)* and selecting an approximate function *p(x)*. The most common and simplest way is to obtain a linear form of that equation as:

Eq. 3.2-20
$$\ln F(\alpha) = f\left(\frac{1}{T}\right)$$

In this way, the activation energy E, is calculated from the slope of this linear plot, whereas the pre-exponential factor A, is deduced from the intercept. Hence, the kinetic parameters can be determined from a single heating rate experiment. Several investigators have also suggested this type of analysis methods (Freeman and Carroll 1958; Achar *et al.* 1966). These procedures assume that a single kinetic model holds for the whole reaction process; whereas the reaction mechanism may be changing and may not be accurately described by a single kinetic model (Brown 2001; Vyazovkin 2001b). In addition, there is the problem of a single heating rate effect, where it was established in section 2.4.3 that determination of the kinetic parameters is strongly affected by the heating rate employed. For these two reasons, model-fitting procedures have been found to be generally unreliable and inaccurate (Sbirrazzuoli *et al.* 1995; Ortega 2002).

3.2.3 Isoconversional Methods

Some kinetic analysis procedures are based on the isoconversional principle, where the reaction rate at a constant extent of conversion α is only a function of temperature. In this case, it is not necessary to define a kinetic model. For this reason, these methods are also often referred to as 'model-free' kinetics (Brown 2001). Two categories of isoconversional methods have emerged in the literature: methods that lead to a linear analysis and those which lead to a non-linear analysis.

(i) Differential isoconversional methods

These types of isoconversional methods do not make any approximation of the temperature integral. These procedures were first derived by Friedman (1964) by taking the logarithm of equation (3.2-1):

Eq. 3.2-21
$$\ln\left(\frac{d\alpha}{dt}\right) = \ln A\, g(\alpha) - \frac{E}{RT_\alpha}$$

Where T_α is the temperature at a particular conversion α. The activation energy is easily calculated from the slope of $ln(d\alpha/dt)$ versus $1/RT_\alpha$.; whereas the pre-exponential factor may only be derived by assigning a kinetic model function $g(\alpha)$. These methods are not reliable as they use instantaneous rate values $d\alpha/dT$, which are sensitive to experimental noise, and therefore are numerically unstable.

(i) Integral isoconversional methods

These methods make use of multiple-heating rate so that equation (3.2-7) is rewritten as:

Eq. 3.2-22
$$\beta = \frac{AE}{F(\alpha)R}\, p(x)$$

For various heating rates, the temperature T_α is measured at a fixed conversion α. A $p(x)$ function is selected, which lead to a linear equation. The two well known

isoconversional methods of this type include the analysis of Kissinger (1957) which can be derived by using the the *p(x)* function of Coats and Redfern (1964):

Eq. 3.2-23

$$\ln\frac{\beta}{T_\alpha^2} = -\frac{E}{RT_\alpha} + C_1$$

The other method is that of Ozawa (1965) and Flynn-Wall (1966), derived by using the *p(x)* function of Doyle (1962):

Eq. 3.2-24

$$\ln\beta = -1.052\frac{E}{RT_\alpha} + C_2$$

C_1 and C_2 are positive constants which include both the kinetic model function $g(\alpha)$ and the pre-exponential factor A. The activation energy alone is determined in these methods, from the slope of the plot of $ln\ (\beta/\ T^2_\alpha)$ versus $1/RT_\alpha$, for the Kissinger method, and plot of $ln\ \beta$ versus $1.052/RT_\alpha$ for the Ozawa-Flynn-Wall method.

(ii) Advanced isoconversional methods

Integral isoconversional methods may systematically give rise to an erroneous activation energy value, if the latter changes with the extent of conversion α. For this reason, Vyazovkin and Dollimore (1996) implemented a non-linear isoconversional method which takes into account the variation of activation energy with the extent of conversion α. In their analysis, the temperature integral is denoted $I(E_\alpha, T_{\alpha,i})$, and evaluated by using the Senum and Yang (1977) approximate function. Experiments are then performed at different heating rates β_i $(i = 1,...n)$. By assuming that the activation energy E is independent of the heating rate and the kinetic model, they derived the following based on equation (3.2-22):

Eq. 3.2-25

$$\frac{I(E_\alpha, T_{\alpha,1})}{\beta_1} = \frac{I(E_\alpha, T_{\alpha,2})}{\beta_2} = \ldots = \frac{I(E_\alpha, T_{\alpha,n})}{\beta_n}$$

By substituting experimental values of T_α and β, the true activation energy E of the process is derived subject to the following condition:

Eq. 3.2-26
$$\sum_{i}^{n}\sum_{j\neq i}^{n}\left[\frac{I(E_\alpha,T_{\alpha,i})\beta_j}{I(E_\alpha,T_{\alpha,j})\beta_i}\right]=\min$$

Although, other non-linear isoconversional methods have been derived (Li and Tang 1999; Sewry and Brown 2002; Budrugeac and Segal 2004), this one is probably the most popular (Starink 2003; Simon 2004). However, these methods are complex and too time-consuming to justify their application in kinetic studies.

3.3 Proposed Kinetic Model Analysis

3.3.1 Analytical Method Selection

The choice between isoconversional and model-fitting kinetics is very important in non-isothermal analysis studies. Model-fitting methods are very attractive as the kinetic parameters are obtained from a single experimental thermogravimetric run. However, these reactivity parameters largely depend on the heating rate, as the kinetic model may vary with the rate of heating. This consequence results from mass and heat transfer effects operating at different heating rates, as discussed in section 2.4.3. This complexity, however, is not taken into account in the formulation of the reaction rate equation.

Modern thermal analyses have therefore recommended the use of isoconversional methods (Vyazovkin and Dollimore 1996; Brown 2001; Vyazovkin 2001a). According to these researchers, isoconversional methods are sufficiently flexible to allow for a change in mechanism during the course of the reaction. Hence, these methods are particularly interesting for processes of unknown, complicated or multistep reaction mechanism, which cannot be characterised by a simple kinetic model. In addition, these authors have suggested that the use of multiple heating rates considerably reduces mass and heat transfer effects.

Nonetheless, integral isoconversional methods only apply to processes for which the activation energy is independent of the conversion α. For complex reaction mechanisms, these procedures generate activation energy values which depend on

the extent of conversion α (Vyazovkin and Sbirrazzuoli 2003). Non-linear isoconversional methods, on the other hand, are far too complex to justify their use in industrial applications (Sewry and Brown 2002), and appear to be very sensitive to experimental noise (Orfao and Martins 2002).

For these reasons, this project seeks to develop an enhanced model-fitting method. Firstly, the mechanism of the reaction is scrutinised, so that a single kinetic model may be defined for a specific rate-controlling mechanism, instead of the overall decomposition reaction, as considered by existing model-fitting methods. Secondly, an appropriate heating rate is identified as suggested in section 2.4.3, in order to minimise thermal effects induced in the sample at various rate of heating.

3.3.2 p(x) – Function

Although the function $p(x)$ has no closed form, 'exact' values may be found by numerical integration, in order to evaluate the accuracy of the different approximate functions $p(x)$ described in section 3.2.1. The 'exact' values of the temperature integral are calculated using the trapezoidal rule with a step size of 0.01, adapted on a MATLAB program (Appendix B). The relative percentage deviation of these $p(x)$ approximations is given in Table 3.3.1 for various values of x. As can be seen in the table, these computed errors are similar to those presented in the literature for similar $p(x)$ functions (Flynn 1997; Tang *et al.* 2003). The function from Senum and Yang (1977) appears to be the most accurate; whereas, Doyle's (1962) approximation presents the largest deviation. The other approximate functions are reasonably accurate with deviations less than 1% for $x > 20$. This error is sufficiently negligible compared to those introduced by other factors (experimental or human errors). Hence, there is no apparent benefit from employing the complex algorithms from Senum and Yang to calculate the activation parameters.

In addition, approximations derived from an integrated expression appear to be more accurate than those derived from expansion series. However, the error first decreases and then increases with x. Coats-Redfern (1964) and Gorbachev (1975)

functions, on the other hand, converge towards a smaller error with increasing x. As the mathematical expression of the $p(x)$ function of Gorbachev may not be valid for large values of x, Coats and Redfern approximation emerges as the most adequate for this study.

3.3.3 Kinetic Model

The most common reaction models for char oxidation systems were presented in section 2.8. It appears that both the shrinking core and progressive conversion models are not sufficiently accurate for describing char oxidation. The random pore model, on the other hand, has successfully been used in char oxidation kinetics. However, this model is rather complex as discussed in 2.8.4. In fact, this model attempts to incorporate structural changes involved during char oxidation, when these changes are not completely known. For these reasons, many investigators have opted for simpler kinetic models that capture the complexity of the reaction in a tractable mathematical manner. Such kinetic models consist of global reaction or volumetric reaction models, as described in 2.8.5. In this way, char oxidation is assumed to take place all over the volume of the porous solid particle. Global kinetic models have extensively been used in the literature for char oxidation studies (Walker Jr 1959; Smith 1982; Smoot and Smith 1985; Van Krevelen 1993), and the reaction rate is given as in equation (2.8-3):

$$\frac{d\alpha}{dt} = k(1-\alpha)^n$$

Olofson (1980) has shown that, in the chemical control regime, carbon reacts with oxygen following a single-step decomposition to produce carbon dioxide. In other words, the reaction is first order kinetics with respect to carbon, and the kinetic model expression is given as:

Eq. 3.3-1 $$g(\alpha) = (1-\alpha)$$

And the rate equation may be rewritten as

Eq. 3.3-2

$$\frac{d\alpha}{dt} = k(1-\alpha)$$

Many researchers have also applied this first order kinetic function, amongst them are Zimbardi (2000) and Hu *et al.* (2001), and more recently, He *et al.* (2002) and Hecker *et al.* (2003). Nonetheless, they did not always verify that this kinetic model was valid for the entire temperature range of oxidation. This verification process is important, since the reaction mechanism changes during the course of the reaction. In this study, however, this first order kinetic model is presumed for a single reaction step in the decomposition of the carbon, within the chemical regime. As demonstrated by Li and Brown (2001) the different reaction steps in char oxidation can easily be segregated by a deconvolution process. They identified the first reaction step to be the direct production of CO and CO_2; whereas, the second reaction step consisted of secondary reactions involving either water, CO or oxygenated complexes. These observations were discussed in section 2.7.3. Hence, the present investigation will only identify the first reaction step, as being valid for a first order kinetic model within the chemical control regime. For this purpose, the temperature interval for the analysis will be clearly identified to account for:

(i) *Temperature boundary for kinetic control.*

(ii) *Temperature boundary for first reaction step kinetics.*

The first condition is established through an Arrhenius plot, as discussed in section 2.7.4. The second condition will be established by means of deconvolution analysis, and will be illustrated in the next chapter.

Table 3.3.1: Relative percentage error between the 'exact' value of the temperature integral calculated from the trapezoidal rule and some approximate p(x) functions, at various x.

x	Doyle 1962	Coats-Redfern 1964	Gorbatchev 1975	Senum-Yang 1977	Starink 1.95 1996	Starink 1.92 2003	Tang et al. 2003
5	-87.3722	-18.8581	-3.4025	-0.0031	15.8732	12.1436	9.0243
10	-65.8649	-5.1769	-1.226	-0.0013	5.1392	3.4784	2.0503
15	-43.7327	-2.3965	-0.63	-0.0011	1.9433	1.1554	0.4624
20	-24.9539	-1.3797	-0.3835	-0.001	0.6274	0.3131	0.0289
25	-11.119	-0.8965	-0.2581	-0.001	0.032	-0.0114	-0.0548
30	-2.4617	-0.6293	-0.1857	-0.0009	-0.2258	-0.1223	-0.029
35	1.4975	-0.4661	-0.1401	-0.0009	-0.306	-0.1403	0.0185
40	1.5574	-0.3592	-0.1095	-0.0009	-0.2857	-0.1194	0.0526
45	-1.3971	-0.2853	-0.088	-0.0009	-0.206	-0.0862	0.0592
50	-6.5231	-0.2322	-0.0723	-0.0009	-0.0901	-0.054	0.0331
55	-13.0833	-0.1926	-0.0605	-0.0009	0.048	-0.03	-0.0265
60	-20.4699	-0.1624	-0.0514	-0.0009	0.1995	-0.0176	-0.1188
65	-28.2055	-0.1388	-0.0442	-0.0009	0.3589	-0.0186	-0.2418
70	-35.9319	-0.1201	-0.0385	-0.0009	0.5225	-0.0334	-0.3936

3.4 Analysis Method and Assessment

3.4.1 Reactivity Model Equation

Since the kinetic model $g(\alpha)$ has been identified, the integral form is given as:

Eq. 3.4-1
$$F(\alpha) = \int_0^{\alpha} \frac{d\alpha}{(1-\alpha)} = -\ln(1-\alpha)$$

Hence the reactivity model equation (3.2-7) may be rewritten as

Eq. 3.4-2
$$-\ln(1-\alpha) = \frac{AE}{\beta R} p(x)$$

The $p(x)$ function of Coats and Redfern is then introduced to evaluate the temperature integral:

Eq. 3.4-3
$$-\ln(1-\alpha) = \frac{AE}{\beta R} \frac{e^{-x}}{x^2}\left(1-\frac{2}{x}\right)$$

Substituting for x = E/RT and taking the logarithm yields:

Eq. 3.4-4
$$\ln\left(-\frac{\ln(1-\alpha)}{T^2}\right) = \ln\left(\frac{AR}{\beta E}\left(1-\frac{2RT}{E}\right)\right) - E/RT$$

Since for a vast majority of solid-state reactions $15 < x < 60$ (Coats and Redfern 1964), thus E/RT >>2, so that the above equation reduces to:

Eq. 3.4-5
$$\ln\left(-\frac{\ln(1-\alpha)}{T^2}\right) = \ln\left(\frac{AR}{\beta E}\right) - E/RT$$

Thus, the activation energy E and pre-exponential factor A, may be obtained from the slope and intercept respectively, of the plot of the right hand side versus $1/RT$.

3.4.2 Heating Rate Selection

Selection of a suitable heating rate is based on the assumption that the presumed kinetic model is valid. In this way, there should exist an optimum-heating rate (or a range of heating rates) at which this kinetic model function is verified. The

derived kinetic parameters E and A can therefore be used to generate the original experimental decomposition curve of the char. These kinetic parameters are deduced from equation (3.4-5) for various heating rates β_i. The experimental weight loss curve may be simulated following the rate equation (3.2-2) for a first order kinetics:

Eq. 3.4-6
$$\frac{d\alpha_{calc}}{dT} = (1-\alpha_{calc})\frac{A}{\beta_i}\exp\left(-E/RT\right)$$

Where α_{calc} is the unknown fractional carbon conversion in this equation. Using the modified Coats-Redfern approximation, simulated weight loss profiles $(1-\alpha_{calc})$ are generated by integration of equation (3.4-6):

Eq. 3.4-7
$$(1-\alpha_{calc}) = -\frac{ART^2}{\beta_i E}\exp\left(-E/RT\right)$$

It should be expected that the experimental weight loss profile $(1-\alpha)$ and the simulated one $(1-\alpha_{calc})$ would not always correspond exactly, at any heating rates. For inappropriate heating rates, the reactivity parameters E and A are not correct, and therefore they cannot reproduce the experimental weight loss profile exactly. At the appropriate heating rate, however, there should be a good fit between the experimental and the simulated profiles. This goodness of fit may be characterised by a standard deviation in the conversion α. This error σ is defined over the predefined temperature range T_r, for an individual heating rate curve:

Eq. 3.4-8
$$\sigma(\beta, T_r) = \sqrt{\frac{\sum_{i=0}^{n}(\alpha-\alpha_{calc})^2}{n}}$$

Where n is the number of experimental data in the temperature range T_r. However, reactions occurring at higher heating rates take less time to reach the upper boundary temperature in the range T_r. Thus, a systematic smaller error σ is generated. For this reason, a similar error σ must be computed over an equivalent time interval t_r:

Eq. 3.4-9
$$\sigma(\beta,t_r)=\sqrt{\frac{\sum_{i=0}^{m}(\alpha-\alpha_{calc})^2}{m}}$$

In this case, m is the number of experimental data in the time rang t_r. The total residual error $\sigma(\beta)$ is finally computed as the average from these two as:

Eq. 3.4-10
$$\sigma(\beta)=\frac{1}{2}[\sigma(\beta,T_r)+\sigma(\beta,t_r)]$$

The minimum error $\sigma(\beta)$ is therefore identified at the optimum heating rate β. At the same time, a sufficiently low minimum error indicates that the presumed kinetic function $F(\alpha)$ is consistent with the chemical reaction process. In other words, at this optimum heating rate, the derived reactivity parameters E and A must correspond to the true kinetic parameters of the process. It is important, nonetheless that the range of heating rates covered must be sufficiently broad to enable accurate determination of this optimum-heating rate.

3.4.3 Reactivity Model Testing

In order to evaluate the accuracy of the proposed kinetic analysis method, a series of tests are necessary. Firstly, the proposed analysis implies that kinetic parameters may be derived from a single heating rate experiment, if the appropriate rate of heating is selected. Hence, the derived kinetic parameters at this heating rate must correspond to those derived using isoconversional methods. These methods, in fact, do not make any assumption on the kinetic model, and provide accurate values for the activation energy. In addition, isothermal techniques are very accurate in estimating both the activation energy E and the pre-exponential factor A. Hence, these two conventional analyses will also be carried out to evaluate the validity of the proposed model-fitting kinetic. Secondly, the underlying assumptions of this novel kinetic approach will be verified by performing a sensitivity analysis. This analysis will aim at establishing whether the selected kinetic model is the most appropriate for coal char oxidation.

Chapter 4

Experimental Details

4.1 Introduction

The present chapter deals with the experimental details undertaken to apply the novel kinetic analysis established in Chapter 3. This chapter is divided in four sections. The first section presents the coal chars selected in this investigation. The second section discusses the method used to prepare the chars and assess some of their physical properties. These characterisation techniques were performed on the chars in order to establish a link with their oxidative reactivity. The third and main section of this chapter describes the thermogravimetric equipment, the experimental set-up and the procedure for carrying out char oxidation experiments. The fourth section deals with the analysis of the experimental data, in order to accurately evaluate the intrinsic reactivity of each char. This final section outlines how to correctly determine the temperature range for kinetic control of the principal chemical reaction. That is, the proposed reactivity analysis is based on modelling the production of CO_2 within the chemical control regime.

4.2 Materials Selection

Eight different types of coal, ranging from anthracite to subbituminous, were selected for this study. In addition, a commercial activated carbon BPL was studied in two distinct particle sizes. This material is derived from bituminous coal and manufactured by Calgon Carbon Ltd (United States). It was selected as a suitable char model, in the development of the new analysis method, as it embraces all different types of coal derived chars. In fact, an activated carbon may be considered as a 'perfect' char, since it is highly homogeneous with a high degree of purity.

The selected industrial coals were provided by Mitsui Babcock Energy Ltd, and Corus UK Ltd. Both companies are based in the United Kingdom. The first one supplied a selection of six industrial coals, from anthracite to subbituminous, as representative samples of coals normally used in boiler power stations. These coals originate from various worldwide locations, and thus they are named after the seam in which they are extracted: Pha Lai (Vietnam), Heze (China), Chang Cun (China), Kellingley (UK), Colombian coal (Colombia) and Power River Basin (or PRB from the United States). Corus UK Ltd, on the other hand, supplied two coals representative of samples normally used in the steel making industry. These two coals are denoted EC2106 (Australia) and EC2038 (United States).

A summary of properties for all these coals is given in Table 4.2.1 and Table 4.2.2. These data include a proximate analysis supplied by the company and verified through carbonisation and oxidation reactions as described in the subsequent sections. In addition, an ultimate analysis performed on the coals by the suppliers is also provided in the table. From these analyses, a coal classification (ASTM D 388 1984) was deduced and is presented in Table 4.2.3, together with other measurements undertaken on the coal chars. These measurements include the total internal and microporous surface area, and also the particle size distribution. Surface areas were measured by means of volumetric adsorption, and particle size was determined by scanning electron microscopy and laboratory test sieving, as detailed in the next sections.

Table 4.2.1: Proximate analysis (moisture free) as supplied by the manufacturers and industries.

Coal samples	Volatile matter (wt %)	Fixed carbon (wt%)	Ash level (wt %)	Calorific value (MJ/kg)
BPL granules	0.0	91.8	8.2	-
BPL crushed	0.0	91.8	8.2	-
Pha Lai	6.1	62.5	31.5	33.9
Heze	10.1	58.2	31.7	34.8
Chang Cun	12.2	70.8	17.0	35.8
Kellingley	31.4	51.1	17.5	34.5
Colombian coal	34.8	54.0	11.2	32.7
PRB	43.6	49.2	7.2	29.5
EC 2106	27.0	62.6	10.4	-
EC 2038	17.2	76.9	5.9	-

Table 4.2.2: Ultimate analysis data supplied by Mitsui Babcock Energy Ltd: corrected for ash and moisture free

Coal samples	C (wt %)	H (wt %)	N (wt %)	S (wt %)
BPL granules	-	-	-	-
BPL crushed	-	-	-	-
Pha Lai	91.6	3.9	1.1	0.6
Heze	89.0	6.4	1.4	2.2
Chang Cun	90.6	4.9	1.5	0.5
Kellingley	82.4	8.3	1.8	2.3
Colombian coal	81.5	6.1	1.7	0.9
PRB	73.8	5.3	0.9	0.2
EC 2106	-	-	-	-
EC 2038	-	-	-	-

Table 4.2.3: ASTM Classification of the received coals, and measured physical properties of the produced chars.

Char sample	ASTM Coal Classification	Internal surface area ($m^2 g^{-1}$)	Microporous surface area ($m^2 g^{-1}$)	Particle size (μm)
BPL granules	Bituminous derived	1074 ± 21	580	1, 000 - 4, 000
BPL crushed	Bituminous derived	1071 ± 21	1057	< 75
Pha Lai	Anthracite	35 ± 1	115	< 75
Heze coal	Semianthracite	94 ± 2	156	< 75
Chang Cun	Semianthracite	105 ± 3	217	< 75
Kellingley	Bituminous (hva)	148 ± 3	207	< 75
Colombian char	Bituminous (hva)	252 ± 5	235	< 75
PRB	Subbituminous (hvc)	265 ± 4	414	< 75
EC 2106	Bituminous (hva)	7 ± 1	29	500 - 1, 000
EC 2038	Bituminous (lvb)	29 ± 1	67	500 - 1, 000

4.3 Char Characterisation

4.3.1 Char Preparation

Chars were produced in a Carbolite CSF tube furnace, controlled by a Eurotherm Type 818 temperature controller. A diagram of the tube furnace is shown in Figure 4.3.1. A silica tube is contained within the furnace and enveloped by crucilite glow bars, which serve as heating elements. The temperature inside the furnace is accurately measured by a platinum and rhodium type S thermocouple, connected to the controller device. The experimental procedure involved loading approximately 5 g of samples onto an alumina dish and placing it on the silica tube inside the furnace. First, the system was purged with N_2 (99.99 % purity) at 1 bar for 2 hours. Then, the temperature was raised at a rate of 2 °C min^{-1} from 20 °C to 100 °C and left for 0.5 hour. This isothermal first stage was required to

ensure that all moisture evaporated and escaped from the vicinity of the sample. Heating was subsequently resumed at the same rate up to 900 °C and held at this temperature for 5 hours. This dwelling time ensured that most of the volatile matter was removed. On completion, the sample was allowed to cool down to room temperature (20 °C), and then removed and weighted. This procedure was repeated three times for each sample to ensure reproducibility of results. This char preparation was in accordance with a British Standard (BS 1016-104 1998) for the determination of volatile matter. The residual char consists of fixed carbon and mineral matter, so that the percentage of volatile matter (including moisture) is calculated as:

Eq. 4.3-1

$$Volatile\ matter = \frac{W_o - W_f}{W_o} \times 100$$

Where W_0 is the initial weight of coal, and W_f is the weight of the residual char. The moisture content may be calculated by measuring the weight of the sample at 100 °C during the isothermal stage. The ash content, on the other hand, is evaluated at the end of each char oxidation experiment.

4.3.2 Surface Area Determination

Both the total internal and microporous surface areas were measured by volumetric adsorption in a Micromeritics ASAP 2010 analyser (Accelerated Surface Area and Porosimetry). A schematic of the system is presented in Figure 4.3.2. Total surface area was measured under N_2 at −196 °C; whereas, microporous surface area was measured under CO_2 at 0 °C. The reason for this change in gas lies in that CO_2 is a smaller molecule (0.33nm) than N_2 (0.36nm), and therefore diffuses better into smaller pores. In addition, Dubinin and Stoeckli (1980) have shown that characterisation of micropore texture of carbon materials is more successfully determined by CO_2 adsorption. They concluded that the microporous surface area contains most of the active surface area, where the chemical reaction takes place. Furthermore, CO_2 gas has a higher critical temperature, allowing for a larger uptake of CO_2 at very low relative pressures, so

that the microporous part of the isotherm is obtained with a better accuracy than in N_2 adsorption at –196 °C (Rouquerol *et al.* 1999). The experimental procedure was similar with both adsorptive gases. This procedure involved weighting a minimum of 100 mg of the char sample and degassing it under vacuum at 150 °C. Degassing was completed when a residual pressure less than 0.04 Pa was reached. The sample container was then left to cool to room temperature (20 °C), and weighted again before being transferred to the analysis port of the adsorption apparatus. For adsorption measurements, the free space (or dead volume) of the sample flask was determined using helium. This gas was selected since it is not absorbed by carbon materials and has a low critical temperature (~ -268 °C). The sample was then outgassed prior to a series of adsorptions over an increasing range of pressures, where the sample flask is immersed in a bath to maintain constant temperature. Incremental doses of the adsorptive gas were injected into the sample flask. After each injection, the pressure was subsequently reduced and the system was allowed to equilibrate. Since the volume of injected gas and the dead volume of the sample flask are known, the amount of adsorbed gas can be calculated.

(i) Internal surface area

The internal surface area of the mesopores (pore diameter between 2 nm and 50nm), is accurately determined by the method of Brunauer – Emmet – Teller (BET) (Brunauer *et al.* 1938). As recommended by British Standards (BS 4359-1 1996), this method was applied in this study, for five points relative pressure in the range of 0.05 to 0.3, whilst the sample flask was immersed in liquid N_2 at – 196 °C. The BET theory was devised for multi-molecular layer systems. The theory assumes that the energy of adsorption is the same as the liquefaction energy for the second and subsequent layers, whilst the first layer has a characteristic energy of adsorption. By balancing the rates of evaporation and condensation of the various adsorbed layers, the BET equation is generally given as:

Eq. 4.3-2

$$\frac{p}{V\left(p^o - p\right)} = \frac{1}{V_m C} + \frac{C-1}{V_m C}\frac{p}{p^o}$$

Where, p is the relative pressure of adsorptive gas; p^o is the saturated vapour pressure of adsorptive gas; V is the amount of adsorbed gas per unit mass of solid; V_m is the monolayer adsorption capacity and C is a positive constant defining the interaction of the adsorbent-adsorbate force. Values of C and V_m are simultaneously deduced from the slope and intercept of the linear plot of $[(p/V)/(p^o-p)]$ versus (p/p^o). These values are shown in Table 4.3.1 for all the chars studied. As can be seen from the table, all C values are negative; suggesting that these chars are probably microporous, and thus the BET equation is not valid in this case. However, this BET surface area may be used as a comparative index between the chars. The specific surface of the char [m^2 g^{-1}] S_{BET}, is now calculated as:

Eq. 4.3-3

$$S_{BET} = \frac{\lambda_{N_2} V_m L}{V^o}$$

Where, λ_{N2} is the molecular cross-sectional area of N_2 equal to 0.162 nm^2 ; L is the Avogadro's number equal to 6.023 x 10^{23} mol^{-1} and; V^o is the molar volume of gas at standard conditions equal to 22.414 dm^3 [STP] mol^{-1}.

(ii) Microporous surface area

Dubinin's theory is certainly the most widely used in the characterisation of micropores texture by adsorption (Hutson and Yang 1997; Rouquerol *et al.* 1999). This theory is based on the concept of micropore filling as opposed to layer formation on the pores walls (Dubinin 1975). For porous materials he considered that micropores are space volumes, which fill up during adsorption instead of forming layers. In this way, the adsorptive gas is in a highly compressed liquid state, and trapped inside the micropore volume. From this concept, several equations have been developed (Dubinin and Stoeckli 1980), yet that of Dubinin and Radushkevich (1947) (DR equation) is the simplest version, which is incorporated in the ASAP 2010 software program:

Eq. 4.3-4

$$log(V) = log(V_0) - \frac{BT^2}{\theta}\left[log\frac{p^0}{p}\right]^2$$

Where, V_0 is the micropore volume capacity; B is a structural constant containing the characteristic adsorption energy E_0; θ is the affinity constant for CO_2 equal to 0.461 and; T is the analysis bath temperature equal to 0 °C. Since the volume V and pressure p are measured during the adsorption process, a straight line may be plotted for *log (V)* versus *[log* (p^0/p) *]*^{2}, from which B and V_0 are deduced from the slope and the intercept, respectively. The values of B and V_0 are given in Table 4.3.2. The microporous surface area of the char [m^2 g^{-1}] S_{DR}, is then calculated as:

Eq. 4.3-5

$$S_{DR} = \frac{\lambda_{CO_2} V_0 L}{V^o}$$

Where λ_{CO2} is the molecular cross sectional area of CO_2 gas equal to 0.170 nm^2.

4.3.3 Particle Size Estimation

Particle size distribution in each char sample was examined using a Jeol JSM-6310 scanning electron microscope (SEM). The suspended particles were carefully deposited onto an aluminium SEM specimen mount covered with carbon tape. This carbon tape enabled side and top views to be obtained. Once prepared, each specimen was successively placed in the SEM chamber, and signals were collected for the backscattered electrons. The accelerating voltage and current in the measurements were 15 keV and 12 nA, respectively. Representative particles from each specimen, with typical magnifications of 200X and 1000X, were photographed to obtain SEM images and determine particle size distribution. An example of these images for Pha lai char and BPL crushed are given in Appendix C. For the granular materials (BPL granules, EC2038 char and EC2106 char), the particle size was measured by means of a laboratory test sieve, with the desired aperture size.

Table 4.3.1: BET parameters V_m and C obtained from a five point analysis in N_2 for the different char samples.

Char samples	V_m, $cm^3\ g^{-1}$	C
BPL granules	246.7	-337.4
BPL crushed	246.1	-297.9
Pha Lai	7.9	-71.6
Heze coal	21.7	-73.9
Chang Cun	24.1	-70.9
Kellingley	33.9	-103.4
Colombian raw coal	57.91	-97.7
Powder River Basin (PRB)	60.9	-159.7
EC 2106	1.7	-29.6
EC 2038	6.7	-40.3

Table 4.3.2: DR parameters Vo and B obtained from adsorption isotherms in CO_2 of the different char samples.

Char samples	V_0, $cm^3\ g^{-1}$	E_0, $kJ\ mol^{-1}$
BPL granules	126.9	19.4
BPL crushed	294.2	11.6
Pha Lai	25.3	22.1
Heze coal	33.7	22.9
Chang Cun	47.5	23.4
Kellingley	45.4	22.9
Colombian raw coal	52.4	20.6
Powder River Basin (PRB)	90.7	22.9
EC 2106	6.3	20.3
EC 2038	14.7	21.7

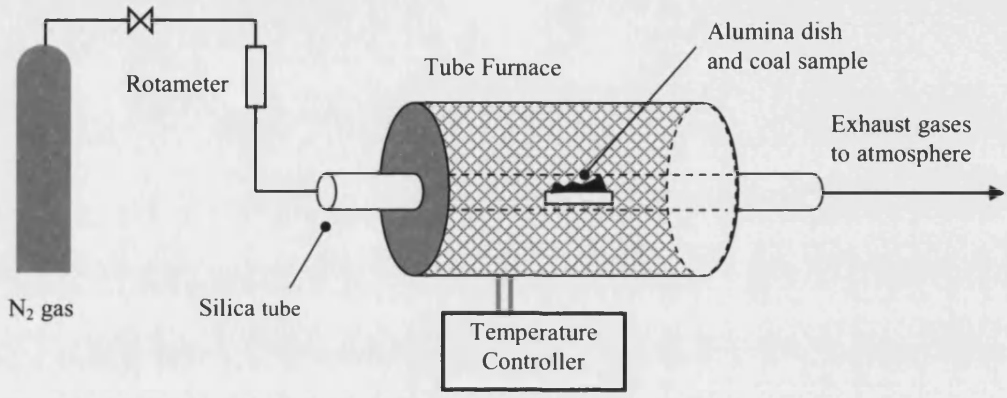

Figure 4.3.1: Schematic of the Carbolite CSF 15' tube furnace set up for the carbonisation of coals samples.

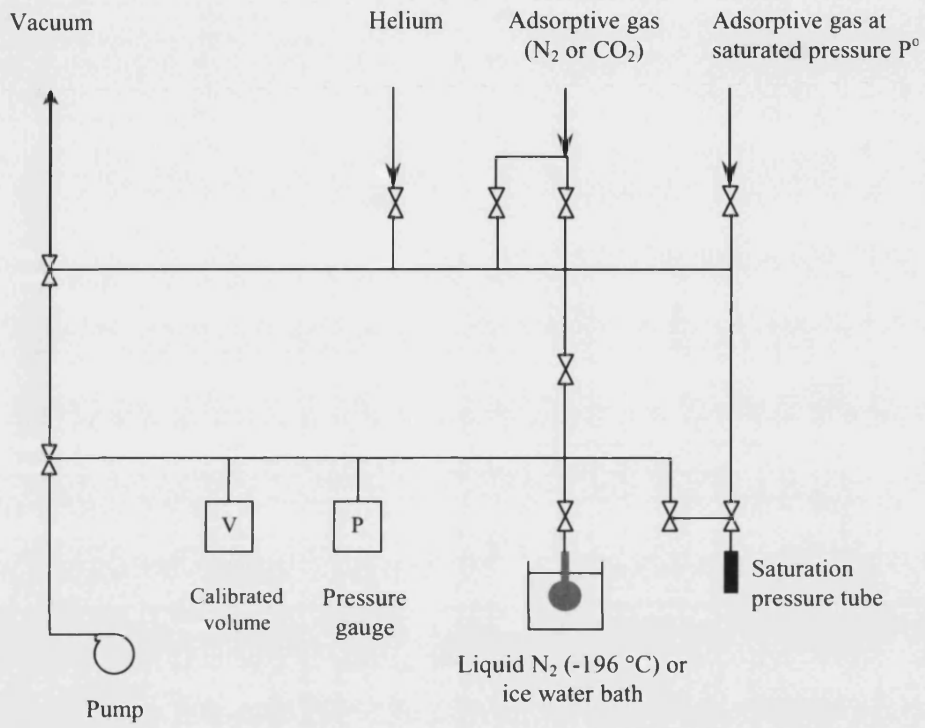

Figure 4.3.2: Schematic of the ASAP 2010 system for surface area analysis under either nitrogen or carbon dioxide.

4.4 Char Reactivity Measurement

4.4.1 The Thermogravimetric Analyser

Thermogravimetry analysis comprises methods that continuously measure the weight of a sample whilst the sample is subjected to a particular temperature programme. The thermogravimetric instrument used in this work is a Setaram TG 92, which consists of a microbalance, a temperature programmable furnace, and a CS 32 controller connected to a computer. These individual components are detailed in the next paragraphs. The experimental set up is presented in Figure 4.4.1.

(i) The microbalance

The microbalance is an electronic beam type, which revolves about a torsion strip. A source light is emitted through a sight glass and received by two photo resistances. This sight glass is attached to the beam balance and fixed with magnetic solenoids. As the weight of the balance changes, the sight glass moves, and partly blocks the path of the light. The intensity of this light received by the photo resistances is amplified, and a current is sent into the solenoids. These coils, subsequently, produce a magnetic force, which restores the balance to its null-point. The movement of the balance is a measure of the weight, which is proportional to the electromagnetic force and to the intensity of the current from the photo resistances. In this way, the sensitivity of the balance is very high, of the order of 0.03 μg. In addition, the balance is equipped with a counterweight pan which helps maintain the load on the balance constant.

(ii) The controller

The CS 32 controller manages and regulates the temperature programme in the furnace, according to sequences set by the operator. In addition, it controls the opening and closing of the gas valves, as well as the acquisition and digitalisation of the weight or thermogravimetric signals *TG* and the temperature *T*. At the

same time, it instantaneously calculates the first derivative of the thermogravimetric signal *dTG*. Through a series of interface, these digitalised signals are then transferred to the computer.

(iii) The furnace

The non-inductively wound TG 92 furnace is mounted vertically and fitted with a graphite tube in the centre line. In this way, the furnace can sustain temperature from ambient to 1750 °C. The graphite-heating element is insulated with a tubular screen and a graphite felt, in order to avoid interactions with the sample. The reacting gas is introduced from the top of the furnace, the argon gas is passed through the heating envelope to prevent the graphite element from corroding, as shown in Figure 4.4.1. In addition, this cylindrical furnace is cooled by water circulating through the system. The temperature inside the furnace is measured by a type S thermocouple made of platinum and rhodium (Pt/Pt Rh 10%). As illustrated in the schematic of the furnace in Figure 4.4.2, this thermocouple is located 6 mm from the crucible, so that the measured furnace temperature is very close to that of the sample. Nonetheless, it is possible that the sample temperature may not correspond exactly to that of the furnace. This temperature difference, however, was corrected through temperature calibration of the furnace, as discussed in the next section.

4.4.2 System Calibrations

(i) Weight change calibration

Weight change calibration of the thermobalance was performed by measuring the weight loss of calcium carbonate $CaCO_3$ (99% purity) upon heating in nitrogen (99.99% purity) at 20 °C min^{-1}. The decomposition reaction is as follows:

$$CaCO_3 \rightarrow CaO + CO_2$$

When heating 35.4 mg of $CaCO_3$ in the TGA, 19.8 mg of CaO should be produced, in theory. However, the thermobalance measured a 20.1 mg production

of CaO, as revealed by Figure 4.4.3. Thus there is an overall error of 0.3 mg, which corresponds to less than 1.8% of the weight change. Measurement of the absolute weight was calibrated by means of standard steel balls of 5 mg, 10 mg and 15 mg, supplied by the manufacturers of the TGA.

(ii) Furnace Temperature Check

The temperature measured by the thermocouple was verified in order to assess the difference with the actual temperature of the sample T_s. The melting point of four pure metals was measured, including: indium, lead and copper. An empty crucible was suspended to the metal inside the furnace, and the temperature was raised at 20 °C min^{-1} in flowing nitrogen at 25 ml[STP]min^{-1}. As the melting point of the metal was reached, it subsequently broke and the crucible fell down, so that an apparent mass loss was observed, as shown in Figure 4.4.4. This experimental melting point temperature was compared to a theoretical value given in Perry and Green (1997). These values are given in Table 4.4.1, where it can be seen that both the experimental and actual temperatures coincide with a negligible maximum error of 2 °C.

(ii) Buoyancy correction

As dry air flows in the vicinity of the sample, a buoyancy force is exerted on the sample. This force causes an apparent mass gain m, which may be calculated by the ideal gas law as:

Eq. 4.4-1
$$m = M_r \frac{PV}{RT}$$

Where M_r is the relative molecular mass of air at standard conditions equal to 29 g mol^{-1}; V is the volume of the sample; P is the pressure of the air. Since this buoyancy force decreases with increasing temperature, the maximum force is exerted at room temperature (25 °C), with a maximum sample load in the crucible (V = 170 µl):

$$m = \frac{29g}{mol} \times \frac{10^{-5} Pa \times \left(170 \times 10^{-6} m^3\right)}{8.314 J/mol/K \times 298K} = 1.99 \times 10^{-11} g$$

Thus, the maximum buoyancy mass represents 6.6 x 10^{-8} % of the sample weight (based on a 30 mg sample). Hence, this buoyancy effect is negligible. In addition, buoyancy effects induced by an empty sample were corrected by subtracting the effects of blank runs (empty sample holder).

4.4.3 Experimental Procedure

For linear thermogravimetric analysis, experiments were performed at heating rates of 1, 5, 10, 15, 20, 30 and 50 °C min^{-1}, whilst the sample was heated from 20 °C to 900 °C. This temperature programme is easily inputted in the computer software of the TGA. First, an empty 170 µl crucible was loaded onto the balance which was then set to zero. Then, approximately 30 mg of char was placed into the crucible, and this initial weight was inserted into the recording software programme. The crucible was made from alumina and hence does not react with carbonaceous materials. The oxidation process subsequently started under dry air (20-v % O_2 and 80-v % N_2) flowing at 25 ml[STP]min^{-1}. During the oxidation process, the weight of the char and the temperature of the sample were recorded every second. The experiment was stopped when the recorded weight remained unchanged, indicating suggesting that all the char had oxidised leaving behind ash residue. Each experiment was repeated two or three times for repeatability purposes.

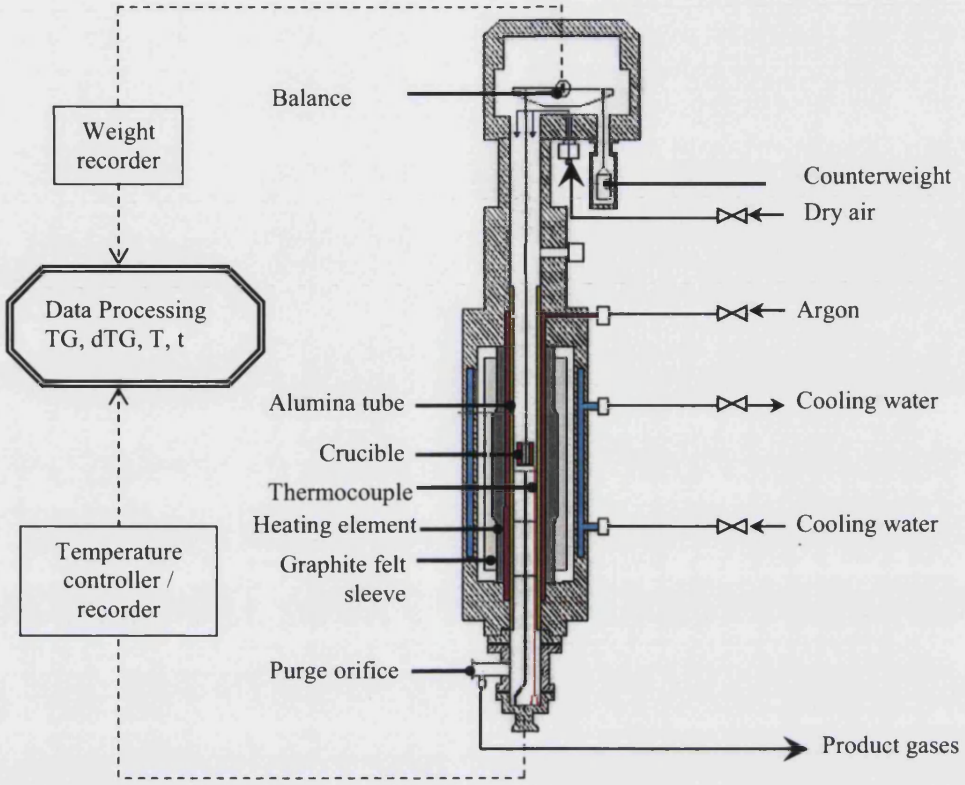

Figure 4.4.1: Experimental set up of the Setaram TG 92 furnace (adapted from Setaram Setsys Evolution model brochure): Thermogravimetric or weight signal TG; Temperature T; first derivative of weight signal dTG.

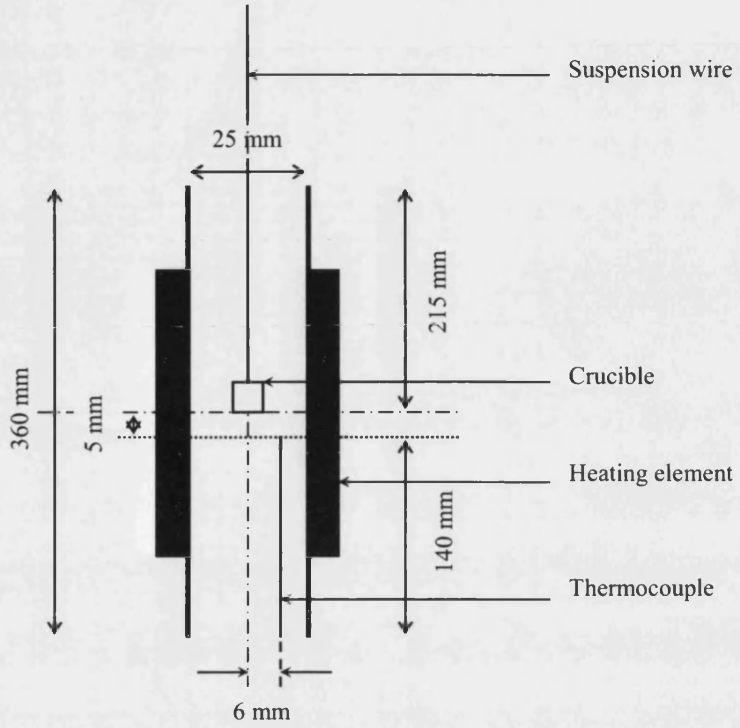

Figure 4.4.2: Schematic diagram of the Setaram TG 92 furnace

Table 4.4.1: Comparison of the experimentally observed melting point temperature and the actual melting point of different metals tested in the TG 92 furnace.

Temperature	Indium	Lead	Copper
Experimental (°C)	156	325	1081
Literature (°C)	157	327	1083

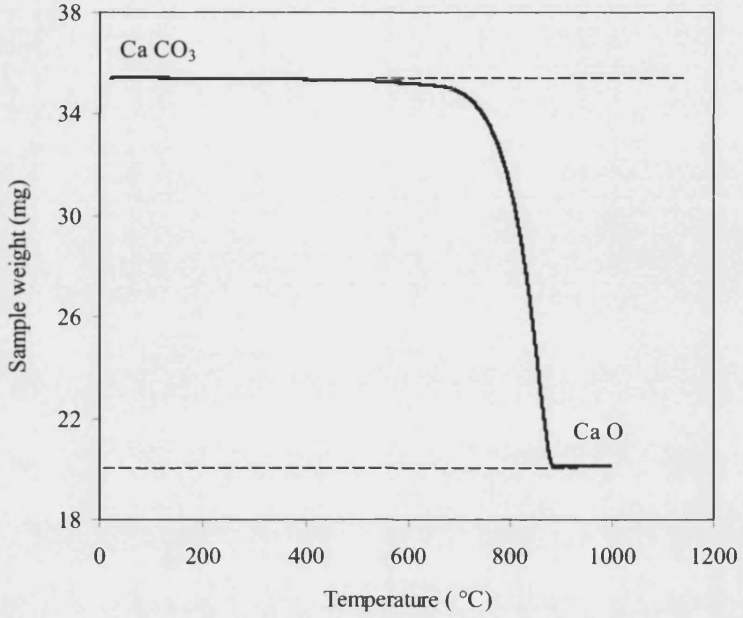

Figure 4.4.3: Weight change of $CaCO_3$ heated in nitrogen (99.99% purity) at 20 °C min^{-1}.

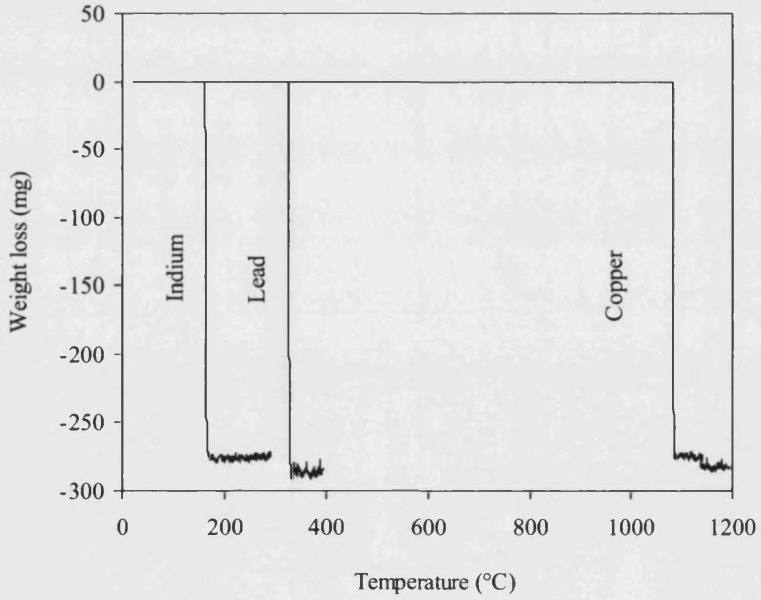

Figure 4.4.4: Experimental melting point temperatures of various metals heated in pure nitrogen at a rate of 20 °C min^{-1}.

4.5 Data Analysis

4.5.1 Reaction Zones

At the end of each experiment, a data file is generated, containing recorded values of weight and temperature as a function of time and the in-built calculation of the derivative of the thermogravimetric curve. An example of a real data series is illustrated in Figure 4.5.1 for the variation of temperature with time at a heating rate of 5 °C min^{-1}. The recorded weight and weight change rate profiles are presented in Figure 4.5.2. It appears from the figure that the oxidation reaction starts at around 413 °C, and is completed as the dTG values reaches zero around 754 °C. This main reaction zone has been highlighted and corresponds to the region used for the kinetic analysis proposed in Chapter 3.

4.5.2 Intrinsic Reactivity Zone

As discussed in section 2.7.4, the chemical reaction may be limited by the kinetics of the reaction, pore diffusion and external diffusion of the reacting gas. Since the present analysis is concerned with intrinsic reactivity data, it is important to perform the analysis within the chemical control regime. This regime may be identified as described in section 2.7.4, by means of an Arrhenius plot of *ln [(1/w) dw/dt]* versus *1/T*. These plots may be obtained for slow oxidation (at 5 °C min^{-1}), in order to accurately determine the maximum temperature for kinetic control. As an example, the reaction zone identified in Figure 4.5.2 is now analysed in the range of 5 to 95-wt% char conversion. The remaining 5-wt% char towards the end of the oxidation process, essentially consists of ash and therefore may be ignored in the analysis. In fact, Russell *et al.* (1998) pointed out that only the first 50% conversion of carbon may be representative of the whole sample, whereas the very first 5% conversion may include desorption of chemisorbed species. The subsequent Arrhenius plot for this oxidation profile is given in Figure 4.5.3. The figure presents two distinct gradients, indicating that two different mechanisms operate in this temperature range. In fact, these two rate-

controlling mechanisms correspond to kinetic control and internal pore diffusion. These two zones are determined by examining the slope of the overall straight line. The point at which this straight line begins to curve is identified as the end of the first controlling zone. This point is indicated by a maximum correlation coefficient $r^2 \leq 0.990$. As shown in the figure, the overall straight line curves after a temperature of 606 °C ($10^3/T$ = 1.65 °C $^{-1}$). At this temperature, the optimum correlation coefficient is equal to 0.995 and decreases considerably beyond this temperature. Thus kinetic control is assumed for temperature below 606 °C during air oxidation of granular BPL; whereas, between 606 and 700 °C, the reaction is essential controlled by diffusion through the porous structure.

4.5.3 Individual Reactions

As discussed in section 2.7.3, char oxidation proceeds via three main reaction steps. These individual reaction steps may be separated by means of deconvolution, as suggested by Katsikas and Popovic (2003). This technique provides a higher resolution of the dTG curve by multi peak fitting using a Gaussian type function. This procedure was conducted through the computer program Origin 6.1® to identify the three reactions. Other researchers have also used this method to separate consecutive reactions in coal or polymer studies (Kim *et al.* 2004; Arenillas *et al.* 2004b). As an example, a deconvolution procedure was applied to the dTG curve in Figure 4.5.2, the goodness of fit of the overall Gaussian function is measured by the correlation coefficient $r^2 > 0.990$. The individual peak reactions are shown in Figure 4.5.4. Reaction I prevails for temperatures below 617 °C, then, both Reactions II and III dominate the overall oxidation process. For kinetic modelling of Reaction I, this temperature emerges as the maximum analysis temperature for the oxidation of granular BPL in air. However, chemical control regime was found to take place up to 600 °C. Thus, the kinetic analysis of granular BPL is performed with experimental data obtained at temperatures below 600 °C, in order to ensure full kinetic control of the primary chemical reaction. A similar analysis was undertaken for all the remaining coal char samples.

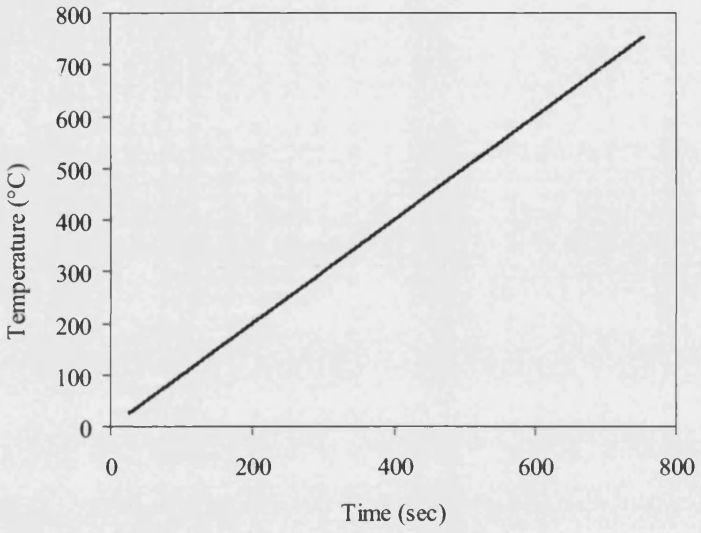

Figure 4.5.1: Relation between heating time and temperature for the oxidation of granular BPL in air at 5 °C min $^{-1}$

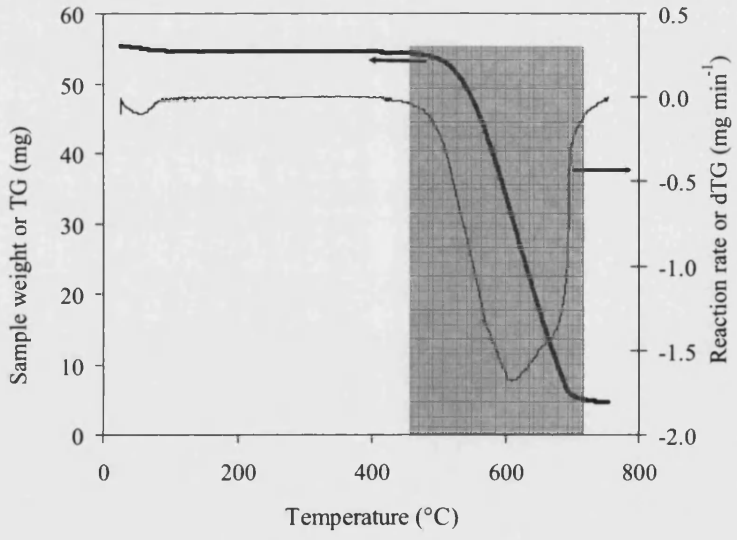

Figure 4.5.2: Weight loss (**—**) and reaction rate (—) profiles of the oxidation of BPL carbon in air at 5 °C min $^{-1}$: the shaded region represents the reaction zone of interest for the kinetic analysis.

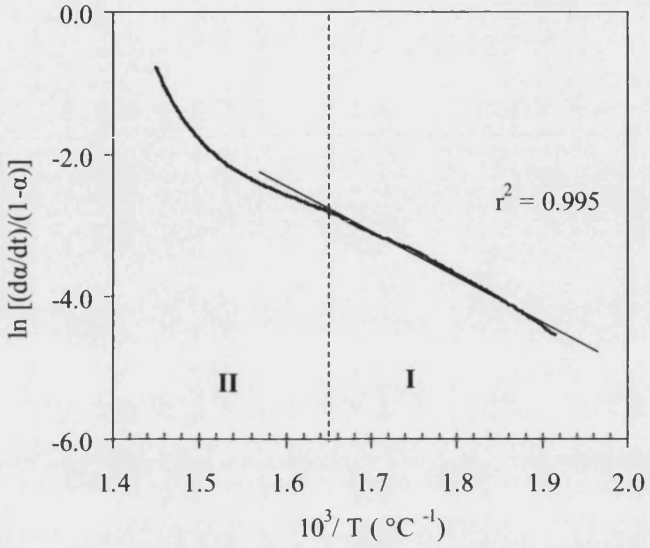

Figure 4.5.3: Rate-controlling regimes for the oxidation of granular BPL carbon in air at 5 °C min $^{-1}$.

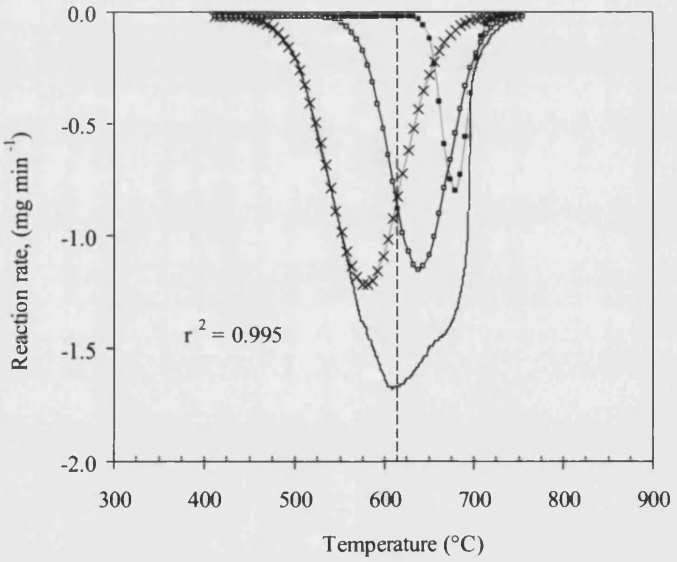

Figure 4.5.4: Gaussian deconvolution of the main dTG curve (–) of the oxidation in air at 5 °C min $^{-1}$ of granular BPL carbon into its individual reactions: (+) reaction I C + O_2 → CO_2; (□) reaction II C + ½ O_2 → CO and; (■) reaction III CO* + ½ O_2 → CO_2.

Chapter 5

Experimental Results

5.1 Introduction

This chapter presents the results of the linear heating rate analysis method developed in Chapter 3. The experiments were conducted according to the method described in Chapter 4. These results are organised in four sections. First, the oxidation profiles of the chars are examined, in order to investigate the various effects of experimental conditions on thermogravimetric data. The second part deals with a study of the kinetic control regime for all the chars, and determination of maximum temperature for the validity of the proposed kinetic analysis. In the third and fourth section, the reactivity parameters derived by this novel kinetic analysis are reported and evaluated for identifying an optimum rate of heating. Due to the large number of figures generated during the experimental runs, similar trends and salient features of the figures are presented for some samples only. These figures have been included at the end of each section for clarity. An additional discussion of these results is presented in Chapter 6, highlighting the key results, together with some suggestions for further research work.

5.2 Oxidation Profile Characteristics

5.2.1 Heating Rate Effect

The expected effects of the rate of heating, as described in section 2.4.3, were observed during the oxidation of all the chars. As an example, the oxidation profile of granular BPL at different heating rates is shown in Figure 5.2.1. These curves represent mean data from experiments reproduced twice or three times and showing good reproducibility. It is clear from the figure that the heating rate influences the shape of the thermogravimetric curve and the temperature interval of the reaction. In fact, the increase in rate of heating led to a shift of the reaction towards a higher temperature 50 % carbon conversion is reached at approximately 500 °C when using a heating rate of 1 °C min^{-1}; whereas, the same conversion is attained above 1200 °C when a heating rate of 50 °C min^{-1} is used. Such changes in residual carbon fraction, and thus in thermogravimetric data, caused by the variation of the heating rate, are the basis for the uncertainty in determining kinetic parameters from a single thermogramme.

In a similar way, the slope of these decomposition curves and the position of a plateau (transition between two reaction peaks) are also influenced by the heating rate. These remarks are best described by the corresponding thermogravimetric rate curves presented in Figure 5.2.2. At high heating rate, the thermogramme is very broad, with two distinct peak reactions. The range at which the plateau is observed, increases with increasing heating rate so that the secondary reactions are being retarded; suggesting that mass-transfer limitations are strongly in operation at these higher heating rates. At low heating rate, however, the second reaction is inhibited and the overall process takes place in a single step. Nonetheless, it is interesting to note that the initial reaction rate (reaction rate before the maximum rate for the first reaction peak is reached) is identical for all the rate curves, indicating that the initial reaction rate is independent of the heating rate.

5.2.2 Particle Size Effect

The oxidation of BPL carbon in two distinct particle sizes was analysed, for a similar sample weight of approximately 30 mg. The larger particles are granular BPL with 1 – 4 mm diameter, and the smaller particles are powder BPL, with particle size less than 75 μm. A comparison of the weight-loss and reaction rate curves for the two particle sizes is shown in Figure 5.2.3 and Figure 5.2.4. It appears that there are no significant effects on the ignition temperature T_o, the temperature of maximum rate T_p and the final decomposition temperature T_f. However, the temperature to reach a specific carbon conversion α, appears to change with particle size. These variations are more pronounced at higher heating rates. The temperature at 50% carbon conversion $T_{0.5}$, for instance, is increased to approximately 50 °C for the larger particles. Nonetheless, it may be noted that the overall shape of the thermogravimetric curves is not affected by the particle size. Although the smaller particles are more reactive, this difference is always less than 1 wt% min^{-1}. As these results were taken from several experiments, it is very likely that particle size is a negligible factor on the reactivity of carbonaceous materials smaller than 4 mm.

5.2.3 Chemisorption Effect

It was found that oxidation of coal chars presented an initial weight increase. This apparent gain in weight is not observed whilst using the activated carbons. As an example, the weight-loss profiles of two coal chars are compared with that of granular BPL, in Figure 5.2.5. This increase in weight before the oxidation reaction takes place, may correspond to the chemisorption phase discussed in section 2.7.2. In fact, the carbon-oxygen reaction consists of an initial uptake of oxygen to form surface complexes, which subsequently oxidise at higher temperatures. This apparent increase in weight was corrected on thermogravimetric data in the main reaction zone. Otherwise, the intrinsic surface reaction rate is disguised by the rate of chemisorption and desorption. It is very likely that that coal chars have more of a fulleroid carbon structure than the activated carbons (Madarasz *et al.* 1994).

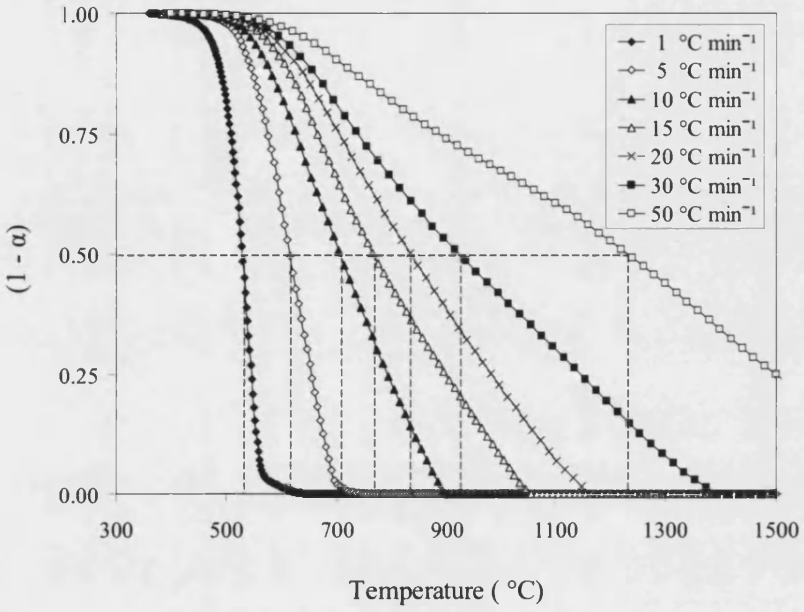

Figure 5.2.1: Influence of heating rate on the weight-loss curve of the oxidation in air of granular BPL, corrected for moisture and ash (sample weight = 40 mg).

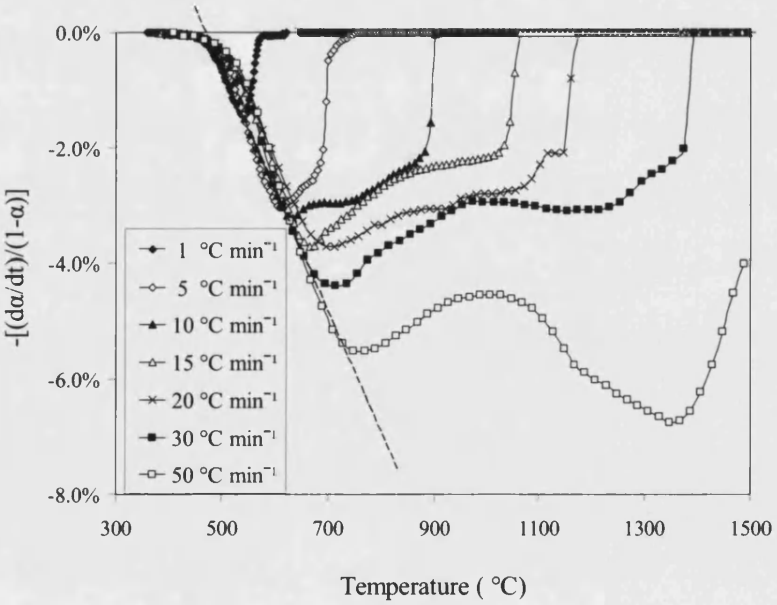

Figure 5.2.2: Influence of heating rate on the reaction rate curves of granular BPL in air.

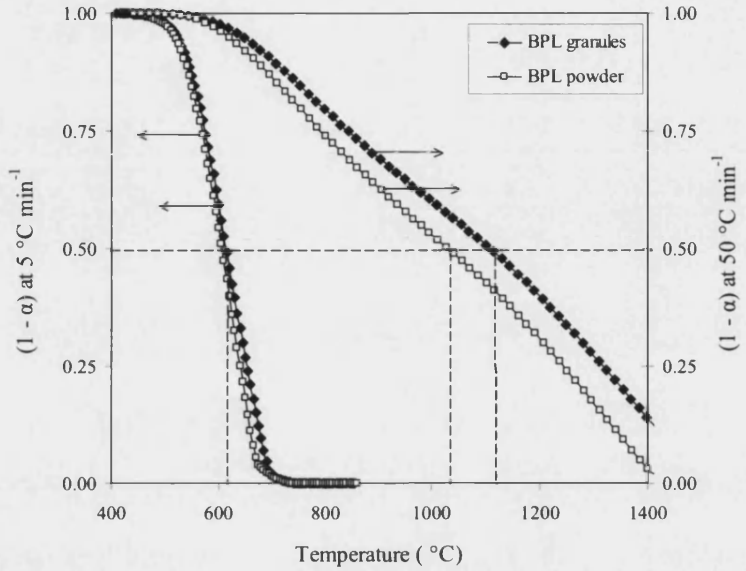

Figure 5.2.3: Comparison of weight loss curves for the oxidation of BPL granules and BPL powder at low and high heating rates.

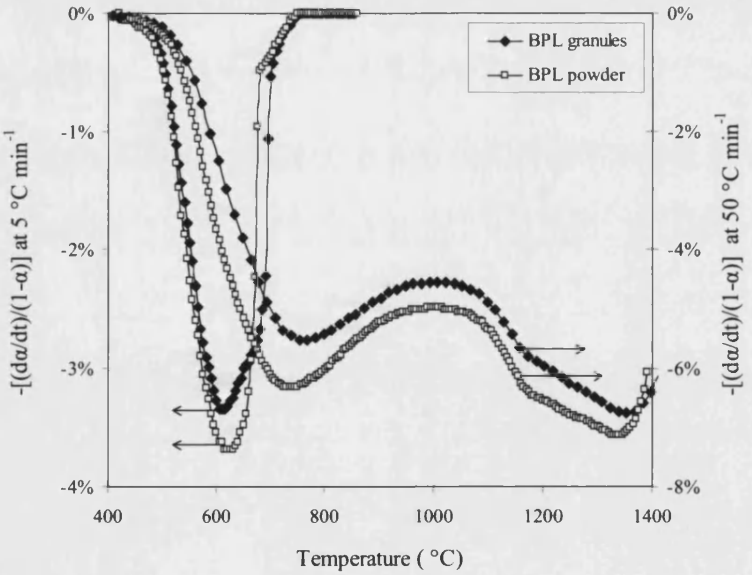

Figure 5.2.4: Comparison of reaction rate profiles of BPL granules and BPL powder at low and high heating rates.

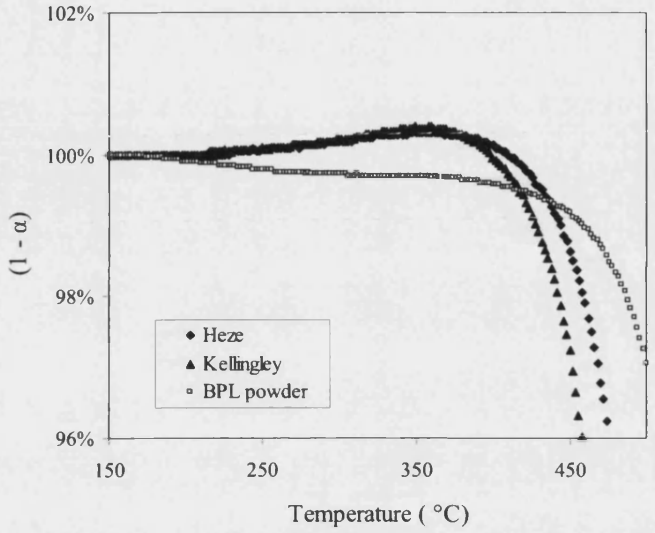

Figure 5.2.5: TG curves for the oxidation at low temperatures of Heze and Kellingley chars in comparison to the activated carbons (BPL powder).

5.3 Maximum Analysis Temperature

5.3.1 Kinetic Control Regime

As discussed in section 2.7.4, as the oxidation process proceeds, the reaction is successively being controlled by different mechanisms. These different rate-controlling zones were identified as suggested in section 4.5.2, by means of an Arrhenius plot. Figure 5.3.1 shows Arrhenius plots of the initial oxidation rate at a heating rate of 5 °C min $^{-1}$, for all the various materials. The resulting maximum temperatures for chemical control (Zone I) are given in Table 5.3.1. It should be noted that the heating rate has no effect on this temperature analysis, since it was established that the initial reaction rate is independent of the rate of heating. As can be seen from Figure 5.3.1, the three rate-controlling zones are clearly identified. The oxidation of both activated carbons and PRB, however, are only controlled by Zone I and II. It is interesting to note, at this stage, that these materials have larger microporous surface areas compared to the others, and

therefore the chemical reaction is kinetically controlled. For the other chars, the first 50-wt% conversion of carbon takes place within Zone I; whereas, the remaining 30% are under the influence of pore diffusion, and the end of the reaction is controlled by external diffusion. The extent of each controlling zones may also be explained by differences in the porous structures of the chars. In fact, rate-controlling regimes through porous particles is rather complex. Wang *et al.* (1999) have recently observed that small pore sizes are kinetically controlled, whilst larger pore structures are either Knudsen or continuum diffusion limited. It is therefore possible that pore size plays an important role in the observed differences in rate-controlling mechanism during the oxidation of the different chars.

5.3.2 Primary Reaction Zone

As discussed in section 4.5.3, the primary reaction zone was defined as the temperature region where the first reaction step was observed on a reaction rate profile. This first peak corresponds to reaction I or both reactions I and II simultaneously. These reactions were defined in section 2.7.3 as follows:

$$C + O_2 \rightarrow CO_2 \qquad \text{(I)}$$

$$C + \tfrac{1}{2} O_2 \rightarrow CO \qquad \text{(II)}$$

$$CO^* + \tfrac{1}{2} O_2 \rightarrow CO_2 \qquad \text{(III)}$$

A Gaussian fitting of the thermogravimetric rate curves for all the chars oxidised at 5 °C min^{-1} is shown in Figure 5.3.2 in order to identify these individual reaction steps. All these curves provided a good fit in modelling three peak reactions, as indicated on the graph by a correlation coefficient $r^2 > 0.990$. The first reaction step was clearly determined for all the chars, and the maximum temperature for its prevalence is given in Table 5.3.1. It appears that, the rate of production of CO_2 is greater than that of CO for most chars, owing to the relatively high amount of oxygen in the gas phase (20-v%). For EC2038 char and EC2106 char, the production rate of CO is larger, which explains that their oxidation reactions were essentially controlled by external and porous diffusion. Reaction III represents

the decomposition of a carbon monoxide complex at the surface of the carbon particle. This reaction may also involve hydrogen atoms detaching from the char surface and reacting away with the produced water, so that different types of reactions may take place for the different types of char depending on their chemical structure. These differences may therefore explain the variation in the extent of this third reaction with each char.

5.3.3 Temperature Range Comparison

Once the chemical control region and the temperature range of prevalence of the primary reaction have been established, the maximum temperature for this analysis can be deduced for each char. In fact, the proposed kinetic analysis is strongly based on intrinsic reactivity of a single step reaction. A summary of maximum temperatures for these two conditions is presented in Table 5.3.1, together with the deduced maximum analysis temperature. In most cases, the primary reaction takes place in Zone I, essentially. In other words, direct production of CO_2 is chemically controlled. A similar observation was recently outlined in the work of Slaoui and Bounahmidi (2004), whilst studying the kinetics of coke combustion in air. For EC2038 char, however, part of this reaction is controlled by pore diffusion. This difference may lie in the chemical and physical properties of this char, especially differences in pore size distribution and the organic carbon structure.

Table 5.3.1: Comparison of temperature range for kinetic control analysis and primary reaction occurrence for all the different chars.

Char samples	T_{MAX} for kinetic control (°C)	T_{MAX} for primary reaction (°C)	T_{MAX} for modelling Analysis (°C)
BPL granules	605	600	600
BPL powder	625	600	600
Pha Lai	570	575	570
Heze	580	575	575
Chang Cun	580	540	540
Kellingley	550	540	540
Colombian	575	570	570
PRB	570	565	565
EC2038	565	600	565
EC2106	605	560	560

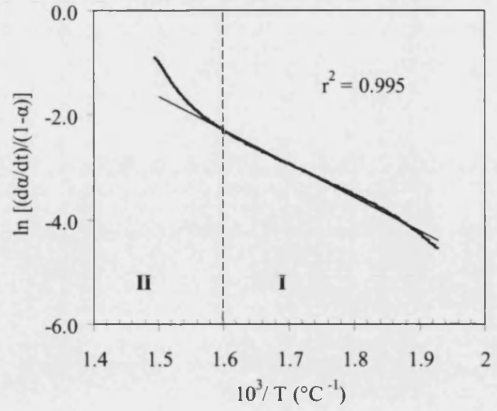

a) BPL (powder)

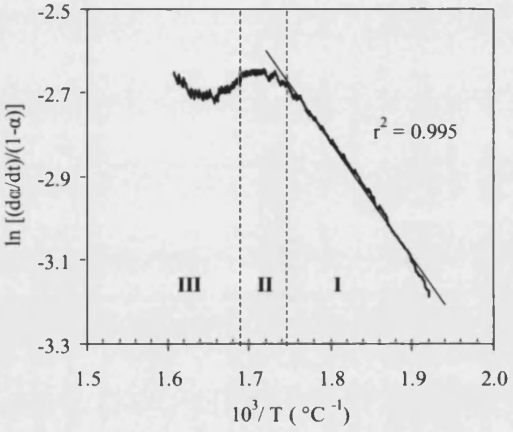

b) Pha lai

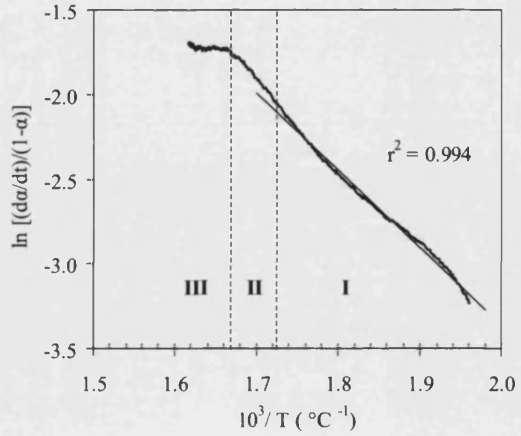

c) Heze

Figure 5.3.1: Rate-controlling regimes for the oxidation in air of the different chars. Straight lines correspond to the estimated mean Zone I behaviour.

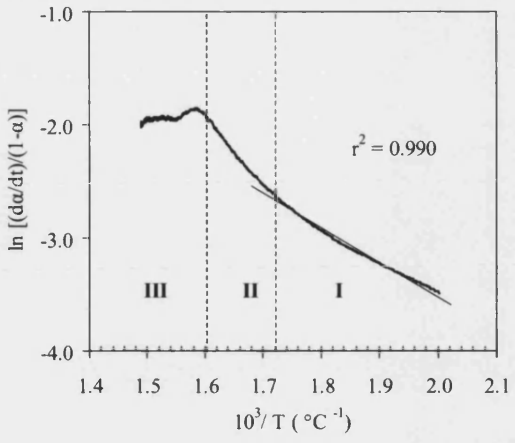

d) Chang Cun

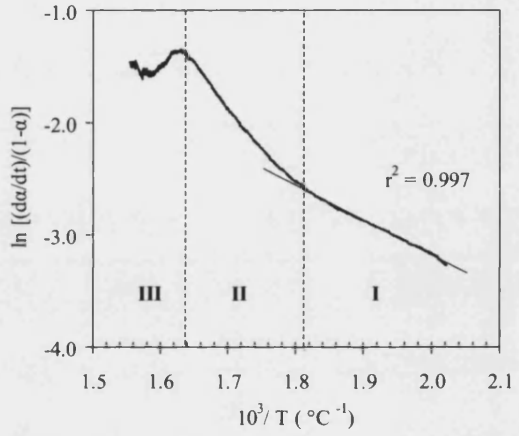

e) Kellingley

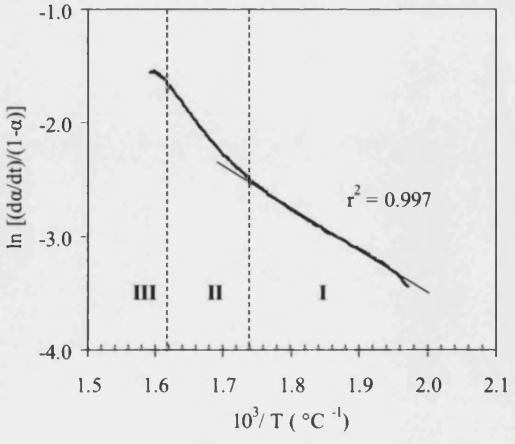

f) Colombian

Figure 5.3.1: continued for:d) Chang Cun; e) Kellingley; f) Colombian

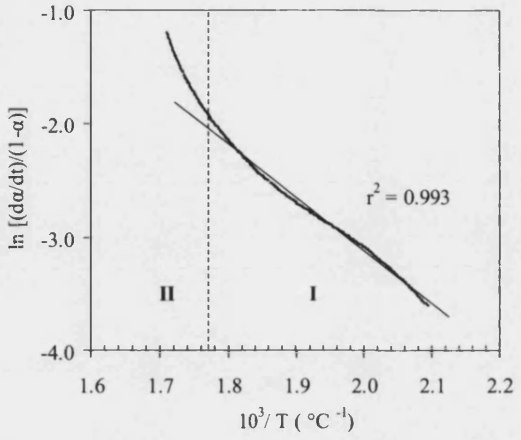

g) PRB

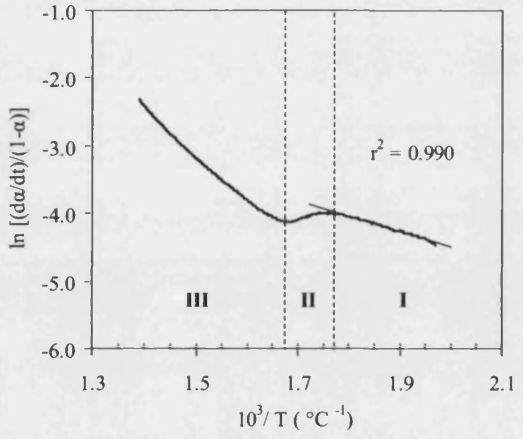

h) EC2038

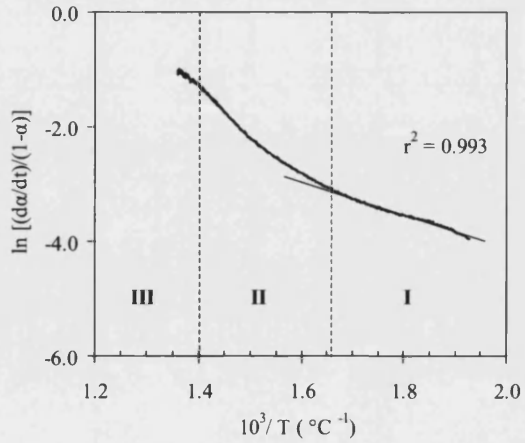

i) EC2106

Figure 5.3.1: continued for: g) PRB; h) EC2038; i) EC2106

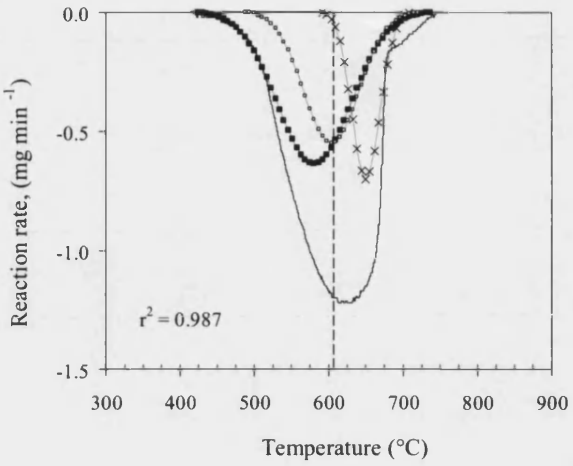

a) BPL (powder)

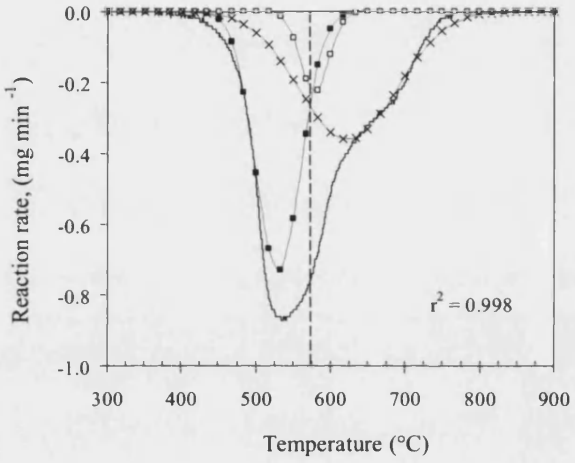

b) Pha Lai

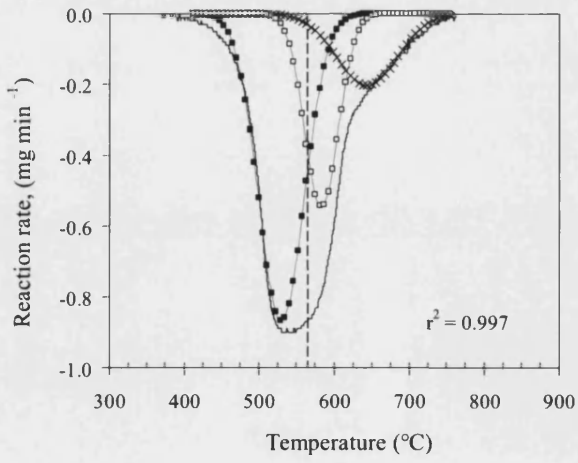

c) Heze

Figure 5.3.2: Deconvolution of the overall reaction rate curve (—) into its three peak reactions for the various chars oxidised at 5 °C min $^{-1}$ in air: (■) reaction I; (□) reaction II; (+) reaction III.

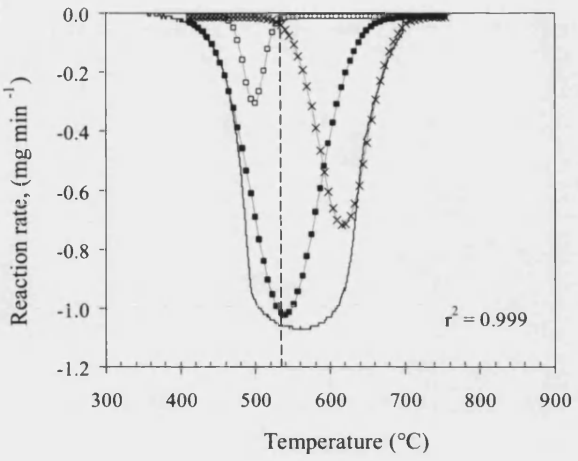

d) Chang Cun

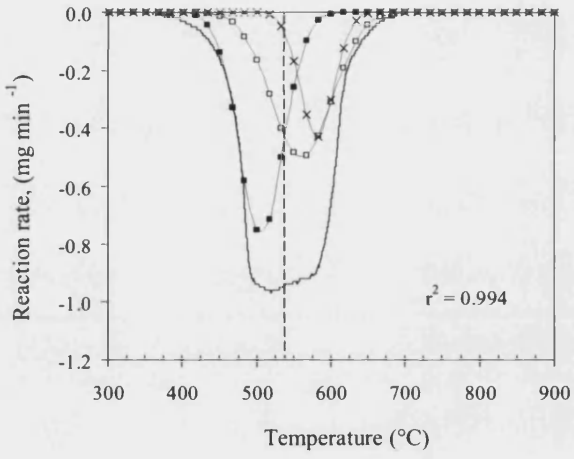

e) Kellingley

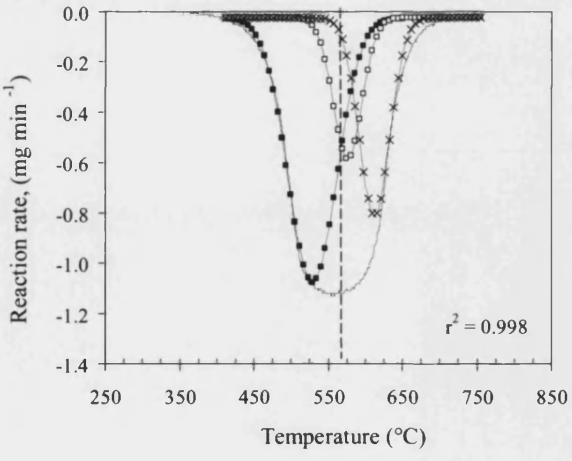

f) Colombian

Figure 5.3.2: continued for: d) Chang Cun; e) Kellingley; f) Colombian

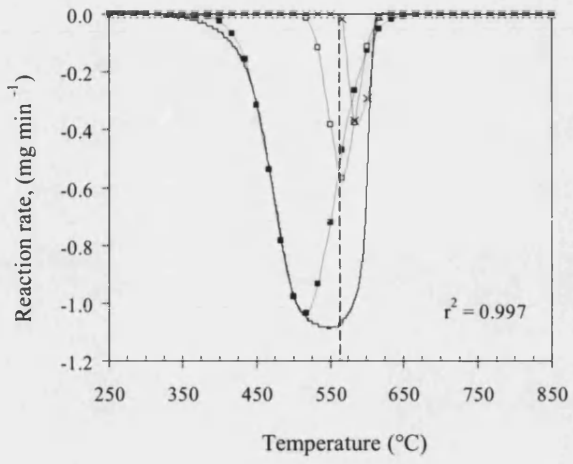

g) PRB

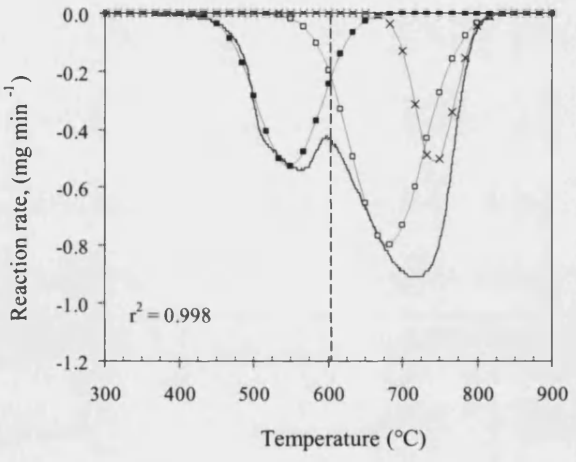

h) EC2038

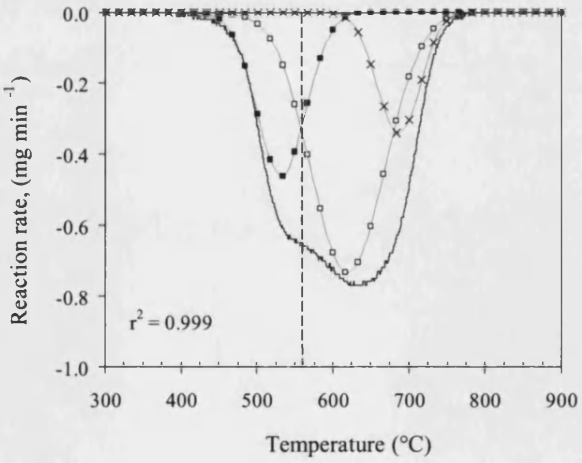

i) EC2106

Figure 5.3.2**:** continued for: g) PRB; h) EC2038; i) EC2106.

5.4 Reactivity Parameters Evaluation

5.4.1 Kinetic Model Fitting

The proposed kinetic analysis, described in Chapter 3, was applied to the different coal chars, so that the description given below was observed with all the coal chars, and is demonstrated here for BPL powder only. Reactivity parameters were evaluated using equation (3.4-5):

$$ln\left(\frac{ln(1-\alpha)}{T^2}\right) = ln\left(-\frac{AR}{\beta E}\right) - E/RT$$

At a specific heating rate β_i, plots of $ln\ [(1/T^2)\ ln\ (1-\alpha)]$ versus $1/RT$ were determined for each char. Then, the activation energy E and pre-exponential factor A were calculated from the slope and intercept of these lines, respectively. This process was performed at heating rates 1, 5, 10, 15, 20 30 and 50 °C min^{-1}. The lines were of good fit, as measured by the correlation coefficient r^2. It was found that, for a heating rate β greater than 1 °C min^{-1}, the correlation coefficient r^2 was always larger than 0.990; suggesting that the kinetic model $g(\alpha) = (1-\alpha)$ accurately described the oxidation reaction of the char within the kinetic control regime at these heating rates. At a heating rate of 1 °C min^{-1}, the correlation coefficient always returned a poor value ($r^2 < 0.990$), with apparent curving in the line. Hence, the kinetic model used is not applicable when using a heating rate of 1 °C min^{-1}. An example of these straight lines is shown in Figure 5.4.1 for the analysis of BPL powder at 1 °C min^{-1} and 10 °C min^{-1}.

5.4.2 Kinetic Parameters

The estimated reactivity parameters E and A for all the chars are given in Table 5.4.1 and Table 5.4.2. These parameters represent the mean value obtained from two or three samples. The standard error of the mean is also given in the table. As can be seen in Figure 5.4.2, the activation energy values decrease with increasing heating rate. This occurrence suggests that strong thermal effects such

as convection currents are in operation during the reaction process, disguising the true activation energy value of the reaction. This variation may be represented in a linear form, as demonstrated by Figure 5.4.3. A similar trend was also pointed out by Serageldin and Pan (1982) who suggested a linear relationships between the activation energy E and the natural logarithm of the heating rate β. A reasonable linearity is observed here for most of the coal chars, with each line having similar slope. It is possible that the activation energy of coal char oxidation is linearly correlated to the rate of heating. For the BPL carbons, however, a different gradient is observed, indicating that these materials are structurally different from the coal chars. Although the physical implications of this relationship remain unclear, it is certainly of great interest from a mathematical and modelling point of view. In fact, this correlation could lead to significant simplifications in the modelling analysis.

5.4.3 Compensation Effect

A linear variation of the activation energy E with the natural logarithm of the pre-exponential factor A was also observed. This phenomenon is known as the kinetic compensation effect (Thomas and Thomas 1967). This compensation effect is plotted in Figure 5.4.4 and shows a good linearity which may be expressed as:

Eq. (5.4-1) $$\ln A = aE + b$$

The parameters a and b, for all the chars are summarised in Table 5.4.3. It can be seen that the value of a are very close for all the chars. It is possible, therefore, that the kinetic compensation effect is independent of the type of chars. This is a useful relationship for correlation in modelling studies. In fact, the proposed kinetic analysis is simplified by requiring only one fitting parameter. Although the significance of this compensation effect is till unclear Brown and Galwey (2002) have suggested that the relationship may describe the behaviour of the material under different experimental conditions, and thus being relative to heat and mass transfer effects.

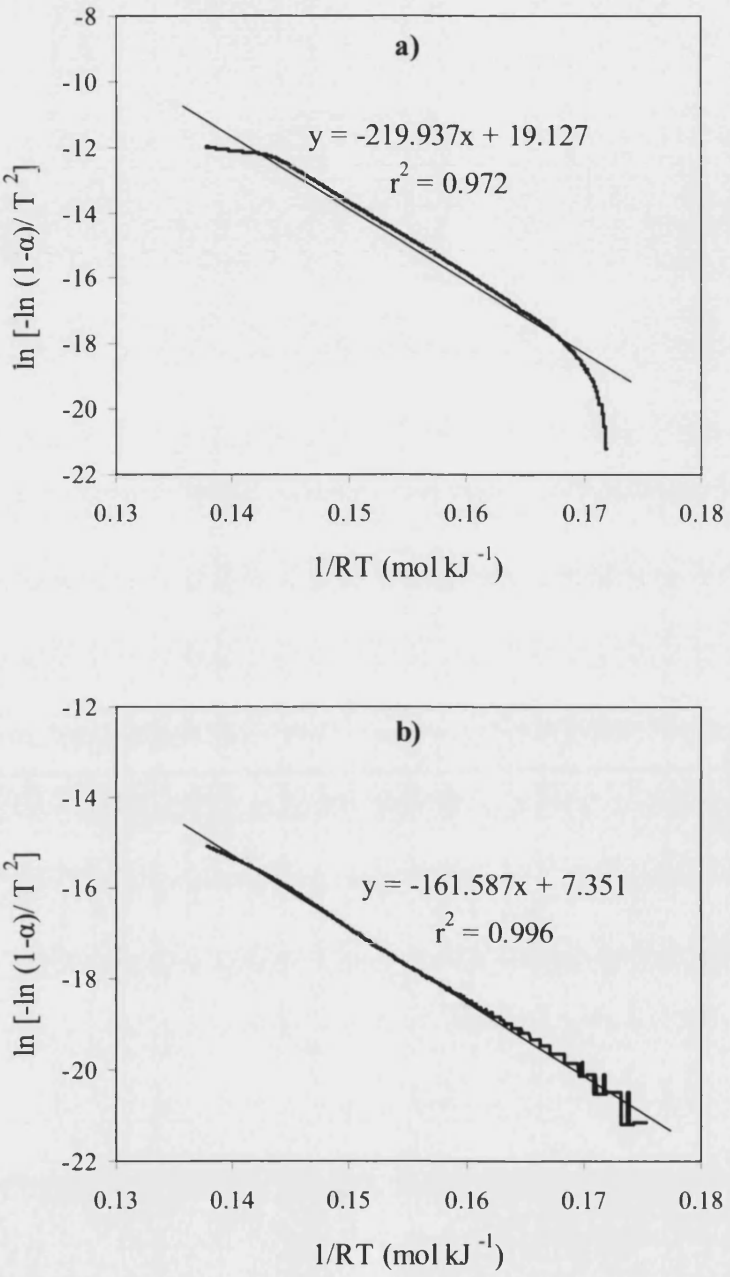

Figure 5.4.1: Fitting of the kinetic model to the oxidation profile of BPL powders at: a) 1 °C min $^{-1}$ and b) 10 °C min $^{-1}$.

Table 5.4.1: Mean activation energy E (± standard error, kJ mol $^{-1}$) estimated by the proposed reactivity model equation (3.4-5)

Heating rate, (°C min $^{-1}$)	Char samples									
	BPL (granules)	BPL (powder)	Pha Lai	Heze	Chang Cun	Kellingley	Colombian	PRB	EC2038	EC2106
1	218.2 ± 2.1	219.9 ± 2.1	175.3 ± 2.7	171.2 ± 2.2	205.9 ± 2.5	161.7 ± 0.8	202.9 ± 1.6	161.1 ± 1.6	160.1 ± 2.3	170.2 ± 1.6
5	190.6 ± 1.3	189.5 ± 2.4	167.8 ± 1.0	161.4 ± 3.0	163.6 ± 1.2	163.9 ± 1.8	158.1 ± 0.8	127.3 ± 0.5	171.1 ± 3.1	176.6 ± 1.5
10	171.8 ± 1.3	165.5 ± 2.8	170.8 ± 0.8	157.1 ± 1.6	160.7 ± 0.2	161.7 ± 0.8	151.6 ± 0.3	119.6 ± 0.2	176.3 ± 0.5	165.6 ± 1.3
15	155.6 ± 1.0	148.8 ± 2.3	168.5 ± 3.4	154.0 ± 0.8	154.2 ± 3.1	154.3 ± 0.6	149.5 ± 1.2	114.4 ± 0.5	175.5 ± 6.1	158.2 ± 0.7
20	135.9 ± 0.8	136.1 ± 2.8	163.5 ± 0.2	153.6 ± 0.7	152.1 ± 1.3	146.1 ± 0.7	148.2 ± 1.3	110.1 ± 0.7	171.9 ± 2.2	151.8 ± 1.0
30	122.9 ± 1.0	122.8 ± 1.1	156.3 ± 0.4	152.0 ± 1.7	147.0 ± 3.1	141.5 ± 0.6	135.4 ± 2.5	108.9 ± 0.5	160.9 ± 2.6	151.4 ± 0.1
50	92.6 ± 0.6	102.8 ± 3.3	151.3 ± 0.9	149.9 ± 4.2	139.2 ± 3.8	134.1 ± 0.5	133.2 ± 5.0	104.3 ± 1.0	143.3 ± 7.4	145.63 ± 0.1

Table 5.4.2: Mean of the natural logarithm of the pre-exponential factor A/s^{-1} (± standard error) estimated by the proposed reactivity equation (3.4-5).

Heating rate,	Char samples									
(°C min $^{-1}$)	BPL (granules)	BPL (powder)	Pha Lai	Heze	Chang Cun	Kellingley	Colombian	PRB	EC2038	EC2106
1	24.9 ± 0.0	25.2 ± 0.0	19.4 ± 0.0	18.8 ± 0.0	25.2 ± 0.0	18.2 ± 0.0	24.5 ± 0.0	18.4 ± 0.0	15.5 ± 0.0	17.6 ± 0.0
5	20.0 ± 0.0	19.9 ± 0.4	17.9 ± 0.1	17.1 ± 0.5	17.7 ± 0.2	18.1 ± 0.3	16.5 ± 0.0	12.3 ± 0.1	17.2 ± 0.5	18.5 ± 0.6
10	17.0 ± 0.0	16.0 ± 0.4	18.3 ± 0.2	16.1 ± 0.2	17.1 ± 0.0	17.4 ± 0.2	15.1 ± 0.0	10.9 ± 0.0	176.9 ± 0.1	16.2 ± 0.5
15	14.3 ± 0.0	13.4± 0.4	17.6 ± 0.5	15.3 ± 0.2	15.8 ± 0.5	16.2 ± 0.1	14.5 ± 4.2	10.0 ± 0.1	17.4 ± 0.9	14.7 ± 0.3
20	11.3 ± 0.0	11.5 ± 0.4	16.6 ± 0.0	15.2 ± 0.0	15.4 ± 0.2	14.9 ± 0.0	14.3 ± 0.2	9.3 ± 0.1	16.8 ± 0.3	13.8 ± 0.4
30	9.3 ± 0.4	9.4 ± 0.2	15.4 ± 0.1	14.9 ± 0.2	14.6 ± 0.4	14.0 ± 0.1	12.1 ± 0.4	9.1 ± 0.1	15.0 ± 0.4	13.4 ± 0.1
50	4.8 ± 0.0	6.4 ± 0.5	14.6 ± 0.2	14.6 ± 0.6	13.3 ± 0.6	12.7 ± 0.1	11.7 ± 0.8	8.4 ± 0.2	12.3 ± 1.2	12.6 ± 0.0

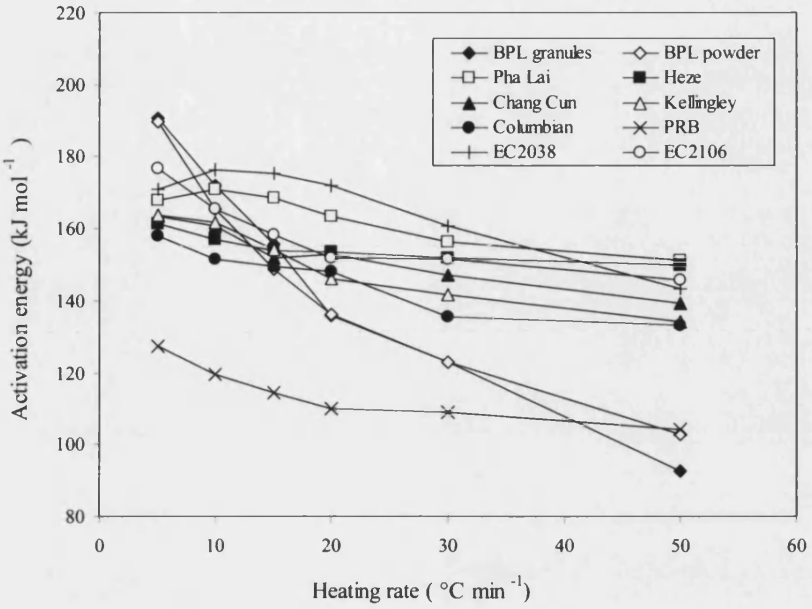

Figure 5.4.2: Variation of activation energy values with heating rate upon oxidation in air of the different chars.

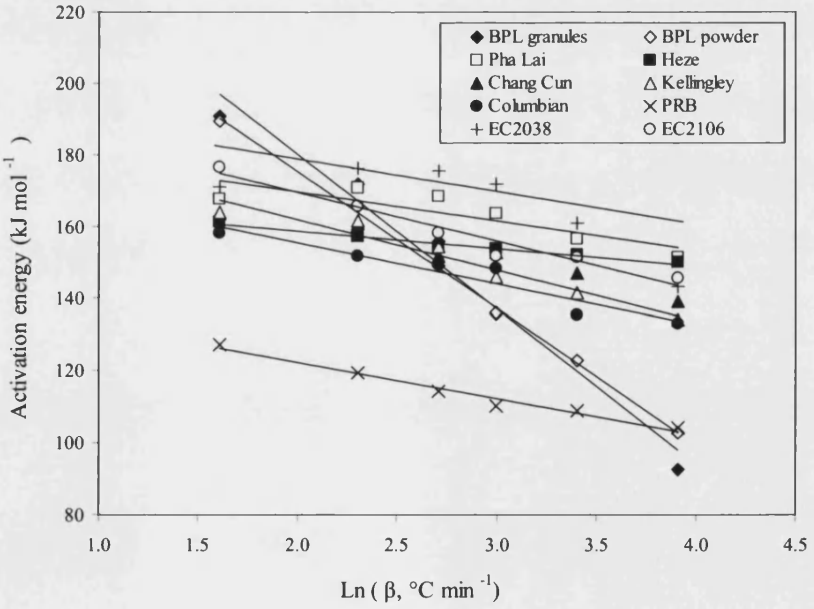

Figure 5.4.3: Linear variation of activation energy with the natural logarithm of heating rate upon oxidation in air of the different chars.

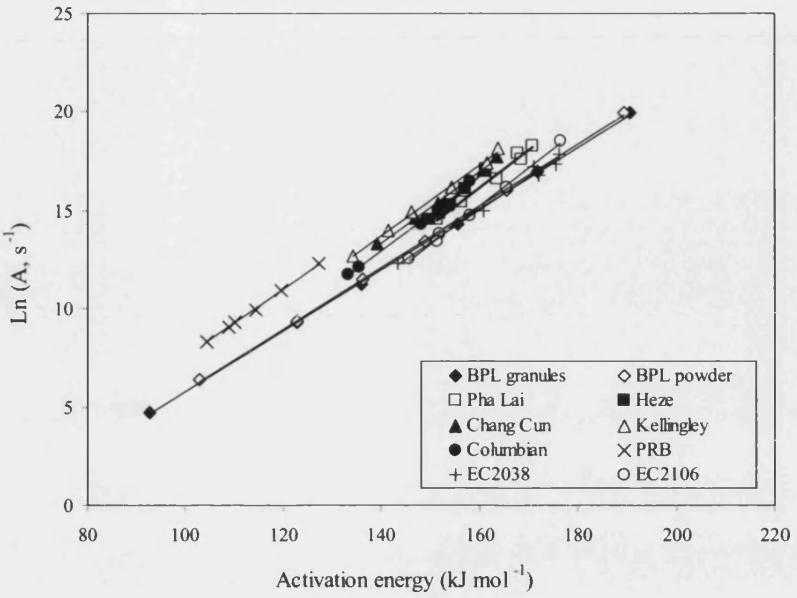

Figure 5.4.4: Correlation between activation energy of the char and the pre-exponential factor at different heating rates.

Table 5.4.3: Parameters a and b for the kinetic compensation effect observed with the different chars

Char sample	a	b
BPL granules	0.16	-9.7
BPL powder	0.16	-9.7
Pha lai	0.19	-14.2
Heze	0.22	-19.3
Chang Cun	0.18	-11.8
Kellingley	0.18	-10.9
Colombian	0.18	-12.9
PRB	0.17	-9.6
EC2038	0.16	-11.4
EC2106	0.19	-15.7

5.5 Optimum Heating Rate Analysis

5.5.1 Char Oxidation Modelling

Given the kinetic parameters derived in the previous section, it is now possible to predict a weight-loss profile for the char in the kinetic control regime. The simulated weight loss profiles are computed by applying equation (3.4-7), discussed in section 3.4.2.

$$(1-\alpha_{calc}) = -\frac{ART^2}{\beta E} exp\left(-E/RT\right)$$

Since the values of E and A are known, the calculated weight-loss profile $(1-\alpha_{calc})$ is easily deduced for the whole temperature range studied. As an example, the simulated curves for the air oxidation of granular BPL, Chang Cun char and EC2106 char are presented in Figure 5.5.1, Figure 5.5.2 and Figure 5.5.3, at various heating rates. The two coal chars are presented as suitable representative of the power station chars and the iron and steel-industry chars, respectively. Simulated weight loss curves for BPL granules have also been published by Sima-Ella *et al.* (2005).

Overall, the shape of the calculated profiles is similar to the experimental ones at the various heating rate. At a rate of heating β = 1 °C min $^{-1}$, however, there is a significant difference between experimental and predicted data. This is somewhat expected, as the kinetic model was found not to be applicable at this heating rate. As the rate of heating increases, the calculated and experimental profiles become more adjacent. After a threshold in the rate of heating, nevertheless, these two profiles start to diverge again. It appears, therefore, that there exists an optimum rate of heating at which the experimental data closely coincide with the calculated ones. A way of accurately estimating this optimum-heating rate is detailed in the next sections.

5.5.2 Root Mean Square Method

The root-mean square (RMS) method is used as a measure of fit in comparing the simulated weight-loss curves with the experimental ones. In this way, it is possible to compare the overall accuracy of the predicted weight loss profiles at each heating rate. This type of error measurement is assessed as detailed in section 3.4.2. The RMS value in equation (3.4-10) and may be rewritten as:

Eq.(5.5.1)

$$\sigma(\%) = \left[\frac{1}{2} \sqrt{\frac{\sum_{i=T_i}^{n=T_{max}} \left(\alpha_{i,calc} - \alpha_{i,exp}\right)^2}{n}} + \frac{1}{2} \sqrt{\frac{\sum_{i=t_i}^{n=t_{max}} \left(\alpha_{i,calc} - \alpha_{i,exp}\right)^2}{n}} \right] \times 100$$

For each heating rate, the RMS value between the simulated conversion profiles and the experimental results was calculated. These values are presented in Table 5.5.1, and are also plotted in Figure 5.5.4. It appears from Table 5.5.1 that the error in the fit are always lower than 2% overall, for any chars, when using a heating rate greater than 1 °C min^{-1}. At this lowest heating rate, the error is very large, reaching almost 5% in the case of PRB. It is clear that this heating rate is not suitable for kinetic modelling of coal char oxidation. On the other hand, the low RMS values at these other heating rates infer that the proposed reactivity model satisfactorily simulates the reaction of carbon with oxygen within the kinetic control regime. It may be noted that the RMS values are different for each char, suggesting that the proposed reactivity model is more suitable for some chars than others.

In addition, it appears that the RMS value always reaches a minimum, for any of the coals studied. It is highly possible therefore that there exists an optimum-heating rate at which the predicted burnout profiles correspond best to the experimental data. At this heating rate, true kinetic parameters are observed since they are not masked by the experimental environment. Furthermore, this minimum RMS value appears to lie in the heating rate range of 20 to 50 °C min^{-1}, for all the chars. In some cases, the minimum RMS value is clearly defined

around a particular heating rate (e.g. BPL granules). In other instances, however, this minimum RMS value does not change significantly between a rate of heating of 20 and 50 °C min^{-1} (e.g. Chang Cun). It may also be noted that, although the error remains unchanged at the higher heating rates, the kinetic parameter values are continuously changing. Therefore, it is clear that at these high heating rates, mass-transfer limitations become important and mask the true value of the kinetic parameters.

As discussed by Sima-Ella and Mays (2005a), it is not possible to ascertain the exact value of the optimum-heating rate, without carrying out a series of experiments at heating rates between 20 and 50 °C min^{-1}. Nonetheless, the optimum-heating rate may be selected as the cut-off point where the RMS value is the smallest and the value of the activation energy does not change significantly. For these reasons, it emerges that the optimum-heating rate is located in the range of 25 to 35 °C min^{-1}.

5.5.3 Relative Error Method

This optimum-heating rate range may be verified by examining the relative error in conversion over the whole temperature range of interest. The previous method was giving an overall picture of goodness of fit, whereas this method aims at looking at the variation in fit in a more qualitative manner. The relative error is determined by difference between the experimental carbon conversion α, and the calculated value α_{calc} at each recorded temperature points:

$$\text{Re}lative\ error\ (\%) = \frac{\left(\alpha_{i,\exp} - \alpha_{i,calc}\right)}{\alpha_{i,\exp}} \times 100$$

A plot of relative error with temperature for BPL granules is shown in Figure 5.5.5 at various heating rates. The overall view shows that the calculated data closely correspond to the experimental ones up to 450 °C, at any given heating rate. At this point the oxidation reaction has not properly started. As the temperature increases, the error also increases and becomes more significant at the lower heating rates of 1 °C min^{-1} to 15 °C min^{-1}. An enlarged view of these

errors is also given in the figure. It appears that a near 0% relative error could be obtained throughout the whole temperature range when using a heating rate between 20 and 30 °C min $^{-1}$. By means of linear interpolation, this optimum heating rate is identified at 27 °C min $^{-1}$. This clearly defined optimum-heating rate is only observed with the BPL carbon materials, however.

For the coal chars, the trend and values in the relative error are very similar for oxidation profiles at rates of heating of 20, 30 and 50 °C min $^{-1}$, as revealed by Figure 5.5.6. The figure represents the variation in relative error of carbon conversion with temperature for the simulation of Chang Cun char and EC2106 char oxidation in air. These profiles were also observed with all the other coal chars. It appears that there are no further changes in the relative error of carbon conversion beyond a rate of heating of 20 °C min $^{-1}$. Hence, this heating rate could be selected as the optimum heating rate. However, the RMS value at a heating rate of 30 °C min $^{-1}$ is always smaller than at 20 °C min $^{-1}$, suggesting that the former heating rate value is better. It is highly possible that the optimum-heating rate is located around a rate of heating of 30 °C min $^{-1}$. For this reason, the optimum heating rate is identified at a range of 25 - 35 °C min $^{-1}$.

5.5.4 True Kinetic Parameters

True intrinsic kinetic data are therefore assumed to be the mean values in the heating rate range of 25 - 35 °C min $^{-1}$. These values are computed by linear interpolation from those derived at 20, 30 and 50 °C min $^{-1}$, as shown below:

$$E_{25^\circ C\,\mathrm{min}^{-1}} = \tfrac{1}{2}\left(E_{20^\circ C\,\mathrm{min}^{-1}} + E_{30^\circ C\,\mathrm{min}^{-1}}\right)$$

$$E_{35^\circ C\,\mathrm{min}^{-1}} = \tfrac{1}{2}\left(E_{50^\circ C\,\mathrm{min}^{-1}}\right) + E_{30^\circ C\,\mathrm{min}^{-1}}$$

$$True\ \ E\text{ - }value\ = \tfrac{1}{2}\left(E_{25\,^\circ C\ \mathrm{min}^{-1}} + E_{35\,^\circ C\ \mathrm{min}^{-1}} \right)$$

A similar calculation applies for the natural logarithm of the pre-exponential factor A. A summary of the resulting mean intrinsic reactivity parameters is given in Table 5.5.2, together with their associated standard error.

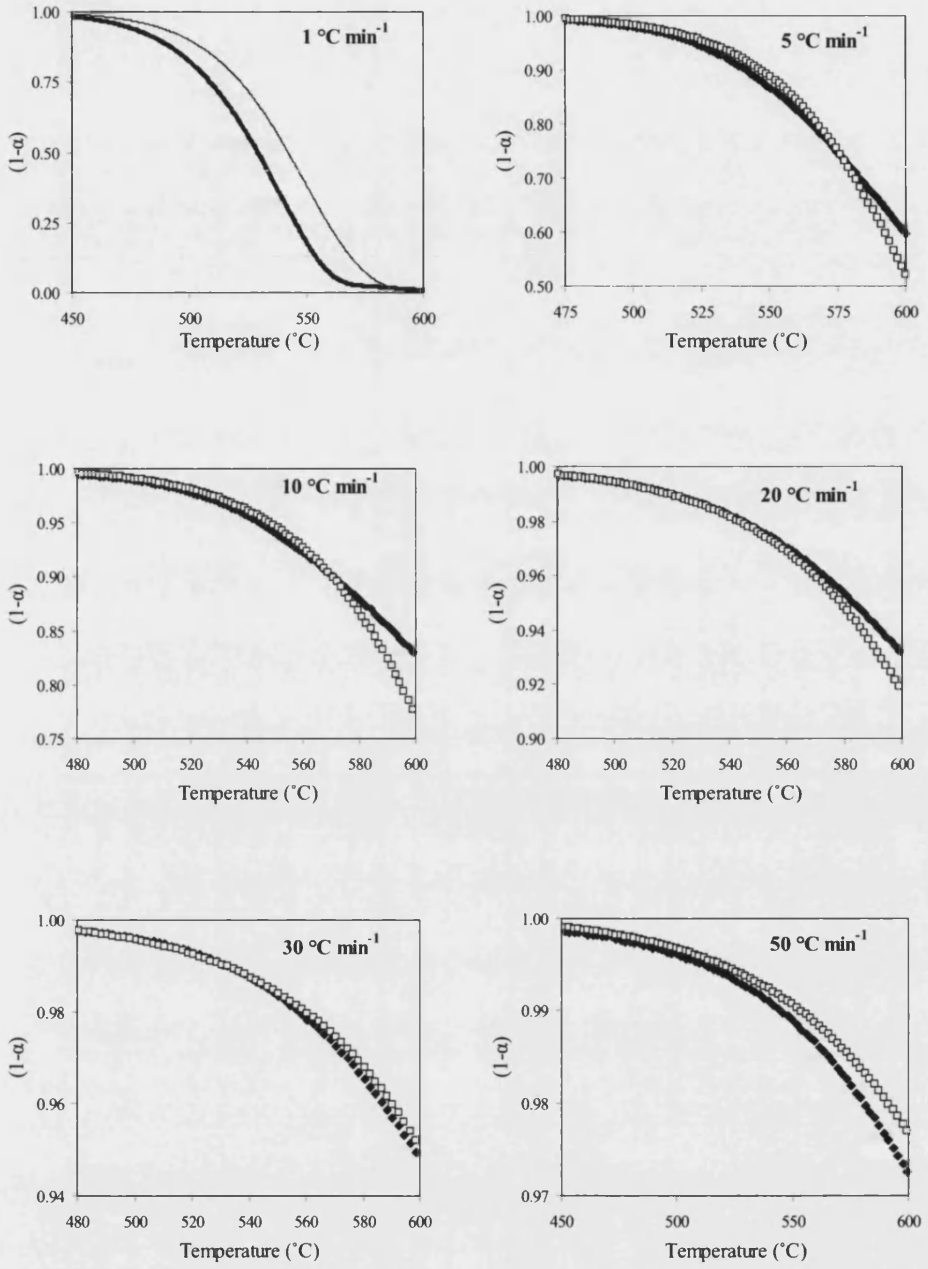

Figure 5.5.1: Comparison between experimental (■) and simulated (□) weight loss profiles for the air oxidation of granular BPL carbon at various heating rates.

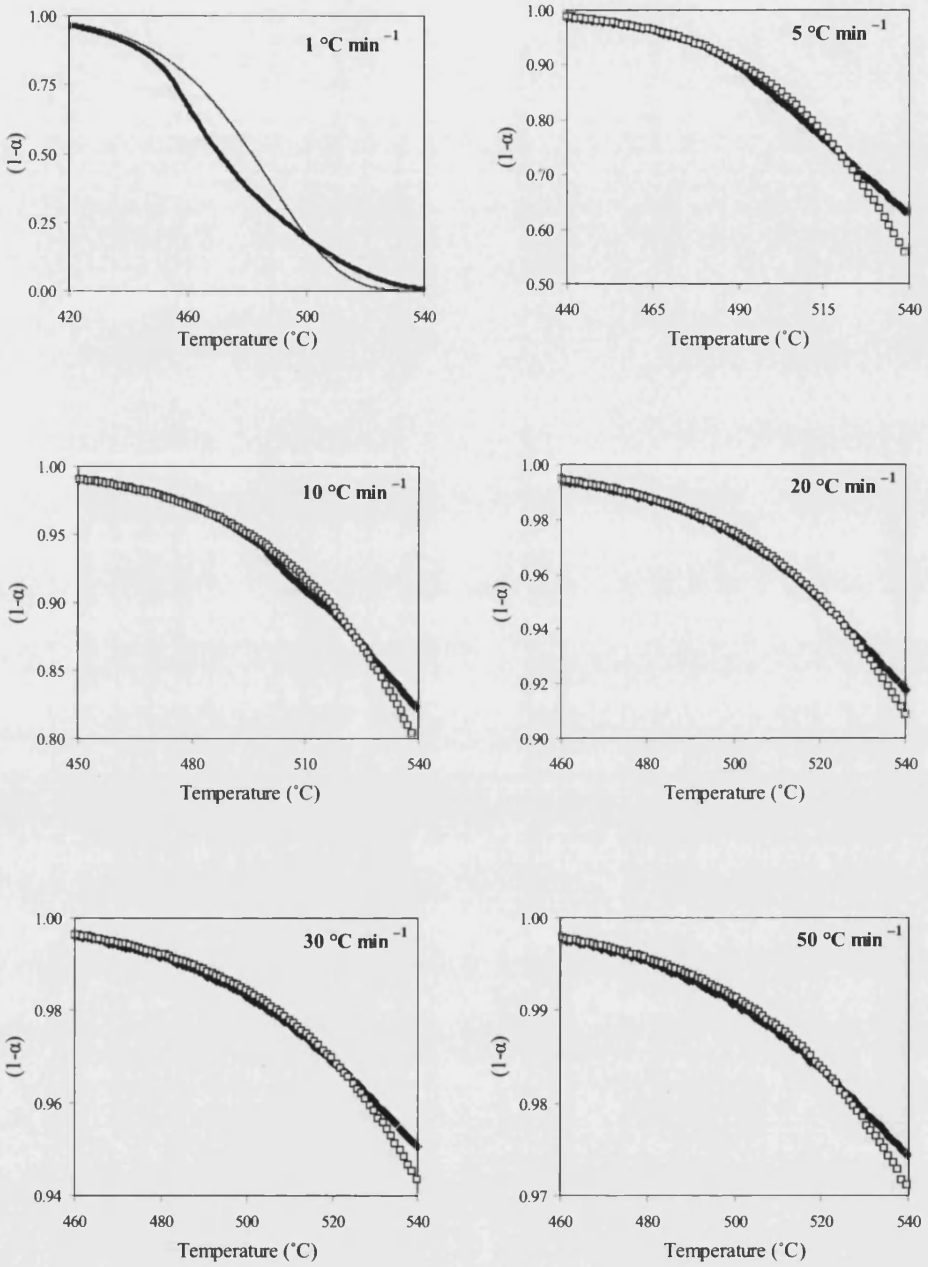

Figure 5.5.2: Comparison between experimental (■) and simulated (□) weight loss profiles for the air oxidation of Chang Cun char at various heating rates.

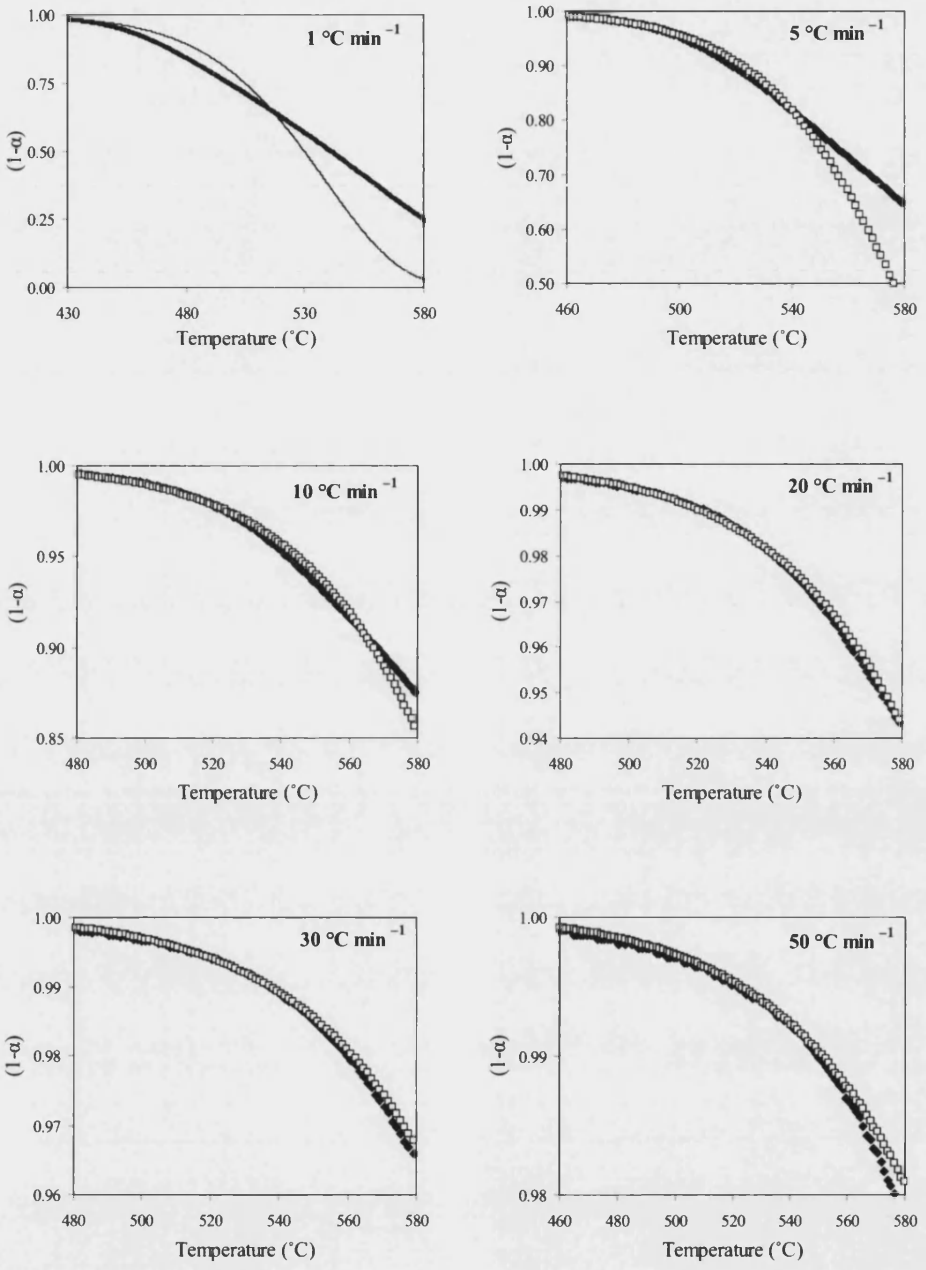

Figure 5.5.3: Comparison between experimental (■) and simulated (□) weight loss profiles for the air oxidation of EC2106 char.

Table 5.5.1: Root mean square (RMS) values in the fit of the calculated thermogravimetric profiles with the experimental data at various heating rates

Heating rate,	Char samples									
(°C min $^{-1}$)	BPL (granules)	BPL (powder)	Pha Lai	Heze	Chang Cun	Kellingley	Colombian	PRB	EC2038	EC2106
1	1.78%	1.84%	4.50%	3.48%	3.48%	2.01%	2.50%	2.42%	4.32%	3.52%
5	1.28%	1.20%	1.03%	1.83%	0.68%	0.78%	0.94%	0.70%	0.50%	0.52%
10	0.89%	0.33%	0.58%	0.93%	0.22%	0.20%	0.43%	0.81%	0.26%	0.22%
15	0.68%	0.11%	0.29%	0.54%	0.14%	0.21%	0.29%	0.61%	0.06%	0.08%
20	0.25%	0.08%	0.22%	0.25%	0.08%	0.20%	0.21%	0.60%	0.03%	0.04%
30	0.09%	0.07%	0.08%	0.15%	0.06%	0.06%	0.07%	0.35%	0.02%	0.03%
50	0.16%	0.12%	0.10%	0.19%	0.06%	0.09%	0.10%	0.42%	0.02%	0.04%

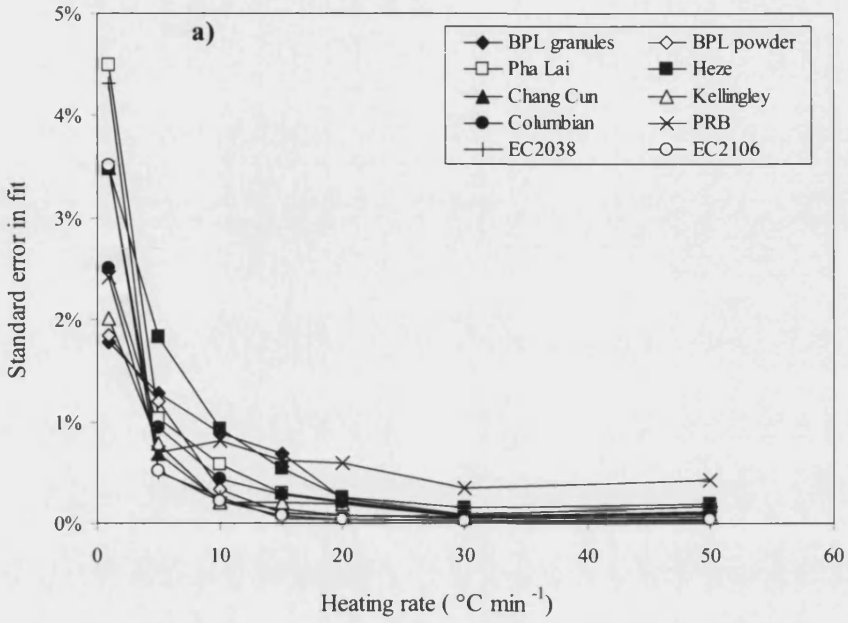

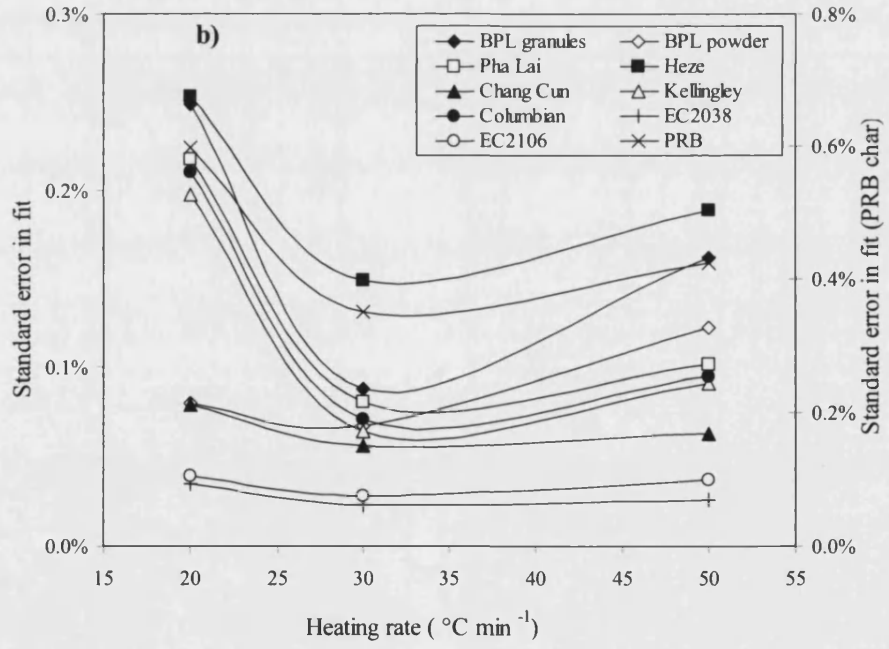

Figure 5.5.4: Variation of standard error with heating rate, in the fit of burnout profiles between the simulated and the experimental data for all the chars: a) overall view; b) enlarged view.

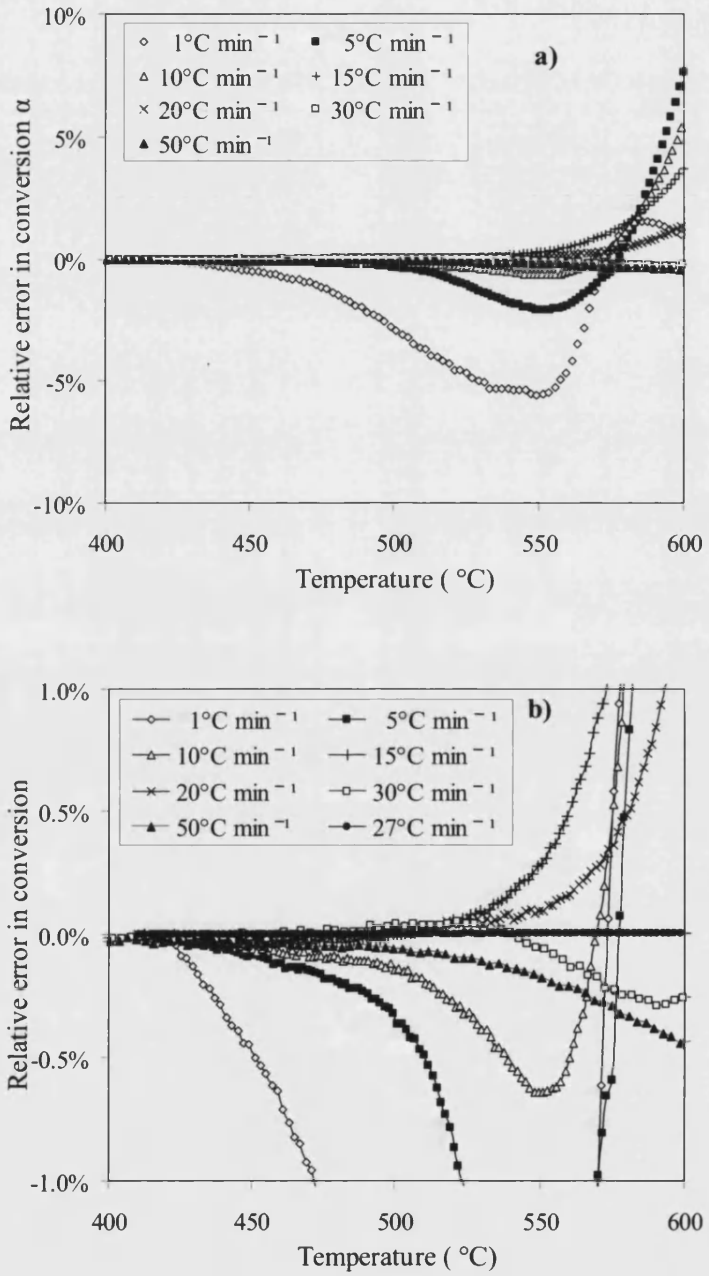

Figure 5.5.5: Relative error in carbon conversion between the simulated burnout profile and the experimental one at different heating rates for oxidation of granular BPL: a) overall view; b) enlarged view.

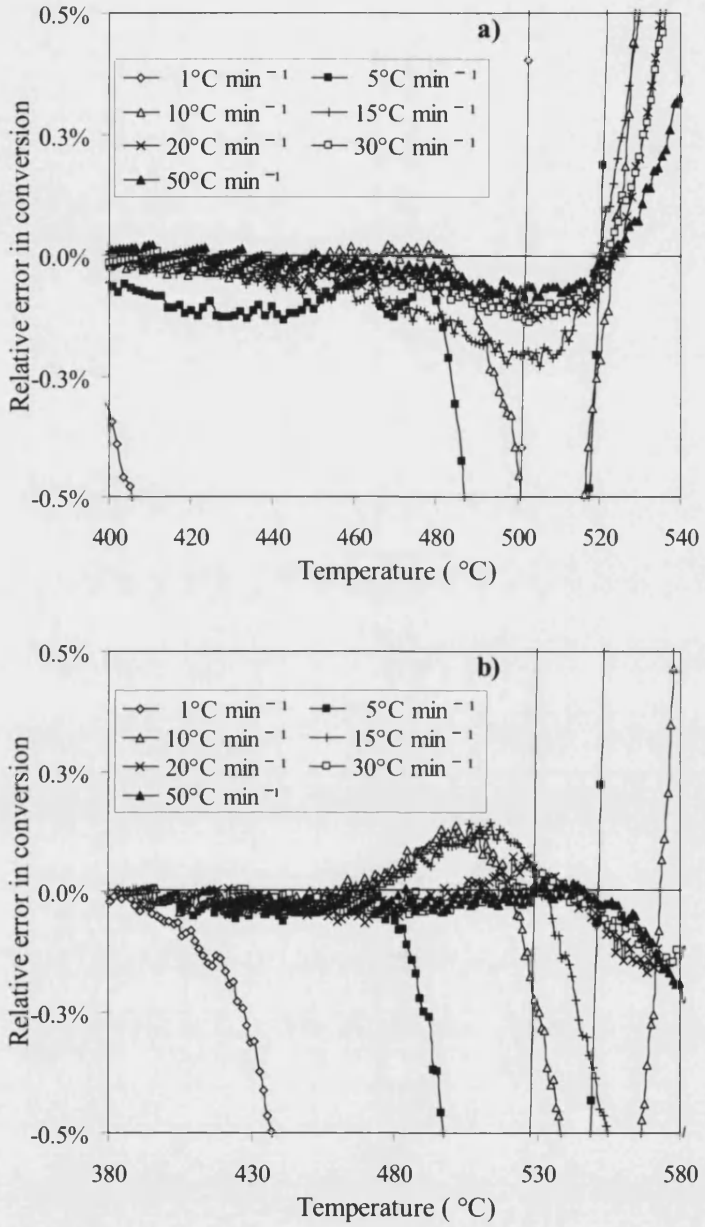

Figure 5.5.6: Relative error in carbon conversion between the simulated burnout profile and the experimental one at different heating rates for oxidation of: a) Chang Cun; b) EC2106.

Table 5.5.2: True intrinsic kinetic parameters (± standard error) derived by the 'optimum-heating rate analysis' for all the different types of chars.

Char samples	E values (kJ mol $^{-1}$)	Ln (A, s^{-1})
BPL granules	122.4 ± 7.0	9.2 ± 1.1
BPL powder	123.6 ± 5.8	9.5 ± 0.9
Pha Lai	157.5 ± 2.4	16.7 ± 0.4
Heze	152.1 ± 2.1	14.9 ± 0.1
Chang Cun	147.3 ± 2.6	14.6 ± 0.4
Kellingley	141.7 ± 2.1	14.1 ± 0.4
Colombian	138.3 ± 3.5	12.6 ± 0.6
PRB	108.6 ± 1.0	9.1 ± 0.2
EC2038	161.4 ± 5.0	15.1 ± 0.8
EC2106	150.8 ± 0.9	13.4 ± 0.2

Chapter 6

Validation of Novel Kinetic Method and General Discussion

6.1 Introduction

The present chapter investigates the accuracy of the proposed kinetic analysis introduced in the previous chapter for different types of coal chars. This chapter is divided into four sections. The first two sections evaluate the intrinsic reactivity parameters of the coal chars by use of existing kinetic analysis procedures, in order to verify the accuracy of the proposed method. These conventional approaches include the time-consuming isothermal analysis, and 'kinetic model-free' isoconversional methods (Kissinger and Ozawa-Flynn-Wall). The third section presents a sensitivity analysis on the novel TGA procedure. In this section, the various assumptions underlying this new kinetic analysis are examined. The fourth section concludes on a general discussion to present the merits of the proposed kinetic analysis.

6.2 Isothermal Techniques

6.2.1 Mathematical Analysis

For the carbon-oxygen reaction, the rate equation was defined by a first order global kinetic in equation (3.3-2) as:

$$\frac{d\alpha}{dt} = k(1-\alpha)$$

For the isothermal experiments, the intrinsic rate constant k is constant. Hence, after separation of variables and by considering the initial conditions t = 0, α = 0, the above equation may be integrated as:

Eq. (6.2-1)
$$\int_0^{\alpha} \frac{d\alpha}{1-\alpha} = \int_0^{t} kt$$

Eq. (6.2-2)
$$-ln(1-\alpha) = kt$$

For an isothermal reaction at temperature T_{iso}, the plot of $-ln(1 - \alpha)$ versus t should generate a straight line with the slope equal to the intrinsic rate constant k. For several isothermal reactions, different values of k are obtained. Hence, the Arrhenius equation (2.4-2) may be used for characterising the dependence of the rate constant with temperature. In this way, an Arrhenius plot is generated by considering its linear form:

Eq. (6.2-3)
$$ln\,k = ln\,A - E/RT$$

Thus, for the set of reactivity k at the various isothermal conditions, a plot of $ln\ k$ versus $1/RT$ should produce a straight line, from which the activation energy E and the pre-exponential factor A are deduced from the slope and intercept, respectively.

6.2.2 Experimental Procedure

Isothermal runs were performed in the TGA furnace described in chapter four. These experiments were carried out in dry air (20-v% oxygen) flowing at 25 ml[STP]min^{-1}. The sample was quickly heated, at 50 °C min^{-1}, to the isothermal temperature T_{iso}, and then kept at this temperature for approximately 10 minutes to ensure a maximum of 5 - 10-wt% carbon conversion. At this weight conversion the initial reaction rate may be measured accurately, so that measurements are taken under a chemical control regime. This procedure was repeated for three different temperatures, selected in the range of the ignition temperature T_0 and the maximum temperature for kinetic control T_{MAX} given in section 5.3.3. These isothermal experiments were conducted on the ten different char samples, and were also corrected for buoyancy effects. In addition, each experiment was repeated twice or three times to test reproducibility.

6.2.3 Reactivity Parameters

The resulting plots for deriving the rate constants k are shown in Figure 6.2.1 using equation (6.2-2), for the oxidation of BPL granules in air, as an example. The corresponding Arrhenius plot is given in Figure 6.2.2. This plot provided a satisfactory good fit, as given by the correlation coefficient of the straight line $r^2 > 0.900$. The activation energy E and the pre-exponential factor A, are deduced from the slope and the intercept of this plot, respectively. These results have also been published by Sima-Ella *et al.* (2005). It was found that, the Arrhenius plots for the other chars, provided a better fit, with correlation coefficient $r^2 > 0.900$, as presented in Table 6.2.1. It may be accepted, therefore, that the applied kinetic model is applicable for the oxidation of coal chars within the chemical control regime. The reactivity parameters for all the different chars are listed in Table 6.2.2. These values represent the mean values for both the activation energy and the natural logarithm of the pre-exponential factor, with their associated standard error. It may also be noted that these parameters are in good agreement with those derived using the optimum-heating rate analysis, in Chapter 5.

Table 6.2.1: Rate constant values for the isothermal oxidation of BPL granules in air at various temperatures

Temperature (°C)	Reactivity, k (s^{-1})	Correlation coefficient, r^2
475	3.834×10^{-5}	0.992
500	6.416×10^{-5}	0.992
525	15.578×10^{-5}	0.997
550	25.259×10^{-5}	0.998
575	34.224×10^{-5}	0.999

Table 6.2.2: Reactivity parameters using isothermal analysis for the oxidation of the different char samples in air.

Char samples	E (kJ mol^{-1})	Ln (A, s^{-1})	Correlation coefficient r^2 for the Arrhenius plot
BPL granules	123.3 ± 10.9	9.7 ± 1.7	0.977
BPL crushed	123.1 ± 23.7	9.4 ± 3.6	0.964
Pha Lai	161.9 ± 4.4	16.8 ± 0.7	0.999
Heze	144.6 ± 5.5	14.2 ± 0.9	0.999
Chang Cun	153.3 ± 6.3	15.9 ± 1.1	0.998
Kellingley	139.9 ± 2.6	13.9 ± 0.5	1.000
Colombian	137.7 ± 10.9	12.8 ± 1.8	0.994
PRB	104.6 ± 12.3	7.4 ± 1.9	0.986
EC2038	158.5 ± 14.0	14.8 ± 2.2	0.992
EC2106	152.4 ± 11.0	13.7 ± 1.7	0.995

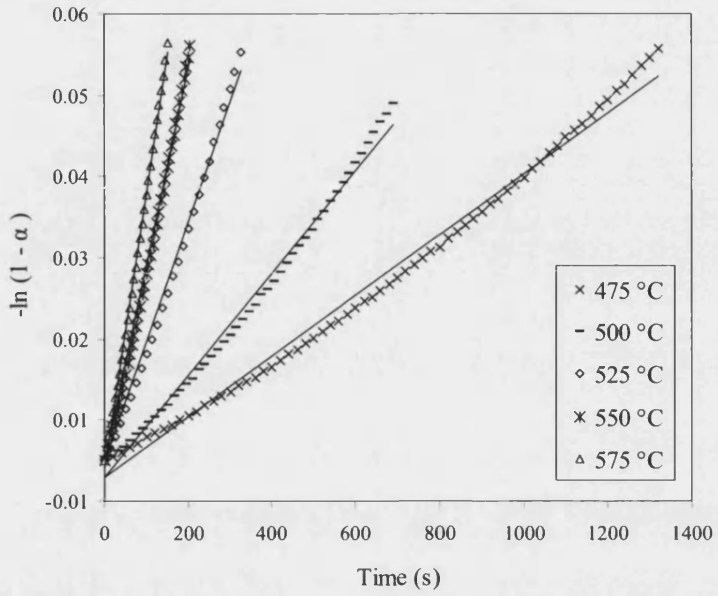

Figure 6.2.1: Determination of the rate constants *k* for various temperatures, through measurement of initial reaction rate according to isothermal method during the oxidation in air of BPL granules

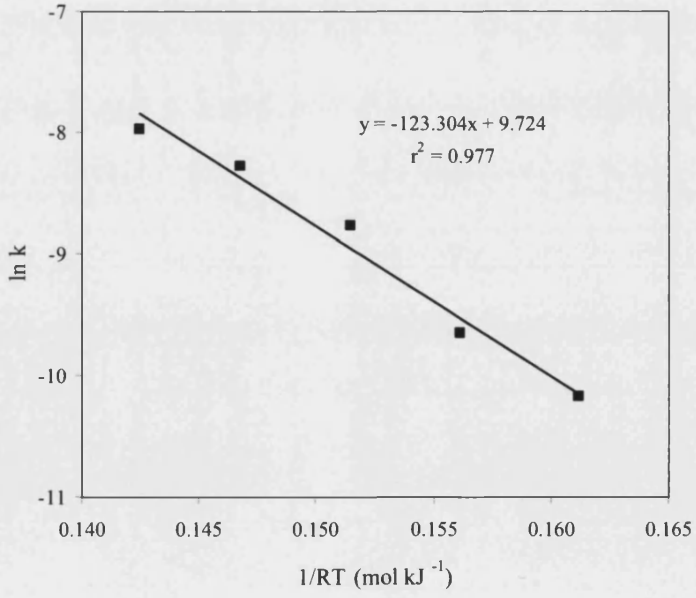

Figure 6.2.2: Determination of reactivity parameters, *E* and *A*, according to isothermal method during the air oxidation of BPL granules.

6.3 Isoconversional Analysis

6.3.1 Kissinger Method

The Kissinger method (1957) was discussed in section 3.2.3. This isoconversional method is still being applied to thermogravimetric data (Chen *et al.* 1993; Mothè Filho 2002; Lopez-Fonseca *et al.* 2005). The mathematical expression is given as in equation (3.2-23):

$$\ln\frac{\beta}{T_\alpha^2} = -\frac{E}{RT_\alpha} + C_1$$

Where the activation energy E is estimated from the slope of $ln(\beta/T^2_\alpha)$ versus $(1/RT_\alpha)$, for a constant conversion α. As previously mentioned, C_1 is a constant, which contains the pre-exponential factor A and the kinetic model $g(\alpha)$. An example of this plot is given in Figure 6.3.1a for the analysis of granular BPL, at various conversions α.

6.3.2 Ozawa-Flynn-Wall Method

The Ozawa-Flynn-Wall method (Ozawa 1965; Flynn and Wall 1966) and is also a very popular isoconversional method still used in thermal analysis studies (Mamleev *et al.* 2004; Lopez-Fonseca *et al.* 2005). The general expression of this method is given as in equation (3.2-24):

$$\ln\beta = -1.052\frac{E}{RT_\alpha} + C_2$$

Where the activation energy E is calculated from the slope of the plot of $ln\ \beta$ versus $1.052/RT_\alpha$. The constant C_2 is a positive constant, which incorporates the kinetic model function and the pre-exponential factor A. An example of this plot is presented in Figure 6.3.1b for the analysis of granular BPL, at various conversions α.

6.3.3 Activation Energy Values

Low carbon conversion α of 3, 5, 8 and 10-wt% were selected in this investigation, in order to perform the isoconversional analysis within the chemical control regime. The resulting mean activation energy values, for all the different coal chars, are presented in Table 6.3.1 and Table 6.3.2 for both the Kissinger and the Ozawa-Flynn-Wall methods. It appears from these tables that the value of activation energy changes with the extent of char conversion α. In some cases, there is no definite trend in the variation (e.g. Heze); whilst, in other instances, there is a continuous decrease in the mean activation energy value with increasing extent of char conversion (e.g. Pha Lai) for the Ozawa-Flynn-Wall method. It is very likely that these two procedures are not entirely isoconversional, since the mean activation energy is not fixed over the char conversion range studied (c.f. section 3.3.1). For this reason, a 5-wt% char conversion is arbitrarily selected as the most convenient, since there are no significant changes in the mean activation energy value at this point (< 10 kJ mol $^{-1}$). In fact, Orfao and Martins (2002) pointed out that these isoconversional methods are highly sensitive to experimental noise in temperature. As observed in section 4.4.2 the measured temperature was always an underestimate of the actual sample temperature at a conversion α. In this way, the calculated activation energy value is always underestimated, and a 95% confidence interval may give a better indication of the actual value. For this reason, the activation energy values for these isoconversional methods are presented in the tables at a char conversion of 5-wt% char conversion with 95% confidence interval.

Table 6.3.1: Mean activation energy values (± 95% confidence interval) derived for various char conversion α using the Kissinger method.

α	Char samples									
(wt %)	BPL (granules)	BPL (powder)	Pha Lai	Heze	Chang Cun	Kellingley	Colombian	PRB	EC2038	EC2106
3	129.5 ± 24.6	130.3 ± 32.6	129.5 ± 0.6	116.2 ± 21.5	143.4 ± 8.3	95.1 ± 13.0	125.0 ± 30.0	132.6 ± 7.8	129.9 ± 29.5	116.9 ± 37.7
5	125.5 ± 31.8	135.8 ± 28.0	129.3 ± 0.4	118.6 ± 19.1	136.1 ± 13.5	111.3 ± 10.2	120.6 ± 28.3	130.6 ± 12.3	127.0 ± 31.7	113.1 ± 44.7
8	117.1 ± 41.5	145.0 ± 20.0	128.5 ± 0.4	120.1 ± 14.7	129.1 ± 32.5	111.8 ± 7.5	114.2 ± 36.0	128.2 ± 26.3	-	-
10	111.9 ± 43.1	154.8 ± 18.7	129.1 ± 3.7	118.5 ± 13.2	123.5 ± 35.8	112.4 ± 12.6	109.5 ± 41.6	124.9 ± 36.3	-	-

Table 6.3.2: Mean activation energy values (± 95% confidence interval) derived for various char conversion α using the Ozawa-Flynn-Wall method.

α	Char samples									
(wt %)	BPL (granules)	BPL (powder)	Pha Lai	Heze	Chang Cun	Kellingley	Colombian	PRB	EC2038	EC2106
3	141.7 ± 24.5	159.3 ± 17.4	140.8 ± 6.1	130.5 ±13.1	134.6 ± 30.2	106.3 ± 13.6	130.4 ± 27.9	137.0 ± 7.0	133.0 ± 27.6	123.2 ± 35.2
5	137.9 ± 31.3	150.2 ± 18.4	137.6 ± 3.0	132.0 ± 14.9	129.4 ± 33.4	122.8 ± 9.7	126.4 ± 26.3	135.3 ± 11.3	135.6 ± 29.7	119.8 ± 41.8
8	129.8 ± 40.8	141.7 ± 26.0	135.7 ± 1.3	130.4 ± 19.4	141.0 ± 12.4	123.5 ± 6.9	120.6 ± 33.5	133.3 ± 24.4	-	-
10	124.7 ± 42.3	136.6 ± 30.3	134.9 ± 3.1	127.7 ± 21.9	147.8 ± 7.4	124.2 ± 12.0	116.2 ± 38.8	130.3 ± 33.9	-	-

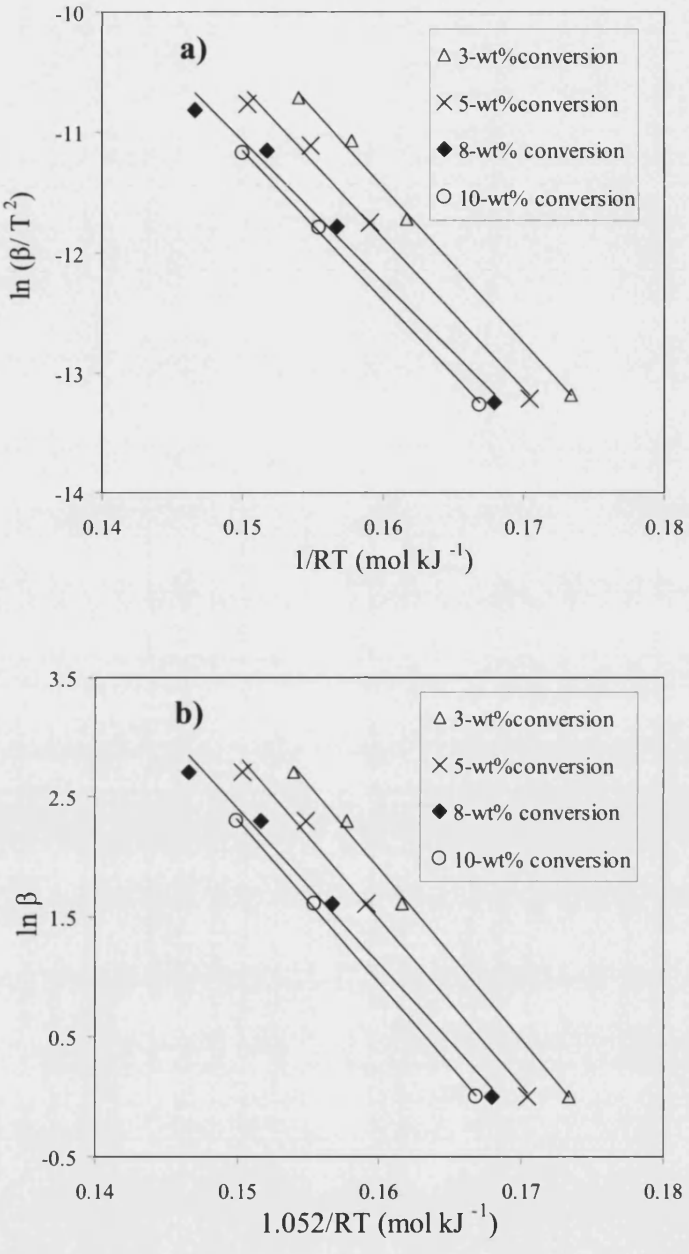

Figure 6.3.1: Isoconversional plots at various carbon conversion for the oxidation in air of granular BPL carbon: a) Kissinger method; b) Ozawa-Flynn-Wall method.

6.4 Sensitivity Analysis: A case study

6.4.1 The Proposed Reactivity Model

The proposed reactivity model was developed through a series of assumptions, which will be tested in this section. Firstly, a global kinetic model was assumed given by equation (2.8-3) as:

$$g(\alpha) = (1-\alpha)^n$$

Then, assuming a first order kinetic model, the reaction rate in equation (3.3-2) was derived as:

$$\frac{d\alpha}{dt} = k(1-\alpha)$$

After mathematical integration, the reactivity model equation was given in terms of the *p(x)* function in equation (3.2-7):

$$F(\alpha) = \int_0^{\alpha} \frac{1}{g(\alpha)} d\alpha = \frac{AE}{\beta R} p(x)$$

Where,

$$p(x) = \int_x^{\infty} \frac{e^{-x}}{x^2} dx \,, x = E/RT$$

In the proposed kinetic analysis, the approximate function of Coats and Redfern (1964) was used, leading to equation (3.4-5) for E/RT >>2:

$$ln\left(\frac{F(\alpha)}{T^2}\right) = ln\left(\frac{AR}{\beta E}\right) - E/RT$$

It is clear that the proposed reactivity analysis is based on three main assumptions: (i) the order of the reaction *n*; (ii) the kinetic model function *g(α)* and; (iii) the approximate function *p(x)*. These three variables are independently tested in the next sections, to ascertain the sensitivity of the proposed kinetic analysis for linear TGA studies. This test is presented for the oxidation in air of BPL granules only, since this material is a suitable model less variable than the coal chars.

6.4.2 Reaction Order Effect

A first order reaction was initially assumed, as is common in the literature. In this section, the reactivity model is tested for different values of reaction order $n \leq 1$. otherwise the rate equation does not describe a decay process for $n > 1$. The integral of the kinetic function $F(\alpha)$ is given as:

Eq. (6.4-1)
$$F(\alpha) = \frac{1}{1-n}(1-\alpha)^{1-n}$$

The reactivity model equation (3.4-5) becomes:

Eq. (6.4-2)
$$ln\left[\left(\frac{1}{1-n}(1-\alpha)^{1-n}\right)/T^2\right] = ln\frac{AR}{\beta E} - E/RT$$

Hence, the activation energy E and pre-exponential factor A are obtained from the slope and intercept of the plot of $ln\ [((1/1-n)(1-\alpha)^{1-n}) / T^2]$ versus $1/RT$, respectively. An example of this plot is given in Figure 6.4.1 for heating rate of 5 °C min^{-1} and 30 °C min^{-1}. At the low heating rates, it was found that the straight lines correlation was not adequate, as their correlation coefficients were very low ($r^2 < 0.900$), with evidence of curving in the lines. At higher heating rates, however, the straight lines fit was more appropriate, with larger coefficient of correlation values. It also appeared that the best fit was obtained at a reaction order $n > 0.9$. It is therefore apparent that the selected kinetic model is the most suitable for describing the carbon-oxygen reaction at the temperature range studied.

6.4.3 Alternative Kinetic Models

Other possible kinetic model functions used in char oxidation were detailed in section 2.8, and include the following:

(i) The shrinking core model

Eq. (6.4-3)
$$F(\alpha) = 1-(1-\alpha)^{1/3}$$

(ii) *A two-dimensional flow diffusion mechanisms*

Eq. (6.4-4) $$F(\alpha)=(1-\alpha)[ln(1-\alpha)]+\alpha$$

(iii) *A three-dimensional flow diffusion model*

Eq. (6.4-5) $$F(\alpha)=\left[1-(1-\alpha)^{1/3}\right]^2$$

Plots of $ln\ [F(\alpha)/T^2]$ versus $1/RT$, at different heating rates, were performed. The activation energy E and the pre-exponential factor A were estimated from the slope and intercept, respectively. It was found that straight lines fitting to these plots were suitable, with high correlation coefficients for all three kinetic model functions. At a rate of heating of 1 °C min^{-1}, however, the correlation was poor, with evidence of curving in the line, as illustrated in Figure 6.4.2. Therefore, these three kinetic models are applicable to the oxidation of carbon with oxygen, at heating rates larger than 1 °C min^{-1}.

The resulting kinetic parameters, from these models, are summarised in Table 6.4.1 and Table 6.4.2. Figure 6.4.3 reveals that the activation energy varies with the rate of heating for all three kinetic models; hence this effect is not dependent on the reaction mechanism. In addition, the activation energy values derived from these kinetic models are very similar to those derived in the proposed analysis with a global kinetic model, except for the diffusion in three-dimension model. This model introduces significant error in the value of activation energy, as being outside the range of those predicted by both the isoconversional analyses (131.7 ± 31.5 kJ mol^{-1}) and the isothermal analysis (123.3 ± 10.9 kJ mol^{-1}). Hence, this model is not appropriate for characterising the oxidation of coal chars in air. The pre-exponential factor values, on the other hand, diverge significantly from the global kinetic model. As indicated in Figure 6.4.4, the other models predict a different compensation effect between the activation energy and the pre-exponential factor.

From these derived kinetic parameters, simulations of weight loss profiles were computed at various heating rates, for each kinetic model function. This procedure was detailed in section 5.5.1. Simulated curves were then plotted and

compared with the experimental data, as illustrated in Figure 6.4.5 for a heating rate of 5 and 20 °C min^{-1}. It appears that the global kinetic model is better than the other kinetic models for simulating the char oxidation process, independently of the heating rate. The other kinetic models always underestimate the fractional char conversion over the temperature range studied.

The RMS value was calculated to assess the goodness of fit of these simulated profiles at different heating rates. This procedure was also detailed in section 5.5.2. As given in Table 6.4.3 and Figure 6.4.9, the errors generated by the global kinetic model are always smaller than those from the other models. It is clear that this model is the most suitable for char oxidation in the kinetic control regime. In addition, there always exists a minimum error, at which simulated data best correspond to the experiments, so that an optimum-heating rate is identified. This optimum-heating rate appears to fall within the same range of 25 – 35 °C min^{-1} for all three kinetic models. It is likely that the optimum-heating rate is related to the TGA instrument, rather than the kinetic analysis.

6.4.4 Alternative p(x) – functions

A series of approximations to the *p(x)* functions were discussed in section 3.2.1. Only the approximate functions, which can be put into a linear form, are discussed in this section. The approximate function of Doyle (1962) and that of Tang *et al.* (2003) are selected for this analysis, as the least and most accurate, respectively. By replacing Doyle's approximation into the reactivity model equation (3.4-5), the following is deduced:

Eq. (6.4-6)
$$ln[-ln(1-\alpha)] = ln\frac{AE}{\beta R} - 5.33 - 1.052\,E/RT$$

On the other hand, Tang *et al.* (2003) approximation, yields the following:

Eq. (6.4-7)
$$ln\left[\frac{-ln(1-\alpha)}{T^{1.89}}\right] = ln\frac{AR^{0.89}}{\beta E^{0.89}} - 0.378 - E/RT$$

The activation energy E and the pre-exponential factor A are obtained from the slope and intercept of $ln[-ln(1-\alpha)]$ versus $1.052/RT$ or $ln[-ln(1-\alpha)/T^2]$ versus $1/RT$. The resulting kinetic parameters are given in Table 6.4.4 and Table 6.4.5. As can be seen in Figure 6.4.7 with different kinetic models, the activation energy value is not affected by the approximate function $p(x)$. In fact, the three functions produce values, which are in statistical agreement. On the other hand, there is a poor agreement on the pre-exponential factor value, from Tang *et al.*(2003). This discrepancy is reflected on a change in the compensation effect as illustrated in Figure 6.4.7.

By using these kinetic parameters, simulations of weight loss were subsequently derived for the different $p(x)$-function, at various heating rates. An example of these simulations is shown in Figure 6.4.8 for a heating rate of 10 and 30 °C min $^{-1}$. It appears that both Coats-Redfern and Doyle approximations generate a better prediction of experimental data than Tang *et al.* approximation, independently of the heating rate. This inadequacy may lie in that the pre-exponential factor values are different, and hence a misrepresentation of the compensation effect. It is clear that Coats-Redfern approximation is the most suitable option, as it provides a correct representation of the char oxidation process; and also, their approximation provides a higher accuracy in the activation energy value compare to Doyle 's $p(x)$-function.

The computed RMS values are summarised in Table 6.4.6, which represent the error in conversion α between the predicted values and the experimental data. It appears that a minimum error always exists. As can be seen in Figure 6.4.10, this minimum error is observed at a similar range of heating rate of 25 and 35 °C min $^{-1}$; suggesting that the optimum-heating rate is also independent of the kinetic analysis used. It is possible, however, that this optimum-heating rate depends on the type of TGA instrument.

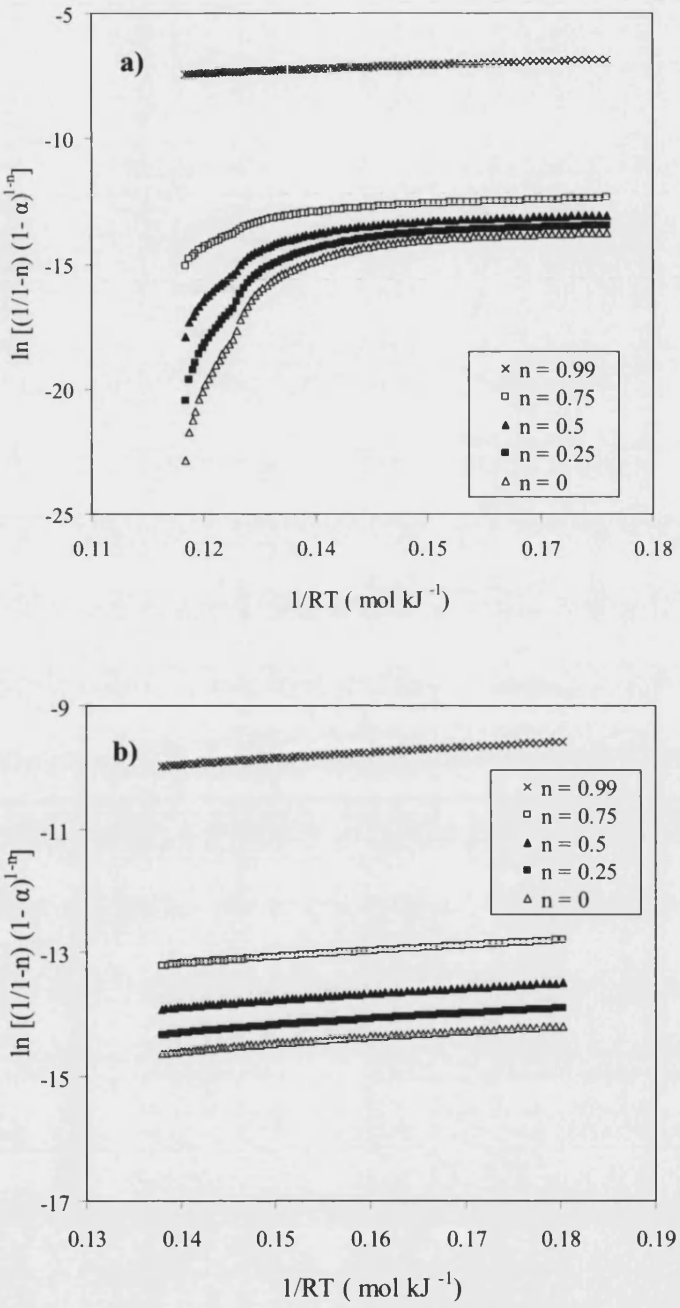

Figure 6.4.1: Effect of reaction order on the kinetic parameters of BPL granules at a heating rate of a) 5° C min^{-1} and; b) 30 °C min^{-1}.

Table 6.4.1: Mean activation energy (± standard error, kJ mol $^{-1}$) values derived for different kinetic models

Heating rate, °C min^{-1}	Activation energy values (kJ mol $^{-1}$)		
	Shrinking core model	Diffusion in 2D model	Diffusion in 3D model
1	199.6 ± 5.2	150.1 ± 7.6	414.0 ± 10.2
5	189.5 ± 2.8	182.7 ± 3.2	393.9 ± 5.2
10	171.8 ± 2.6	168.6 ± 2.8	358.5 ± 5.2
15	155.6 ± 2.0	155.6 ± 2.0	325.9 ± 3.6
20	136.3 ± 1.6	134.7 ± 1.8	284.1 ± 3.4
30	123.4 ± 2.0	122.1 ± 2.0	261.4 ± 4.2
50	93.3 ± 1.2	92.3 ± 1.2	201.2 ± 2.4

Table 6.4.2: Mean values of the natural logarithm of the pre-exponential value (± standard error) derived for different kinetic models

Heating rate, °C min^{-1}	ln (A, s^{-1})		
	Shrinking core model	Diffusion in 2D model	Diffusion in 3D model
1	21.4 ± 0.0	14.1 ± 0.1	51.1 ± 0.0
5	17.8 ± 0.0	17.7 ± 0.0	43.9 ± 0.0
10	14.3 ±0.0	14.8 ± 0.0	37.1 ± 0.0
15	11.2 ± 0.0	11.9 ± 0.0	30.9 ± 0.0
20	8.0 ± 0.1	8.8 ±0.1	24.7 ± 0.0
30	5.6 ± 3.2	6.5 ± 0.3	20.0 ± 0.0
50	0.6 ± 0.0	1.5 ± 0.0	10.2 ± 0.1

Table 6.4.3: Root mean square values in the fit of calculated thermogravimetric profiles with the experimental data of the oxidation of BPL granules at various heating rates for different kinetic models.

Heating rate, °C min^{-1}	Root mean square values (%)		
	Shrinking core model	Diffusion in 2D model	Diffusion in 3D model
1	5.23%	5.87%	5.77%
5	3.49%	4.17%	4.18%
10	2.47%	2.56%	2.33%
15	1.48%	1.57%	1.37%
20	1.18%	1.19%	1.02%
30	0.93%	0.94%	0.87%
50	0.95%	0.95%	0.88%

Table 6.4.4: Mean activation energy values (± standard error, kJ mol^{-1}) derived for different approximate functions of p(x).

Heating rate, °C min^{-1}	Activation energy values (kJ mol^{-1})		
	Coats-Redfern	Doyle	Tang et al.
1	218.2 ± 2.1	219.7 ± 4.0	218.9 ± 4.2
5	190.6 ± 1.3	193.5 ± 2.4	191.3 ± 2.6
10	171.8 ± 1.3	175.6 ± 2.4	172.6 ± 2.6
15	155.6 ± 1.0	160.2 ± 1.8	155.9 ± 1.9
20	135.9 ± 0.8	141.3 ± 1.6	136.6 ± 1.7
30	122.9 ± 1.0	128.8 ± 2.0	123.6 ± 2.1
50	93.0 ± 0.6	100.0 ± 1.1	93.3 ± 2.4

Table 6.4.5: Arithmetical mean values of the natural logarithm value of the pre-exponential factor (± standard error) derived for different approximate functions of p(x).

Heating rate, °C min^{-1}	ln (A, s^{-1})		
	Coats-Redfern	Doyle	Tang et al.
1	24.9 ± 0.0	25.20 ± 0.0	25.01 ± 0.0
5	19.9 ± 0.0	20.50 ± 0.0	18.47 ± 0.0
10	16.9 ± 0.0	17.71 ± 0.0	14.79 ± 0.0
15	14.4 ± 0.0	15.23 ± 0.0	11.66 ± 0.0
20	11.3 ± 0.0	12.45 ± 0.0	8.42 ± 0.0
30	9.3 ± 0.4	10.66 ± 0.0	6.06 ± 0.3
50	4.7 ± 0.0	6.64 ± 0.0	1.04 ± 0.0

Table 6.4.6: Root mean square values in the fit of calculated thermogravimetric profiles with the experimental data of the oxidation of BPL granules at various heating rates for different approximate functions of p(x).

Heating rate, °C min^{-1}	Root mean square values (%)		
	Coats-Redfern	Doyle	Tang et al.
1	1.20%	19.73%	1.95%
5	0.87%	1.22%	5.42%
10	0.62%	0.65%	2.92%
15	0.46%	0.26%	1.64%
20	0.17%	0.08%	1.26%
30	0.07%	0.08%	0.97%
50	0.16%	0.09%	0.99%

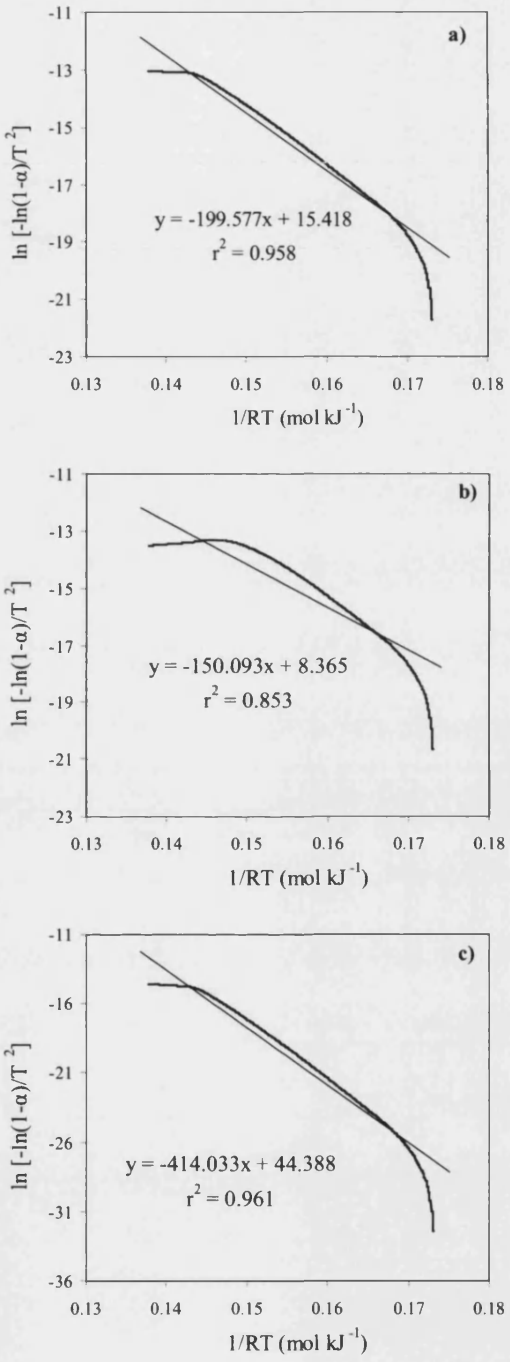

Figure 6.4.2: Fitting of the kinetic model in the oxidation profile of BPL granules at 1 °C min^{-1} using a) shrinking core model; b) 2-dimensional diffusion model and ; c) 3-dimensional diffusion model.

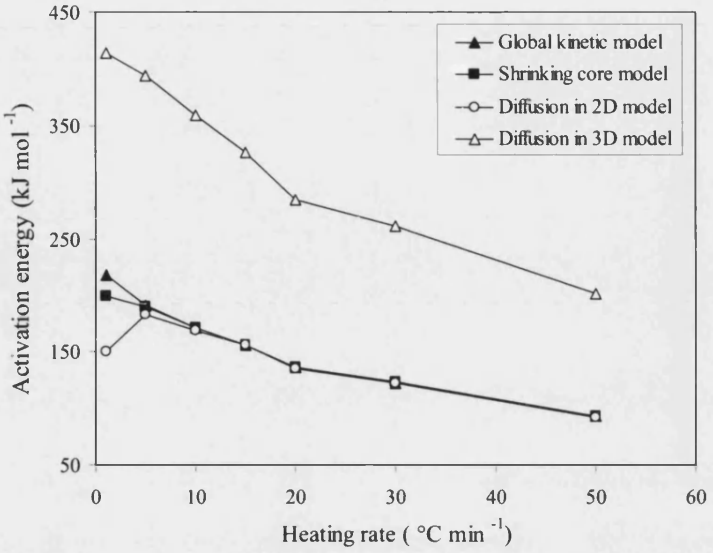

Figure 6.4.3: Effect of heating rate on the activation energy value for the oxidation in air of BPL granules using different kinetic models.

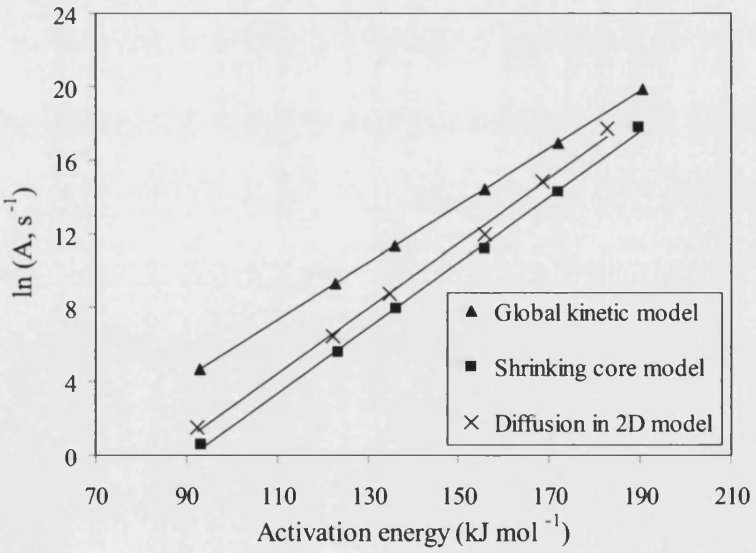

Figure 6.4.4: Effect of different kinetic models on the compensation relationship for the oxidation in air of BPL.

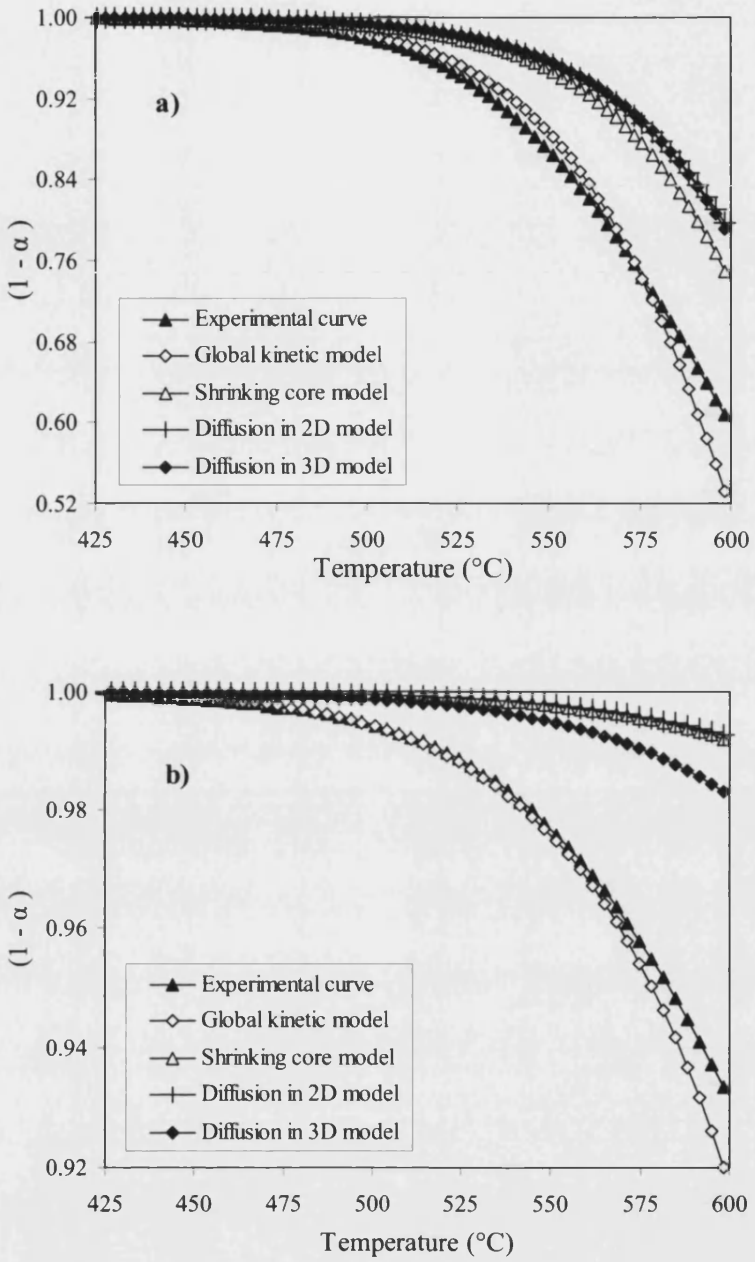

Figure 6.4.5: Comparison between experimental and simulated weight loss profiles for the oxidation of BPL granules using different kinetic model: a) 5 °C min^{-1} and; b) 20 °C min^{-1}.

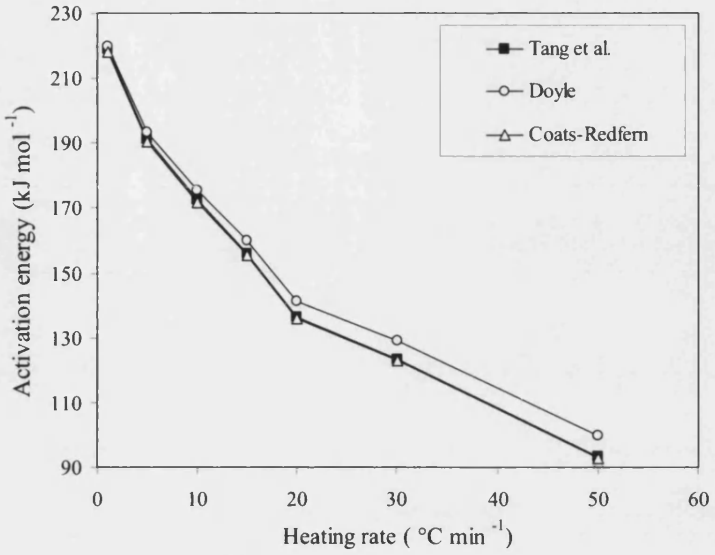

Figure 6.4.6: Effect of heating rate on the activation energy value for the oxidation in air of BPL granules using different approximate functions of p(x).

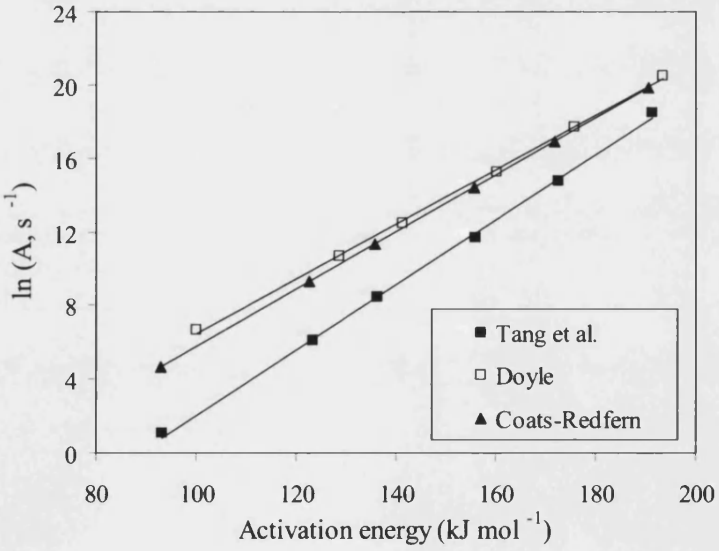

Figure 6.4.7: Effect of different approximate functions of p(x) on the compensation relationship for the oxidation in air of BPL.

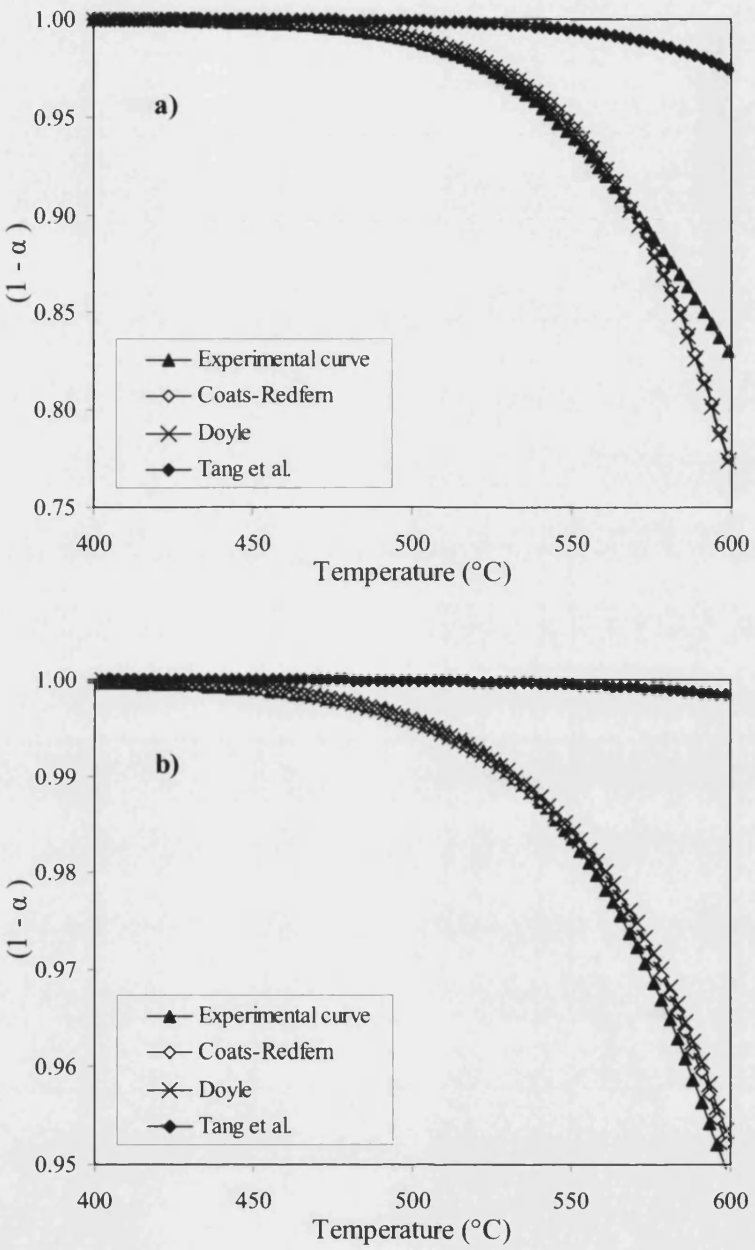

Figure 6.4.8: Comparison between experimental and simulated weight loss profiles for the oxidation of BPL granules using different approximate functions of p(x) a) 10 °C min^{-1} and; b) 30 °C min^{-1}.

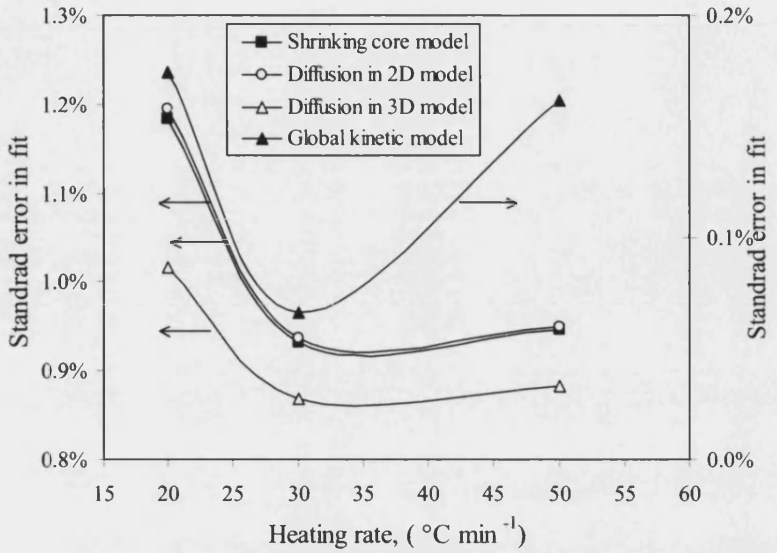

Figure 6.4.9: Enlarged view of the variation in standard error with heating rate, in the fit of burnout profiles between simulated and experimental data for the oxidation of BPL granules using different kinetic models.

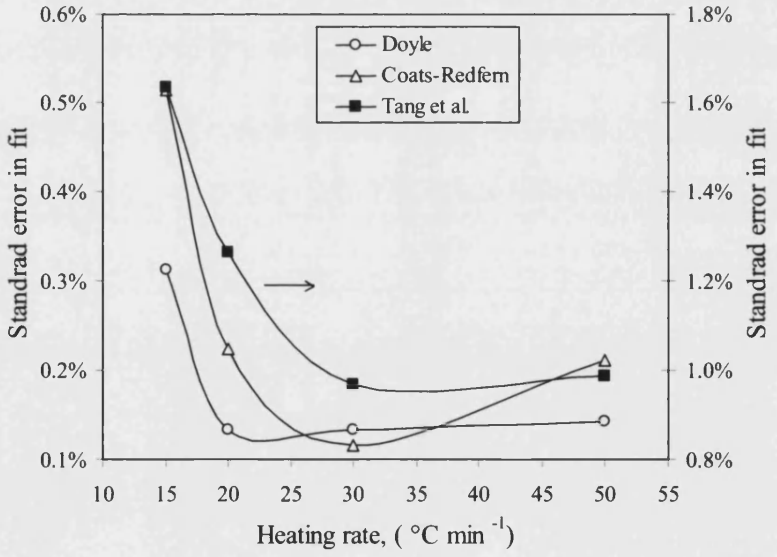

Figure 6.4.10: Enlarged view of the variation in standard error with heating rate in the fit of burnout profiles between simulated and experimental data for the oxidation of BPL granules using different approximation to the function p(x).

6.5 General Discussion

6.5.1 Validation of the Proposed kinetic Analysis

It appears that the activation energy values derived by both the isoconversional and isothermal analyses fully coincide with those predicted by the proposed kinetic analysis at the optimum-heating rate as shown in Table 6.5.1. In addition, those results correspond with those presented in the literature for similar materials, as given in Table 6.5.2. The novel method, nonetheless, presents a higher degree of accuracy than the other techniques. It may be concluded therefore that the novel kinetic analysis is more accurate and simpler than existing techniques for deriving the intrinsic reactivity parameters of a chemical process.

6.5.2 Optimum-Heating Rate and Char Types

The existence of an optimum heating rate appears to be independent of the assumptions postulated in the proposed kinetic analysis: this optimum-heating rate is unrelated to the kinetic model $g(\alpha)$, and the approximation $p(x)$. In addition, it was found that this optimum heating rate was independent of the types of char and particle size. It is highly possible that the optimum-heating rate is an instrumental factor, so that each TGA instrument possesses an optimum-heating rate range at which true kinetic data are obtained. In this way, only one single experimental TGA run is required once this optimum-heating rate has been established. As Vyazovkin (2001a) pointed out, errors in quoted activation energy values are often due to the experimental process. Hence, this novel TGA technique, which efficiently identifies an optimum-heating rate, is an invaluable tool for measuring the true activation parameters of a coal char oxidation process.

Furthermore, the optimum-heating rate analysis may be used to identify the reaction mechanism of a chemical process. It emerged that different chars presented different RMS values when comparing simulated and experimental burnout profiles. For most of the chars studied, the RMS value was smaller than 0.1%; whereas, for other chars such as Heze and PRB, the minimum RMS value

was significantly larger. The large RMS error indicates that the kinetic model selected is not entirely suitable, so that a different kinetic model would provide a better representation of the burnout profile. As a subbituminous coal, PRB char would most probably oxidise with a different reaction mechanism. In addition, it is possible that the high ash level in Heze char may play a critical catalytic role in the oxidation profile, so that a different kinetic model applies. Nonetheless, these different kinetic models do not affect the value of the activation energy, as observed in the previous sections. Hence, it is apparent that the optimum-heating rate analysis could be used to accurately estimate the activation energy value, and at the same time assess the validity of the selected kinetic model.

6.5.3 Kinetic Parameters as Index for Materials Comparison

The intrinsic reactivity of coal chars has widely been used as a measure of comparing different materials. This measure is sometimes represented as the maximum or overall reaction rate $(d\alpha/dt)_{max}$, evaluated under an arbitrary heating rate (Tang *et al.* 2005). The kinetic parameters E and A, however, may provide a better comparative index for coals of different rank. As an example, the activation energy E alone is mentioned in this section, since it correlates linearly with the pre-exponential factor A, as noted in section 5.4.3. In Figure 6.5.1, both the activation energy and the maximum reaction rate are plotted against the rank of the parent coal. It appears from the figure that activation energy gives a better indication of the change in reactivity with the type of coals. A correlation may be drawn, suggesting that coals with more than 75-wt% carbon (daf) possess a similar activation energy during oxidation in air. On the other hand, there is no obvious relationship between the type of coal and the maximum reaction rate. In addition, a linear relationship may be established between the activation energy of the char and the elemental carbon content of the coal, as illustrated in Figure 6.5.2; whereas, there is still no correlation with the maximum reaction rate. From these observations, it appears that activation energy of char oxidation increases with increasing coal rank. This conclusion, however, cannot be extracted from the maximum reaction rate data. It is clear that the activation energy is a better

measure for comparing different coals. It is not surprising, nonetheless, that activation energy increases with coal rank. As presented in section 2.3.3, a highly ordered carbon structure is more difficult to break up, and therefore requires a higher energy of activation. However, both EC2038 and EC2106 chars have larger activation energy values than the coal chars of higher rank. This discrepancy may lie in that the intrinsic reactivity of the char is more dependent on maceral content rather than coal rank, as pointed out by Alonso *et al.* (2001b). They observed that the activation energy value of the char upon oxidation decreases in the sequence: vitrinite-rich high rank coal, to inertinite rich coal, followed by vitrinite-rich low rank coals. Hence, it is possible that EC2038 coal has a larger vitrinite content compared to the other anthracite coals; whereas, EC2106 coals has a larger inertinite content than the other bituminous coals. In fact, southern hemisphere coals, such as EC2106, generally consist of high inertinite maceral coals (Lester and Cloke 1999; Magasiner *et al.* 2002).

6.5.4 Kinetic Parameters and Material Structure

It was observed in section 2.4.1 that the intrinsic reactivity of coal chars is strongly related to the structure of the material. This characterisation is examined in this section in terms of the activation energy and the surface area of the unreacted char. As previously mentioned, this discussion is based on the activation energy alone, although it is possible to correlate directly with the pre-exponential factor. The activation energy of the char is plotted against both the internal and microporous surface area, in Figure 6.5.3. It emerges from the figure that activation energy decreases with increasing surface area, implying that chars with a low surface area require a higher energy of activation before they can react. A larger available surface means that more active sites posses the minimum kinetic energy for the reaction to take place, as established in sections 2.3.3 and 2.3.4. In this way, the activation energy required to start the reaction is reduced.

These linear correlations are somewhat typical of carbonaceous materials within the chemical control regime, as pointed out by Arenillas *et al.* (2004a). For this

reason, they may be used to predict the reactivity of a coal char in air. It may be noted that few scattered points arise in these linear correlations. For BET surface area, both the Australian char (EC2106) and the Colombian char fail to follow the linear trend. As southern hemisphere coals, it is possible that these chars have a high inertinite content, which cannot be depicted by BET surface area measurements. For microporous surface area, only the activation energy of EC2106 char upon oxidation is outside the linear correlation. Since Colombian coal is located at the edge of the southern hemisphere, it is very likely that its inertinite content is significantly lower than that of the Australian coal (EC2106). In this way, microporous surface area measurements may have a larger tolerance of inertinite content than BET measurements.

It may be concluded, therefore, that the degree of precision in the activation energy value has led to a correlation with structural properties. This relationships could be useful in predicting and understanding structural changes of the char during combustion processes under kinetics control regime, as suggested by other researchers (Chen *et al.* 2004).

Table 6.5.1: Comparison of activation energy values (kJ mol $^{-1}$, ± standard error) derived by the proposed kinetic analysis with those obtained using existing kinetic analysis methods.

Char samples	Proposed analysis	Isothermal analysis	Kissinger Method	Ozawa-Flynn-Wall method
BPL granules	122.4 ± 7.0	123.3 ± 10.9	125.5 ± 31.8	137.9 ± 31.3
BPL powder	123.6 ± 5.8	123.1 ± 23.7	135.8 ± 28.0	150.2 ± 18.4
Pha Lai	157.5 ± 2.4	161.9 ± 4.4	129.3 ± 0.4	137.6 ± 3.0
Heze	152.1 ± 2.1	144.6 ± 5.5	118.6 ± 19.1	132.0 ± 14.9
Chang Cun	147.3 ± 2.6	153.3 ± 6.3	136.1 ± 13.5	129.4 ± 33.4
Kellingley	141.7 ± 2.1	139.9 ± 2.6	111.3 ± 10.2	122.8 ± 9.7
Colombian	138.3 ± 3.5	137.7 ± 10.9	120.6 ± 28.3	126.4 ± 26.3
PRB	108.6 ± 1.0	104.6 ± 12.3	130.6 ± 12.3	135.3 ± 11.3
EC2038	161.4 ± 5.0	158.5 ± 14.0	127.0 ± 31.7	135.6 ± 29.7
EC2106	150.8 ± 0.9	152.4 ± 11.0	113.1 ± 44.7	119.8 ± 41.8

Table 6.5.2: Literature values of activation energy of various chars determined in the kinetic controlled region during air oxidation.

Coal char type	Comparable sample	Activation energy (kJ mol $^{-1}$)	Reference
Anthracite	Pha lai, Heze, Chang Cun, EC2038	151 - 167	Smith (1978)
Semianthracite (China)	Heze, Chang Cun	150 ± 4	Chen *et al.* (2004)
Bituminous coal char	Kellingley, Colombian	134	Smith (1978)
Bituminous (USA) Bituminous (UK)	Kellingley	137 142	Hecker *et al.* (2003) Field (1970) cited by Smith (1982)
Bituminous (Columbia)	Colombian	132	Feng *et al.* (2003)
Subbituminous (USA)	PRB	110	Hecker *et al.* (2003)
Microporous carbons	BPL	130	Floess et al (1991) cited by Russell *et al.* (1998)
Carbon Black	BPL	132 ± 3	Lopez-Fonseca *et al.* (2005)
Series of chars	All materials	130 - 175	Trangmar (1989) cited by Russell *et al.* (1998)
Series of chars	All materials	143 ± 43	Varhegyi *et al.* (2001)

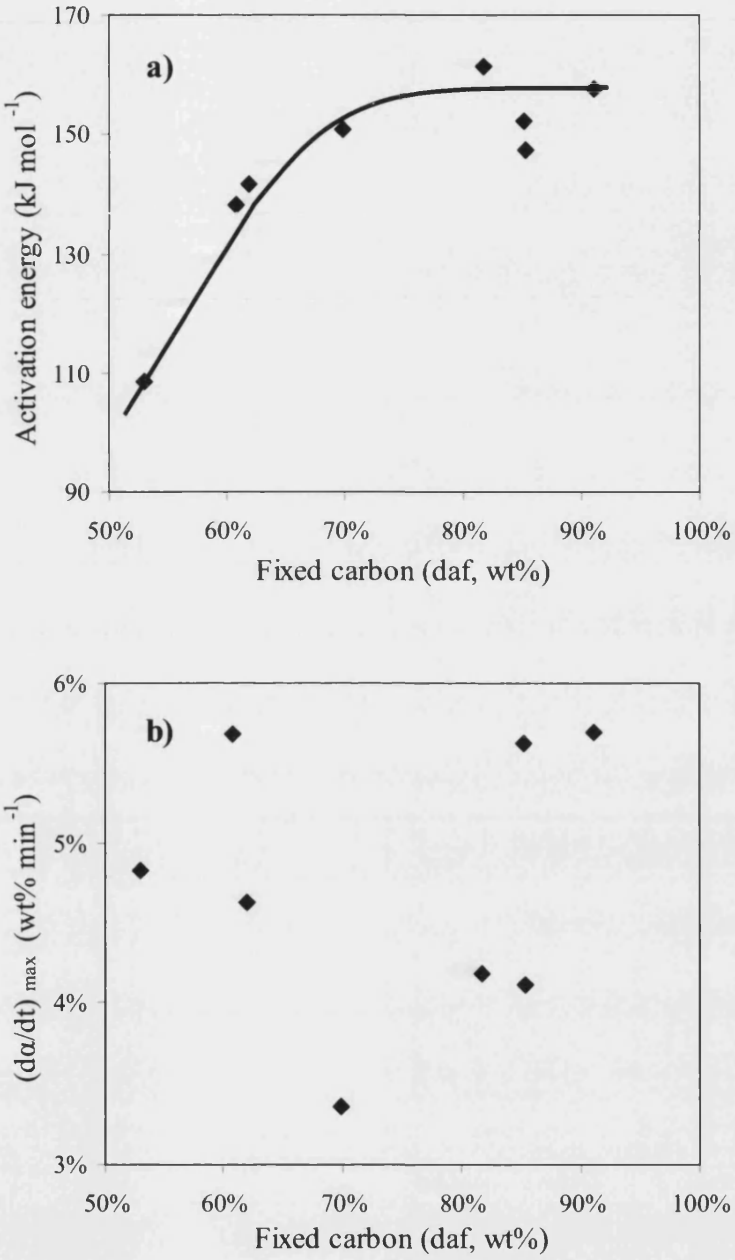

Figure 6.5.1: Evaluation of different reactivity index as a measure of comparing different coal chars in terms of the fixed carbon content of the parent coal: a) activation energy and; b) maximum reaction rate and at 30 °Cmin^{-1}.

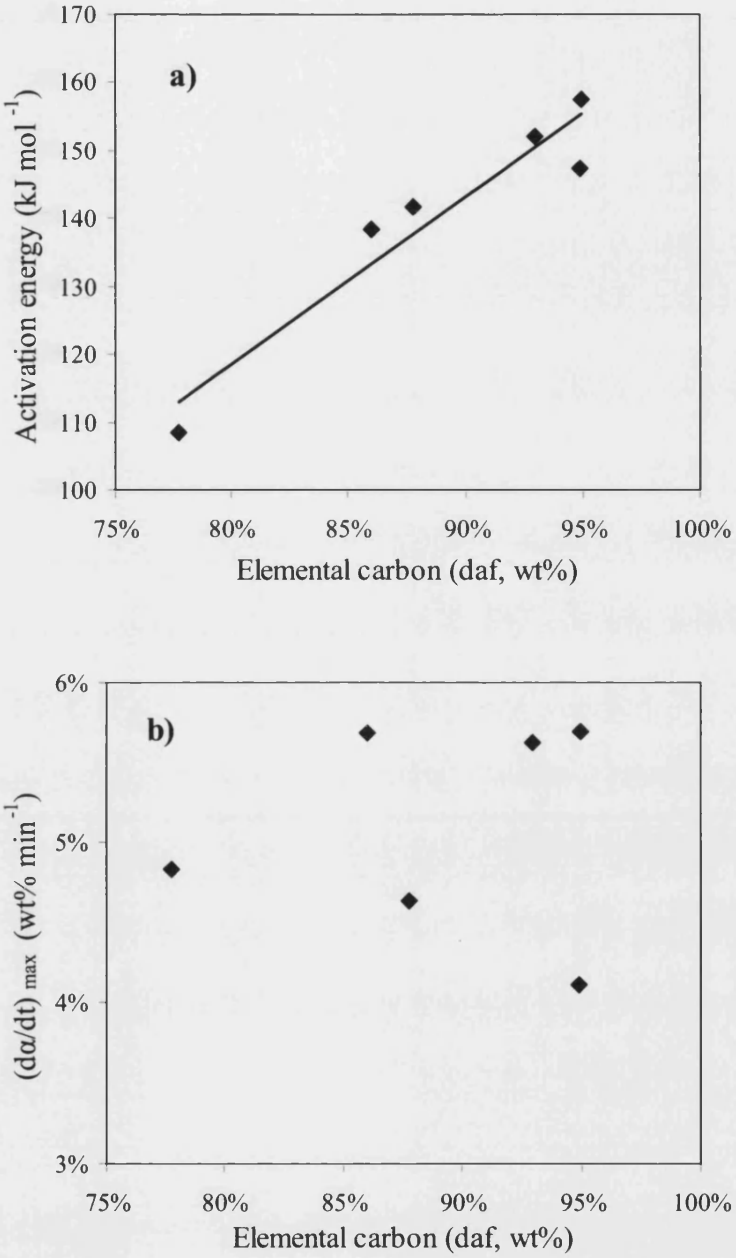

Figure 6.5.2: Evaluation of different reactivity index as a measure of comparing different coal chars in terms of elemental carbon composition of the parent coal: a) activation energy and; b) maximum reaction rate and at 30 °Cmin^{-1}.

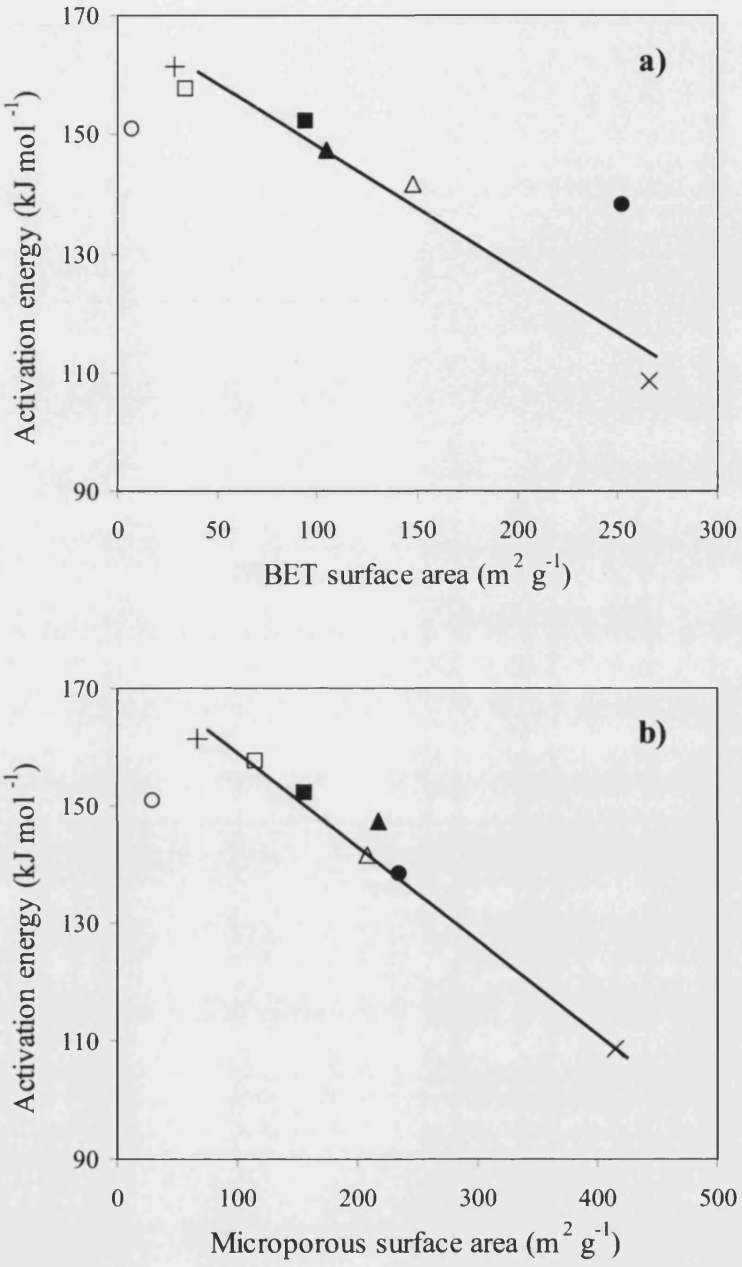

Figure 6.5.3: Relation between activation energy during oxidation in air and the structural properties of the char: a) elemental carbon content; b) microporous surface area for the different coal chars: (□) Pha Lai; (■) Heze; (▲) Chang Cun; (Δ) Kellingley; (●) Colombian; (x) PRB; (+) EC2038; (○) EC2106.

Chapter 7

Sample Controlled Thermal Analysis of Coal Chars

7.1 Introduction

Although, sample controlled thermal analysis (SCTA) are a common focus of thermal analysis today, these novel techniques are still not applied in the coal industry (Sorensen 2003b; Criado and Perez-Maqueda 2005). The main reason may lie in that the applications of SCTA have not fully been developed for evaluating the kinetic parameters of a chemical process. In this chapter the use of SCTA methods is reviewed in order to provide a new insight into coal char characterisation. This chapter is divided into five parts. The first section presents the underlying problems of existing SCTA methods, with respect to the kinetic analysis. In the second section, a novel method is developed, which is derived from one of the existing SCTA approach. The third and fourth sections deal with the implementation of this novel technique based on a model material (BPL granules), in order to assess the accuracy of the kinetic analysis. Once this methodology has been fully established, it is subsequently applied to the industrial coal chars in the final section of this chapter.

7.2 Review of Kinetic Parameters using SCTA

7.2.1 Constant Rate Thermal Analysis (CRTA)

As described in section 2.6.3, in constant rate thermal analysis (CRTA) methods the temperature is controlled in such a way to maintain the reaction rate constant. The reaction rate for char oxidation was given in equation (3.3-2), by introducing the Arrhenius equation for the rate constant *k*:

Eq. 7.2-1
$$\frac{d\alpha}{dt} = (1-\alpha)A\exp\left(-E/RT\right)$$

In this case, however, the reaction rate is maintained constant to a value C = dα/dt, so that the above equation may be rewritten as:

Eq. 7.2-2
$$C = (1-\alpha)A\exp\left(-E/RT\right)$$

Taking the natural logarithm of the above equation yields:

Eq. 7.2-3
$$-\ln(1-\alpha) = \ln\left(\frac{A}{C}\right) - E/RT$$

Both the activation energy *E* and the pre-exponential factor *A* may be determined from linear plots of $-ln(1-\alpha)$ versus $1/RT$, from the slope and intercept respectively. However, a single CRTA curve may lead to erroneous kinetic parameters, which may depend on the selected value of the reaction, rate constant *C*. In order to eliminate this dependence on the reaction rate value, Perez - Maqueda *et al.* (1996) have considered taking the first derivative of equation (7.2-2), leading to the following:

Eq. 7.2-4
$$\frac{1}{(1-\alpha)}\left(\frac{d\alpha}{dT}\right) = -E/RT^2$$

By rearranging the above equation, the following is derived:

Eq. 7.2-5
$$T^2\frac{d\alpha}{dT} = -\frac{E}{R}(1-\alpha)$$

A plot of the left-hand side of the above equation versus (1 - α) is independent of the reaction rate constant C, and the activation energy is deduced from the slope. Determination of the pre-exponential factor A, however depends on the value of the reaction rate C. For this reason, Gotor *et al.*(2000) have suggested the use of master plots, which identify the kinetic parameters by combining various reaction rate C values. This method, nonetheless, is complicated and can be time-consuming, and also, they use of the rate of weight change $d\alpha/dT$. However, numerical differentiation is very dependent on experimental noisy. It is clear that CRTA methods are inadequate for evaluating the activation energy E and the pre-exponential factor A.

7.2.2 Rate Jump Controlled Thermal Analysis

The rate-jump method was developed to make the evaluation of kinetic parameters simpler. The reaction rate is imposed a value C_1 at a constant temperature T_1, then the temperature is abruptly changed T_2. and the reaction rate values jump to a constant C_2. For each reaction rate constant C_1 and C_2, equation (7.2-2) is rewritten as:

Eq. 7.2-6
$$\ln C_1 = \ln A(1-\alpha) - E/RT_1$$

Eq. 7.2-7
$$\ln C_2 = \ln A(1-\alpha) - E/RT_2$$

By assuming that the extent of conversion α is not significantly changed during the temperature jump, the activation energy E of the process is therefore deduced by combining both equation (7.2-6) and equation (7.2-7) as:

Eq. 7.2-8
$$E = \frac{RT_1T_2}{(T_2 - T_1)} \ln \frac{C_1}{C_2}$$

It is clear from the above equation that determination of the activation energy is dependent on the values of C_1 and C_2, but also on the assumption of a constant conversion α, which may vary in practice.

7.2.3 Stepwise Isothermal Analysis (SIA)

As discussed in section 2.6.3, SIA technique is a combination of isothermal steps in a single linear heating process, so that the reaction rate oscillates between a maximum and a minimum imposed value. Since the idea is to consider only the isothermal stages, the kinetic analysis is similar to that of an isothermal process, which was presented in section 6.2.1. Thus, the kinetic parameters are obtained by means of equation (6.2-3):

$$\ln k = \ln A - E/RT$$

During SIA oxidation, however, the isothermal steps may have a short duration, and hence these steps combined with the heating stage. In this way, it becomes difficult to separate these isothermal reactions. The isothermal kinetic analysis thus becomes inadequate since the temperature is not entirely constant. In fact, Sorensen (2003c), who introduced the SIA technique in the late seventies, recently observed that accurate kinetic parameters cannot be derived by this method.

7.3 Development of Step-ramp Analysis

7.3.1 Principles

It is clear that current SCTA methods are not adequate for deriving accurate kinetic parameters. However, the SIA method may in principle be very useful in deriving both the activation energy E and the pre-exponential factor A from a single experimental run. In order to clearly identify each isothermal step, however, the temperature should be forced to remain constant for an identified period of time. After this isothermal step, the temperature may be increased linearly usually, so that the overall process takes place at clearly defined isothermal reactions. This technique may be termed step-ramp oxidation as it combines isothermal step in a single linear temperature increase, as shown in Figure 7.3.1. The duration of each isothermal step is to be determined by a series

of optimisation methods. A similar idea has recently been proposed by Sorensen (2003c), who suggested that, after a maximum of 10-wt% conversion the temperature should be forced to increase to 5 °C. He referred to this alternative method as forced stepwise isothermal analysis (FSIA).

It is clear that the step ramp method is an alternative to the FSIA, with the benefit that both the temperature increase and overall weight loss are not restricted to a specific value. In fact, a 5 °C temperature increase is very small and difficult to conduct on a thermogravimetric analyser without significant temperature overshooting. Also, maintaining the overall weight loss below 10-wt% is difficult. In the step ramp oxidation, however, these parameters may be optimised in order to obtain accurate kinetic parameters. The weight loss is monitored by adjusting the heating rate β applied to the transition between each isothermal step, the temperature interval ΔT between each isothermal step, and the duration of each isothermal steps Δt.

7.3.2 Experimental Procedure

All step ramp oxidation experiments were performed in the thermogravimetric analyser as described in chapter four. The temperature programme, however, differs. Approximately 30 mg of char was reacted with dry air, containing 20-v% oxygen, flowing at 25 ml min^{-1} [STP]. The temperature programme consisted of a fast heating stage of 40 °C min^{-1} to reach the first isothermal step, and then, a desired step ramp programme was applied. This step ramp programme specified the duration of each isothermal step, the heating rate employed to move from one isotherm to the next, and the temperature interval between each isotherm. At the beginning of each isotherm the weight of the sample is tared, in order to monitor the overall weight change of the particular isothermal step. The final temperature of the analysis was selected as the one derived in section 5.3.3 for ensuring kinetic control. Each experiment was repeated twice or three times and showed good reproducibility. An example of such a step ramp oxidation procedure together with the resulting weight loss profile is shown in Figure 7.3.2, in the case of

granular BPL. In this case, each isothermal step was allowed to proceed for 15 minutes, and the temperature was raised every 50 °C at a rate of 25 °C min^{-1}. The weight change has been converted to extent of conversion α. These data are used for the kinetic analysis as presented in the next section. The different isothermal steps have been numbered from 1 to 5.

7.3.3 Kinetic Analysis

The kinetic analysis for a step ramp process is similar to that of an isothermal reaction discussed in the previous chapter. For each isothermal temperature T_i, the rate constant k_i, is calculated from the linear plot of equation (6.2-2):

Eq. (7.3-1) $$-ln(1-\alpha) = k_i t$$

The goodness of fit of the above equation is measured by the correlation coefficient r^2. Good linearity is considered when $r^2 > 0.990$. As an example, the rate constants for the experiment in Figure 7.3.2 are evaluated in Figure 7.3.3. The correlation coefficients of these linear plots are also given in the figure. It is clear from Figure 7.3.3 that isotherms at 400 °C and 600 °C are not linear. At 400 °C, it is most likely that the oxidation process has not started; whereas at 600 °C, the amount of weight loss is excessive for equation (7.3-1) to be verified. Hence, for the isotherm at 600 °C, only the first part of the weight loss curve may be considered, for which the correlation coefficient $r^2 = 0.990$. At this point, the overall weight loss approximates 60-wt% instead of 91-wt%, originally. Therefore, it is important that weight loss during each isothermal step is kept to a minimum. Once the rate constants k_i have been determined, they can now be incorporated into an Arrhenius equation in order to evaluate the kinetic parameters as in equation (6.2-3):

Eq. 7.3-2 $$ln\, k_i = ln\, A - E/RT_i$$

The activation energy E and the pre-exponential factor A are derived from the slope and intercept, respectively, of the plot of $ln\ k_i$ versus $1/RT_i$. Figure 7.3.4

illustrates the resulting Arrhenius plot of the step ramp oxidation of BPL granules in air. In this case E = 161.1 ± 6.4 kJ mol^{-1} and ln A = 15.8 ± 0.1. It may be noted, at this stage, that these kinetic parameters differ considerably from those derived using existing thermogravimetric techniques, and presented in section 6.2 and section 5.5.4. It is possible, therefore, that the kinetic analysis of a step ramp process is affected by the size of the isothermal step, the heating rate employed between each step and the temperature interval between each isotherm. The effects of these three parameters on the kinetic analysis are investigated in the next section.

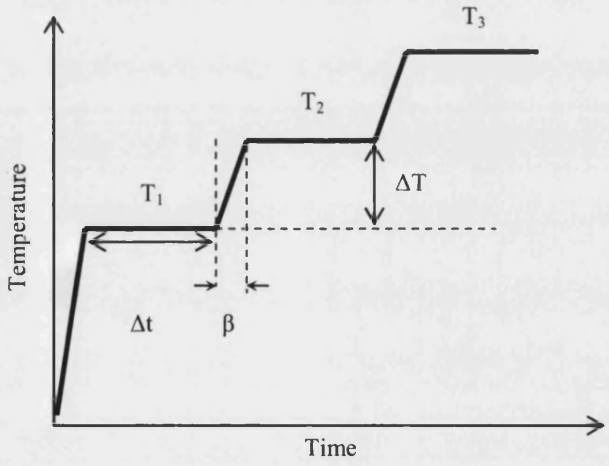

Figure 7.3.1: Schematic of the different controlling parameters (β, ΔT, Δt) required in the temperature programme of a step-ramp reaction.

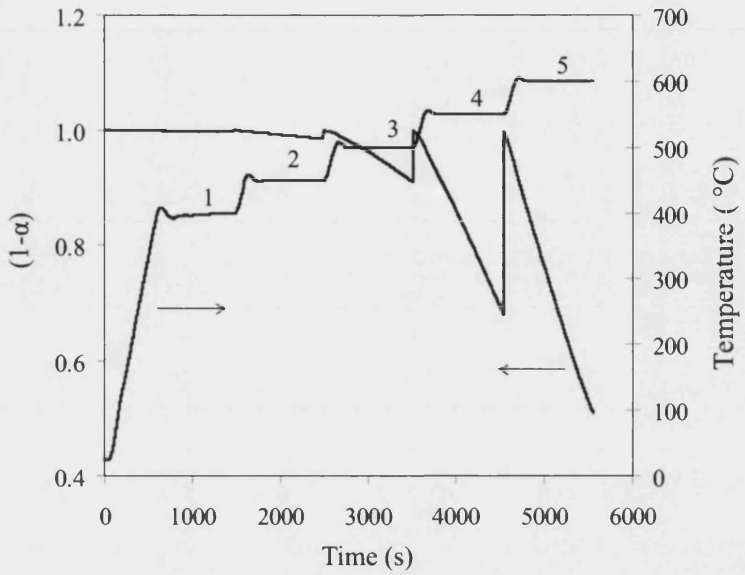

Figure 7.3.2: Example of a step-ramp temperature programme for the air oxidation of BPL granules with the resulting weight loss in each isotherm: 15 minutes isotherms and a heating rate of 25 °C min^{-1} between each step numbered from 1 to 5.

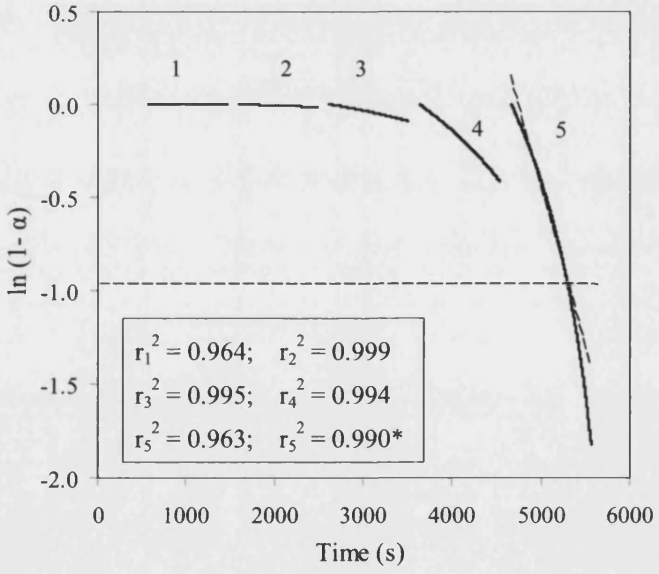

Figure 7.3.3: Evaluation of rate constants *k* derived for each isothermal step following step ramp oxidation of BPL granules in air. The correlation coefficients for each isotherm is given as r_i^2; straight line in the fifth step is represented by the dashed line for $r_5^2 = 0.990$*.

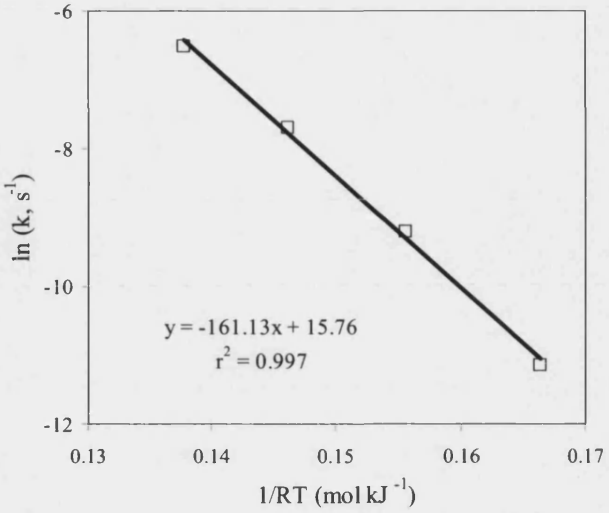

Figure 7.3.4: Arrhenius plot to evaluate the activation energy E and pre-exponential factor A of the step ramp oxidation of BPL granules in air.

7.4 Reactivity Parameters Derivation

7.4.1 Heating Rate Effect

In this section the effect of the heating rate in the resulting kinetic analysis of a step-ramp process is investigated. This investigation is carried out on BPL granules only, as it is considered a suitable model carbon, owing to its homogeneity and purity. The temperature programme consisted of: constant isotherm duration Δt of 15 minutes; constant temperature interval between each step ΔT of 50 °C. Three step-ramp programmes were performed assigned with a specific heating rate of 15, 25 and 50 °C min^{-1}. These step ramp temperature programmes are given in Figure 7.4.1a, and the resulting reaction rate profile is given in Figure 7.4.1b. It emerges from the figure that the decomposition profile is similar regardless of the heating rate applied. The kinetic parameters were subsequently derived as described in the previous section. These values are given in Table 7.4.1. It is clear from the table that the heating rate employed between

each isothermal step has no effect on the resulting kinetic parameters. Hence, any heating rate β may be used during a step-ramp oxidation reaction.

7.4.2 Temperature Interval Effect

The effect of the temperature difference between each isothermal step was also investigated using BPL granules. Both the heating rate β and the duration of each isothermal step Δt were kept constant at 25 °C min^{-1} and 15 minutes, respectively. The temperature between each step was increased either by 25 °C, 50 °C or 75 °C. These temperature programmes are shown in Figure 7.4.2a, and the corresponding weight loss curves are given in Figure 7.4.2b. It emerges from the figure that the individual reaction steps 1 to 4 take place at a much higher temperature while using a larger temperature increment, so that the reaction rate is almost doubled by increasing the temperature interval by 25 °C.

The derived kinetic parameters are given in Table 7.4.2. These parameters appear to decrease with increasing the temperature interval. Nonetheless, these kinetic parameters do not correspond to the true values derived in 6.2 and 5.5.4, where $E = 122.4 \pm 7.0$ $kJmol^{-1}$ and $Ln\ (A, s^{-1}) = 9.2 \pm 1.1$. It is possible that the larger temperature interval forces lower energy sites to be activated at higher temperatures so that the observed activation parameters are reduced. Hence, it is clear that the selected temperature interval between each isotherm has considerable effects on the resulting kinetic analysis.

7.4.3 Step Size Effect

Three different step sizes of 15, 5 and 1 minutes were investigated during the step ramp oxidation of granular BPL. Both the heating rate β and the temperature interval ΔT between each isothermal step were maintained constant at 25 °C min^{-1} and 50°C, respectively. These temperature programmes together with their corresponding reaction rate profiles are given in Figure 7.4.3. It is clear from the figure that these step ramp modes generate different reactivity profiles. In fact,

the longer the isothermal step, the larger the reactivity. These observations are best described by the resulting kinetic parameters presented in Table 7.4.3. These activation parameters appear to increase with increasing the duration of the isotherm. It may be noted, nonetheless, that the shortest isothermal step produces activation parameters closer to the true parameters of the process. At this stage, the material has undergone negligible weight loss, and hence lesser structural changes.

In conclusion the kinetic analysis of a step ramp process is strongly affected by both the temperature interval and the duration of each isothermal step. This dependency is related to the variation in reaction rate, and hence to the overall weight loss of the material during the isothermal stage, which in turns relates to the available surface area. These different factors are assessed on the accuracy of the kinetic analysis in the next section.

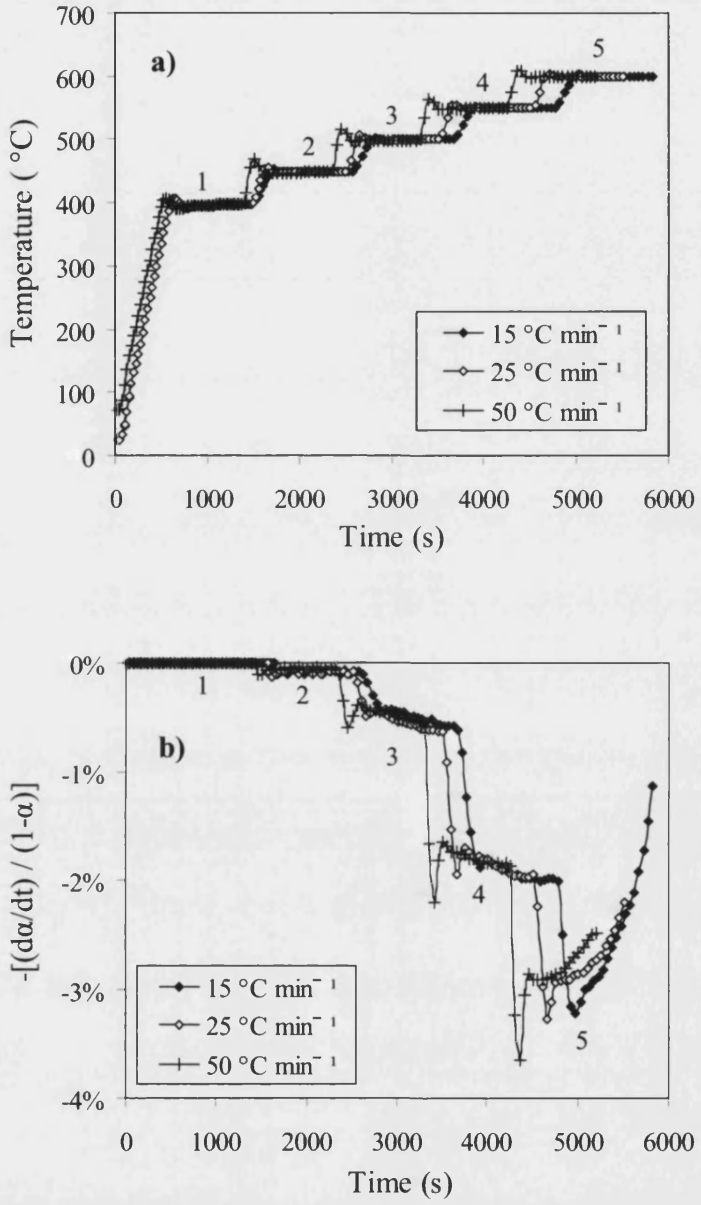

Figure 7.4.1: Effect of the selected heating rate in a step ramp process during the oxidation of BPL granules in air: a) temperature programmes; b) resulting action rate profiles.

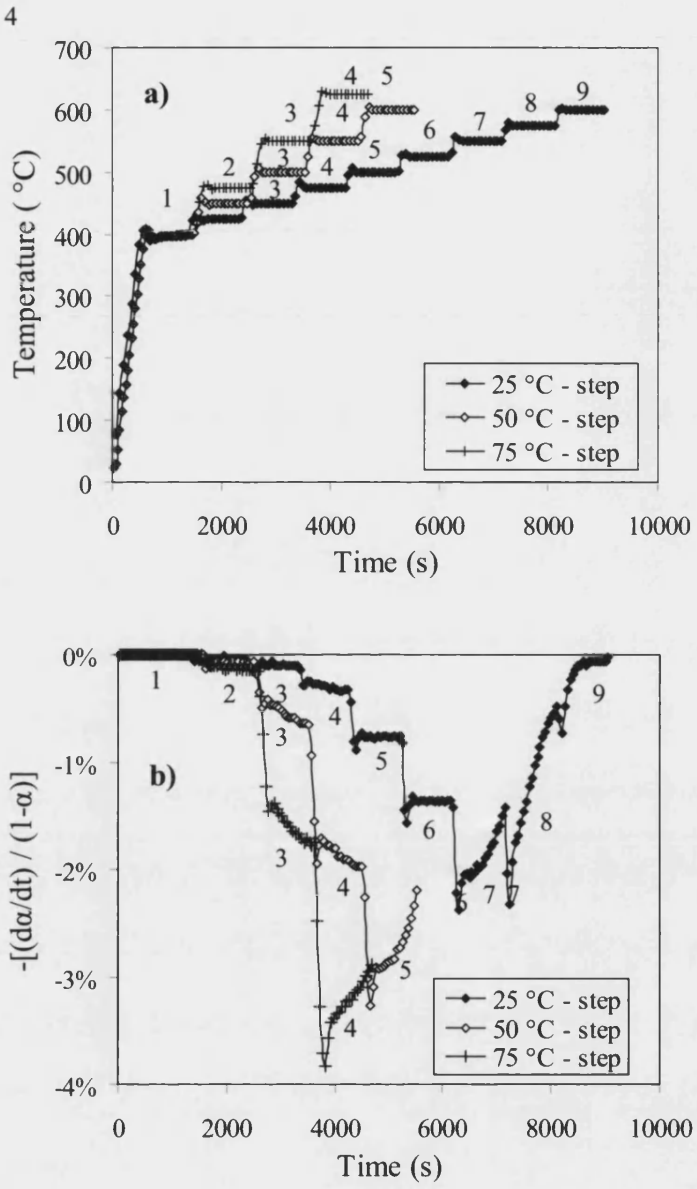

Figure 7.4.2: Effect of the temperature interval between each isotherm in a step ramp process during the oxidation of BPL granules in air a) temperature programmes; b) reaction rate profiles.

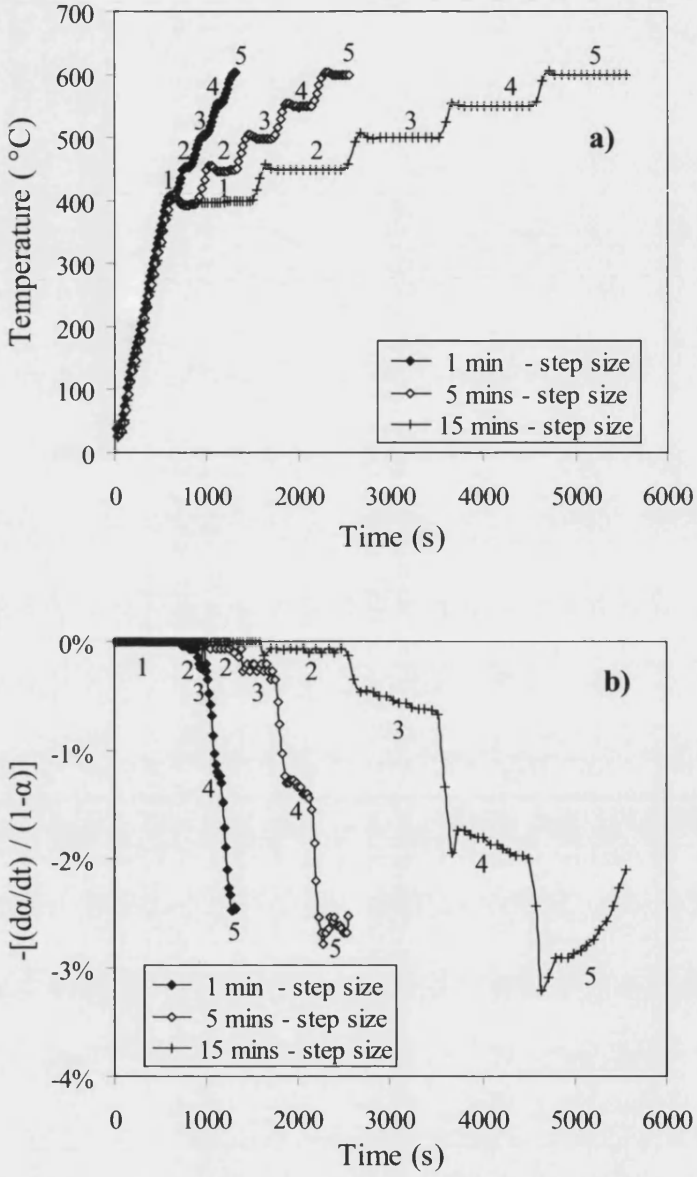

Figure 7.4.3: Effect of the duration of the isothermal step in a step ramp temperature programme during the oxidation of BPL granules in air: a) temperature programmes; b) reaction rate profiles.

Table 7.4.1: Kinetic parameters derived for the step ramp oxidation of BPL granules in air by applying different heating rate between the isothermal steps. Both temperature interval and step size are kept constant at 50 °C and 15 minutes, respectively. (± standard error).

Parameters	$\beta = 15$ °C min $^{-1}$	$\beta = 25$ °C min $^{-1}$	$\beta = 50$ °C min $^{-1}$
E – value (kJ mol $^{-1}$)	168.3 ± 6.0	161.1 ± 6.4	163.6 ± 11.2
Ln (A, s $^{-1}$)	16.8 ± 0.9	15.8 ± 1.0	15.7 ± 1.7

Table 7.4.2: Kinetic parameters derived for the step ramp oxidation of BPL granules in air following different temperature interval between the isothermal steps. Both heating rate and step size are kept constant at 25 °C min $^{-1}$ and 15 minutes, respectively. (± standard error).

Parameters	$\Delta T = 25$ °C	$\Delta T = 50$ °C	$\Delta T = 75$ °C
E – value (kJ mol $^{-1}$)	186.1 ± 3.7	161.1 ± 6.4	151.2 ± 23.6
Ln (A, s $^{-1}$)	20.1 ± 0.6	15.8 ± 1.0	13.8 ± 3.6

Table 7.4.3: Kinetic parameters derived for the step ramp oxidation of BPL granules in air following different step duration. Both heating rate and temperature interval are kept constant at 25 °C min $^{-1}$ and 50 °C, respectively. (± standard error).

Parameters	$\Delta t = 1$ minute	$\Delta t = 5$ minutes	$\Delta t = 15$ minutes
E – value (kJ mol $^{-1}$)	139.4 ± 21.6	158.5 ± 12.2	161.1 ± 6.4
Ln (A, s $^{-1}$)	11.6 ± 3.2	13.7 ± 1.0	15.8 ± 1.0

7.5 Step-ramp Analysis Accuracy

7.5.1 Maximum Weight Loss

In this section, the effect of weight loss on the kinetic analysis of a step-ramp oxidation is investigated. For this analysis, BPL granule was oxidised in air following various step-ramp programmes. Details of these temperature programmes are summarised in Table 7.5.1, for which the experiments have been numbered from 1 to 6. The overall weight loss of the material after each isothermal step was recorded and is given in Table 7.5.2. The resulting activation energy values are also included in the table, for each experiment. For ease of discussion, only the activation energy values are presented; although, the pre-exponential factor was also calculated. It may be recalled that the actual activation energy of the oxidation of BPL in air was established in the previous chapter as 122 ± 7 kJmol^{-1}.

It emerges from these tables that a correct activation energy value is obtained for an overall weight loss smaller than 10-wt%, as suggested by Sorensen (2003c). Hence, for the other experiments 2-6, the activation energy is recalculated by only considering the isotherms at which a 10-wt% is not exceeded. These recalculated values are also included in Table 7.5.2 as E – 10-wt%. It appears that these new values still deviate from the expected true activation energy value. In some cases, these recalculated values are lower and in other instances, they are much larger than the actual activation energy value. Hence, there is no evident trend in the influence of the overall weight conversion on the determination of the kinetic parameters. In other words, minimising the overall weight loss cannot be the sole factor dictating the accuracy of the activation parameters. In fact, weight loss relates to the changes in the structure of the material, and to the available surface area in particular. It is possible that the accuracy of the kinetic analysis is related to changes in surface area, rather than overall weight loss.

7.5.2 Surface Area Influence

It was noted that the step-ramp experiment #1 led to kinetic parameters that agree with the new method presented in Chapter 5. In this experiment, the overall weight conversion was maintained below 10-wt% within a specific temperature range of 500 to 600 °C. It is possible, therefore, that these two conditions must be satisfied in order to obtain accurate kinetic parameters. For this reason, the changes in surface area with both weight conversion and temperature were investigated. The BET surface area of BPL granules was measured at various degrees of conversions following various oxidation temperature programmes. These surface area measurements were performed as described in chapter 4. The various temperature programmes included: two linear heating rates of 10 and 25 °C min^{-1} and two step ramp programmes as given in Table 7.5.1.

The change in available surface area with degree of char conversion is illustrated in Figure 7.5.1a. It appears that the available surface area increases with the degree of weight conversion, at first, before reaching a maximum value. In any case, the maximum surface area seems to occur at a conversion below 20-wt%. It is possible therefore, that the kinetic analysis becomes inadequate beyond this weight conversion. Maintaining this overall weight loss alone, however, does not lead to accurate kinetic parameters. The corresponding change in surface area with temperature is given in Figure 7.5.1b. It appears from the figure that there exists a temperature interval where the surface area of the oxidising char is always larger than that of the unreacted char. This temperature interval corresponds to 475 - 600 °C, where accurate kinetic parameters were derived in experiment #1. Hence, activation energy values for experiments 2-6 were recalculated by only considering the isotherms between 475 – 600 °C. These new values are also included in Table 7.5.2, as activation energy E – (500 °C – 600 °C).

It emerges from the table that, the recalculated activation energy values are closer to the actual activation energy value of the process. Although the resulting activation energy values are still in disagreement, experiment #2 presents a reasonable activation energy value. In this experiment, the overall weight loss approximates 20-wt%, which has been identified as the maximum weight loss

required for the analysis. It is clear that an accurate kinetic analysis of a step-ramp oxidation process is derived by maintaining the overall weight loss to a minimum within a clearly defined temperature range. For BPL granules, a maximum weight conversion of 20-wt% is identified to apply in the temperature range of 475 °C – 600 °C.

7.5.3 Mass Transfer Limitations

Analysing a step-ramp oxidation process by monitoring the weight loss and predetermining a 'reactive temperature' range to perform the analysis can be complicated. The combination of weight loss and surface area may, however, indicate a change in the rate-controlling mechanism. In fact, Smith (1982) and also Smoot and Smith (1985) have suggested that structural changes relate to a specific rate-controlling mechanism during oxidation of coal chars. They observed that the surface area increases to a maximum value at first, whilst the chemical reaction is kinetically controlled. Then, the surface area of the oxidising char decreases and falls below that of the unreacted char. At this point, the chemical reaction is limited by mass transfer effects. These changes may be observed through incremental weight loss (< 5-wt%) between each isothermal reaction. It emerges that a correct kinetic analysis of step-ramp oxidation requires accurate determination of the rate-controlling mechanisms.

In light of this, further experiments were carried out for which an incremental weight loss of 5-wt% (maximum) was monitored between each isothermal step. This new set of experiments is numbered from 7 to 10, and their corresponding step-ramp temperature programmes are given in Table 7.5.3. The resulting weight loss after each isotherm is given in Table 7.5.4, together with the calculated activation energy values. For each experiment, a shaded region has been highlighted. This area corresponds to the chemical control regime identified through an Arrhenius plot, as given in Figure 7.5.2. The limit for chemical control regime terminates at the point where the Arrhenius plot begins to curve, and hence the correlation coefficient $r^2 < 0.990$.

It appears from the table that activation energy values computed within the chemical control regime are in good agreement with the actual activation energy of the process. On the other hand, activation energy values derived by only considering an overall weight loss smaller than 20-wt%, does not necessarily lead to accurate reactivity parameters, as illustrated by experiment #8. In addition, the activation energy values computed by using only the isotherms comprised between 475 – 600 °C are also in good agreement with the actual activation energy. Nonetheless, experiment #9 produces a slightly inadequate value. It may be concluded therefore, that accurate kinetic analysis of a step-ramp oxidation process may be carried out as follows:

(i) Maintain weight loss during each isotherm to a minimum (<5-wt%)

(ii) Identify the chemical control regime through an Arrhenius plot, after at least 1-wt% char conversion is reached to account for chemisorption effects.

(iii) Perform the kinetic analysis detailed in section 7.2.3, for the isotherms comprised in the chemical control regime.

This approach in the kinetic analysis of a step-ramp oxidation is more attractive and much simpler than measuring the surface area of the material at different conversions. Hence, this novel approach can now be tested on industrial coal chars to verify its applicability.

Table 7.5.1: Temperature programme conditions employed in the step ramp oxidation of BPL granule in air.

Experimental conditions	# 1	# 2	# 3	# 4	# 5	# 6
β (°C min $^{-1}$)	25	25	25	50	50	25
ΔT (°C)	50	50	50	50	75	25
ΔL (min)	1	5	15	15	15	15

Table 7.5.2: Weight loss values (wt %) and mean activation energy values resulting from the different step-ramp temperature programmes during the air oxidation of BPL granules. Actual E-value = 122 ± 7 kJ mol^{-1}.

Temperature (°C)	# 1	# 2	# 3	# 4	# 5	# 6
375	-	-	-	-	0.14%	-
400	0.00%	0.04%	0.25%	0.07%	-	0.32%
425	-	-	-	-	-	1.03%
450	0.00%	0.20%	1.66%	1.14%	1.29%	2.70%
475	-	-	-	-	-	7.57%
500	0.18%	1.67%	10.58%	8.69%		20.30%
525	-	-	-	-	17.90%	43.25%
550	2.25%	9.70%	42.50%	37.98%	-	75.60%
575	-	-	-	-	-	96.55%
600	8.35%	27.56%	91.63%	84.94%	97.91%	99.90%
E (kJ mol $^{-1}$)						
E - Overall		158 ± 12	161 ± 6	163 ± 11	146 ± 24	178 ± 4
E - 10-wt %	139 ± 22	177 ± 4	158 ± 11	190 ± 1	183 ± 0	162 ± 9
E - 500–600 °C		146 ± 25	150 ± 6	145 ± 13	100 ± 0	174 ± 9

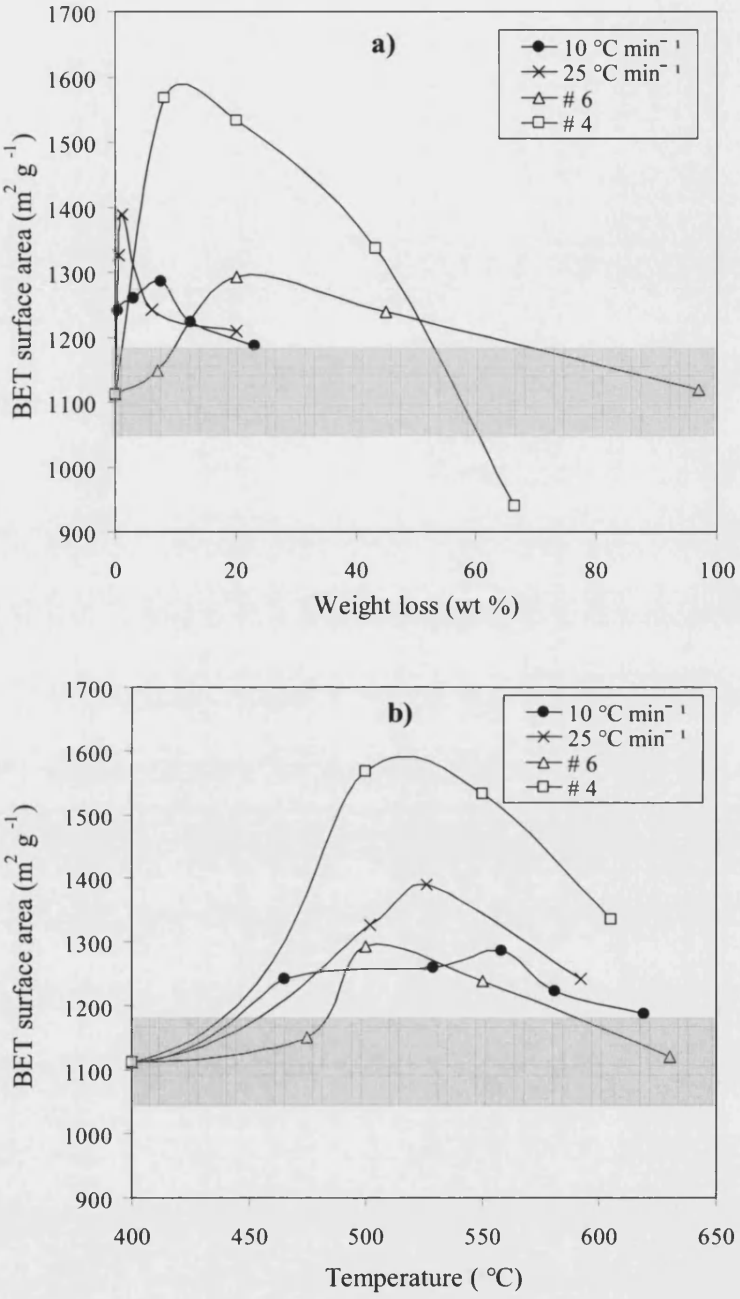

Figure 7.5.1: Changes in surface area with a) degree of conversion and b) temperature, following the oxidation in air of BPL granules at various temperature programmes: weight loss is corrected for moisture and ash content. Shaded region corresponds to the BET surface area of the unreacted BPL.

Table 7.5.3: Temperature programme conditions employed during the step ramp oxidation of BPL granules in air, aiming to minimise the overall weight loss after each isothermal step: Δt (min) and β ($°Cmin^{-1}$).

Temperatures (°C)	# 7		# 8		# 9		# 10	
	Δt	β	Δt	β	Δt	β	Δt	β
400	10	40	15	40	15	40	15	40
425	5	10	5	5	-	-	-	-
450	3	15	1	10	5	20	5	15
475	1	15	1	15	-	-	-	-
500	1	20	½	15	½	20	3	15
525	1	20	¼	15	-	-	-	-
550	½	20	¼	15	¼	20	2	15
575	¼	30	¼	15	-	-	-	-
600	¼	30	¼	15	½	20	1	15

Table 7.5.4: Effect of overall weight loss (wt %) on the mean activation energy values resulting from the different step-ramp temperature programmes during the air oxidation of BPL granules. Activation energy from optimum-heating rate method: E-value = 122 ± 7 $kJ\ mol^{-1}$.

Temperatures (°C)	# 7	# 8	# 9	# 10
400	0.14%	0.13%	0.41%	0.45%
425	0.36%	0.36%	-	-
450	0.55%	0.52%	1.13%	1.34%
475	0.93%	0.81%	-	-
500	1.69%	1.34%	1.91%	4.10%
525	3.25%	2.97%	-	-
550	4.80%	4.06%	4.06%	11.80%
575	6.71%	8.62%	-	-
600	9.19%	13.28%	9.49%	23.75%
E (400-600 °C), $kJ\ mol^{-1}$	135 ± 5	149 ± 5	115 ± 5	126 ± 5
E (500-600 °C), $kJ\ mol^{-1}$	106 ± 11	127 ± 12	96 ± 10	108 ± 13
E (shaded area), $kJ\ mol^{-1}$	119 ± 13	142 ± 12	124 ± 5	136 ± 6

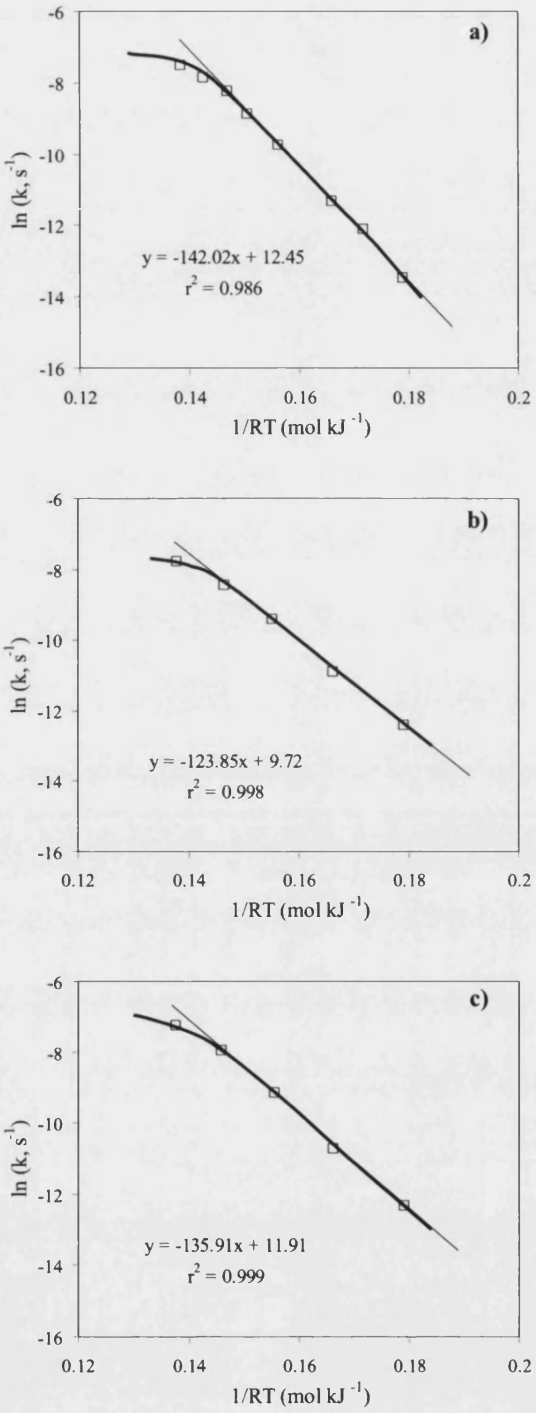

Figure 7.5.2: Arrhenius plots for the oxidation in air of BPL granules following various step ramp programmes, in order to identify the rate-controlling mechanisms zones in experiments a) experiment # 8; b) experiment # 9 and c) experiment #10.

7.6 Coal Chars Analysis

7.6.1 Step – ramp Oxidation

Step-ramp oxidation was performed on the industrial coal chars, following the experimental procedure described in section 7.2.2. The duration of each isothermal step Δt, the heating rate β employed to move to the next step, and the temperature interval between each step ΔT, were adjusted to maintain a maximum weight conversion of 5-wt% in each isothermal step. An example of such a temperature programme is given in Table 7.6.1 for the step-ramp oxidation of Heze char in air. The resulting weight loss after each isothermal reaction is given in Table 7.6.2. These tables have also been produced for the other chars and included in Appendix D.

7.6.2 Mass Transfer Effects

Arrhenius plots for each experiment were derived in order to evaluate the upper temperature limit for chemical control. In the case of Heze char, the chemical control zone has been highlighted in Table 7.6.2. It appears from the table that mass transfer effects become significant above 525 °C. The start of the chemical control regime is identified from a weight conversion greater than 0.5-wt%, in this case. Plots for determining the rate constant at the low temperature isotherms were not linear ($r^2 < 0.990$); suggesting that the intrinsic reaction has not properly started. It is highly possible that this early stage corresponds to the chemisorption phase.

By compiling data from all the different experiments, it is possible to identify the kinetic control regime zone more accurately. In this way, an overall Arrhenius plot was derived for each char, as presented in Figure 7.6.1. The different rate-controlling mechanisms have clearly been identified in the figure, where zone I represents the chemical control regime, and zone II corresponds to internal pore diffusion. The extent of each rate-controlling mechanism is different for each char. This dissimilarity may lie in the structure difference of the chars, as

discussed in section 5.3. The maximum temperature for chemical control was also determined as the point where the straight line of the Arrhenius plot began to curve. This point was selected at the optimum correlation coefficient r^2 value.

These maximum temperatures are listed in Table 7.6.3, and are contrasted with those evaluated during the optimum- heating rate analysis, presented in section 5.3.3. It emerges from the table that mass transfer effects occur at considerably lower temperatures during step-ramp oxidation, compared to linear heating mode. Hence, it is possible that the step-ramp temperature programme may significantly affect the structure of a char upon oxidation. This effect was also observed in Figure 7.5.1, where step-ramp oxidation of BPL granules induced an earlier maximum change in surface area, compared with the linear heating oxidation process. In this way, the early decrease in structural changes during step-ramp oxidation, leads to an earlier appearance of mass-transfer effects.

7.6.3 Kinetic Parameters

From the Arrhenius plots, given in Figure 7.6.1, the reactivity parameters were estimated within the chemical control regime (Zone I). These kinetic parameters are summarised in Table 7.6.4. It emerges from the table that these values are in close agreement with those derived using the optimum heating rate technique (Table 5.5.2) and isothermal methods (Table 6.2.2). It may be concluded therefore, that step ramp oxidation is a highly accurate tool in thermogravimetric analysis, when correctly applied. In fact, it is more complicated in practice than the optimum heating rate analysis. A summary of the benefits from each kinetic analysis method is contrasted in Table 7.6.5.

Unlike the FSIA method, this novel approach is not restricted to a maximum overall weight loss of 10-wt% and an increase of 5 °C between each isotherm. Instead, the weight loss between each isotherm needs to be minimised (< 5-wt%) so that mass transfer effects can be taken into consideration. Hence the step – ramp technique offers a new insight into SCTA for evaluation of kinetic parameters.

Table 7.6.1: Temperature programme conditions employed during the step ramp oxidation of Heze char in air: Δt (min) and β (°C min^{-1}).

Temperatures (°C)	# 1		# 2		# 3		# 4	
	Δt	β	Δt	β	Δt	β	Δt	β
375	5	50	5	50	-	-	-	-
400	1	10	1	15	2	40	1	40
425	1	15	1	20	-	-	-	-
450	1	15	½	20	1	25	1	15
475	1	15	½	20	-	-	-	-
500	¼	15	¼	20	½	25	1	15
525	¼	15	¼	30	-	-	-	-
550	¼	15	¼	30	½	25	1	15
580	¼	15	¼	30	½	25	1	15

Table 7.6.2: Weight loss (wt %) and mean activation energy values resulting from the different step-ramp temperature programmes during the air oxidation of Heze char. Shaded area corresponds to the chemical control zone. Activation energy value derived from optimum-heating rate analysis *E*-value = 152 ± 2 kJ mol^{-1}

Temperatures (°C)	# 1	# 2	# 3	# 4
375	0.04%	0.04%	-	-
400	0.10%	0.21%	0.34%	0.31
425	0.38%	0.40%	-	-
450	0.61%	0.78%	0.97%	1.19%
475	2.07%	1.54%	-	-
500	4.09%	2.94%	2.92%	5.30%
525	8.96%	5.03%	-	-
550	16.63%	8.49%	10.71%	19.25%
580	24.98%	12.90%	23.75%	39.31%
E (375-580 °C), kJ mol^{-1}	132 ± 7	128 ± 6	115 ± 10	118 ± 10
E (shaded area), kJ mol^{-1}	159 ± 4	153 ± 3	155 ± 0	147 ± 0

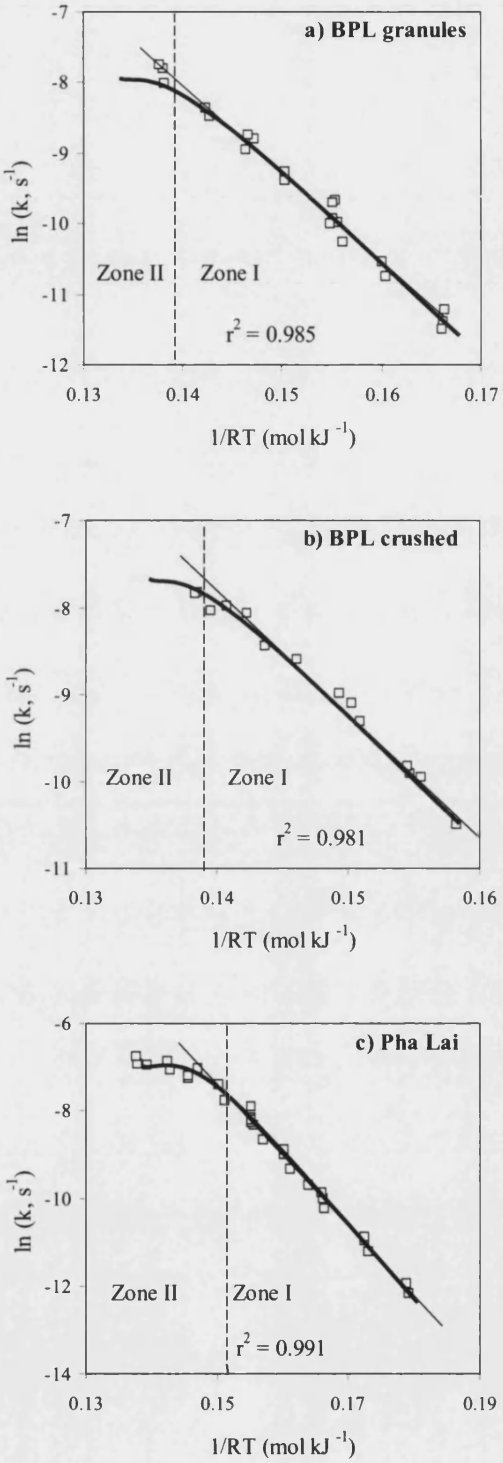

Figure 7.6.1: Kinetic parameters derived in the chemical control regime presented with measure of fit of the curve in this zone: Zone I is the chemical control regime, and Zone II is the porous or diffusion control regime.

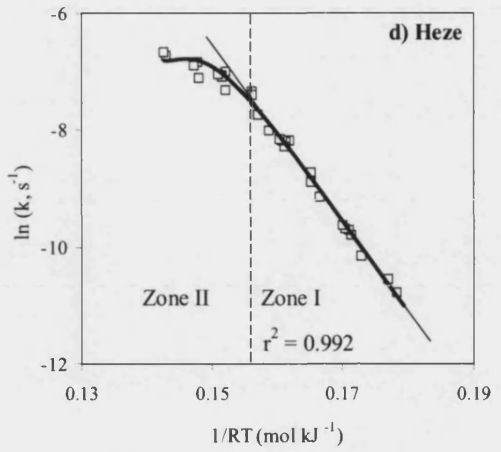

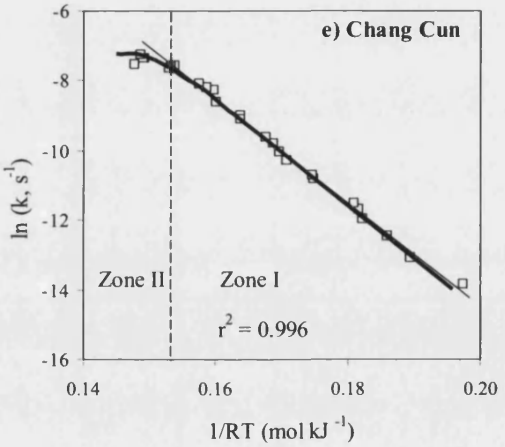

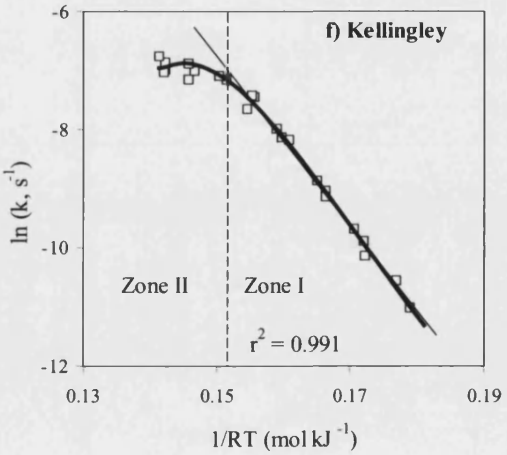

Figure 7.6.1: Continued for : d) Heze; e) Chang Cun and; f) Kellingley char

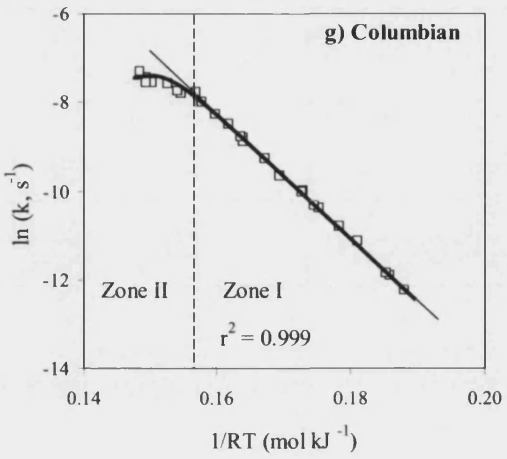

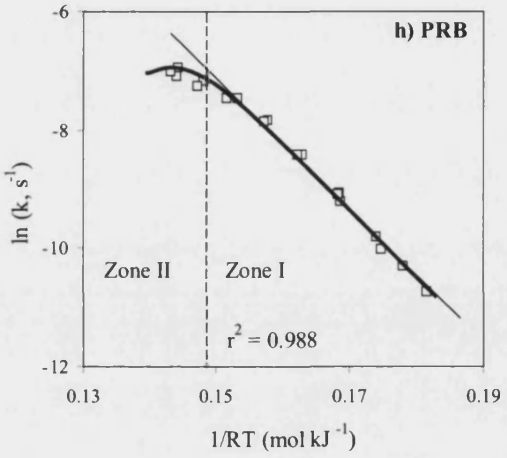

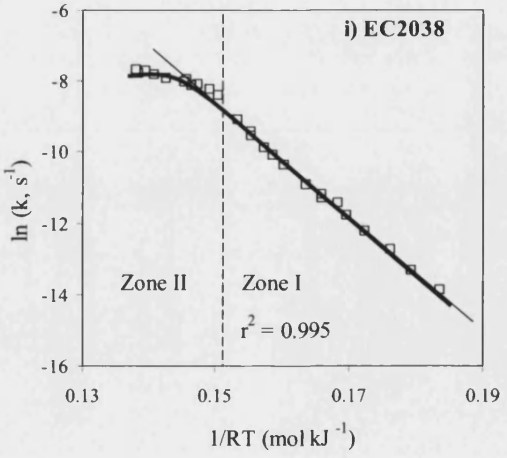

Figure 7.6.1: Continued for : g) Columbian; h) PRB and; i) EC2038 char

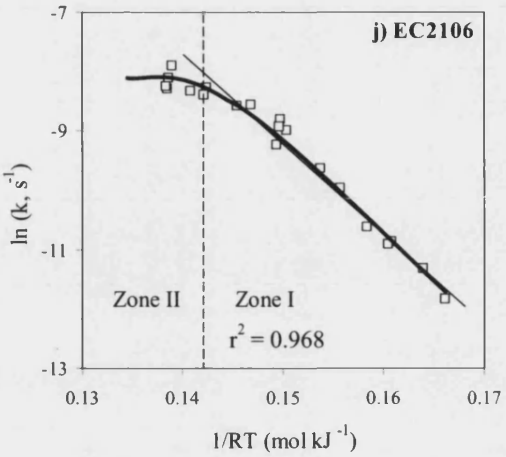

Figure 7.6.1: continued for EC2106.

Table 7.6.3: Comparison of temperature range for chemical control analysis using different temperature programmes during the air oxidation of the different chars.

Char samples	Maximum temperature in step ramp analysis (°C)	Maximum temperature in linear heating rate analysis (°C)
BPL granules	600	600
BPL crushed	600	600
Pha Lai	525	570
Heze	525	575
Chang Cun	515	540
Kellingley	525	540
Columbian	525	570
PRB	540	565
EC2038	525	565
EC2106	575	560

Table 7.6.4: Reactivity parameters using step ramp analysis for the oxidation of the different chars in air.

Char samples	E (kJ mol $^{-1}$)	ln (A, s $^{-1}$)
BPL granules	127.0 ± 4.4	10.3 ± 0.7
BPL crushed	129.5 ± 5.2	10.7 ± 0.8
Pha Lai	161.0 ± 3.8	16.8 ± 0.6
Heze	152.5 ±3.3	15.6 ± 0.5
Chang Cun	147.8 ± 2.3	15.1 ± 0.4
Kellingley	142.9 ± 3.8	14.7 ± 0.6
Columbian	140.1 ± 1.2	13.5 ± 0.2
PRB	110.8 ± 3.5	9.5 ± 0.6
EC2038	160.1 ± 3.0	15.4 ± 0.5
EC2106	151.2 ± 7.6	13.9 ± 1.2

Table 7.6.5: Comparison of existing TGA methods with the novel step-ramp analysis from a practical point of view.

TGA method	Number of experiments required	Total experimental time (hr)	Simplicity of the experimental procedure	Simplicity of the kinetic analysis	Dependence on heating rate
Isothermal	**3**	**> 10**	Yes	Yes	No
Linear TGA	1	< 3	Yes	**No**	**Yes**
Isoconversional TGA	**3**	**> 10**	Yes	Yes	No
Novel linear TGA	**1**	**< 3**	**Yes**	**Yes**	**No**
Step-ramp	1	< 3	**No**	Yes	No

Chapter 8

Conclusions and Future Work

8.1 General Conclusions

This work has demonstrated that conventional thermogravimetric techniques are either time-consuming, mathematically complex, or unreliable for an accurate determination of intrinsic reactivity data for coal chars. As stated in section 2.9, the objectives of this investigation were to develop a new thermogravimetric analysis technique, which is quicker and more reliable than these conventional techniques. This work has culminated in devising such a novel approach. The novel single heating rate thermogravimetric technique clearly distinguishes the chemical control region for analysis of kinetic data, and segregates the actual oxidation reaction occurring within this temperature region. In this way, the proposed kinetic analysis is able to accurately model the oxidation of coal char in the chemical control regime. Furthermore, a statistical best-fit criterion has been devised in order to identify the optimum-heating rate, at which the kinetic analysis is not affected by the rate of heating. In fact, the kinetic parameters derived at this optimum-heating rate were in close agreement with those derived using existing analysis techniques, and values presented in the literature for similar materials. The proposed new analysis has the highest degree of accuracy, as indicated by a narrower error margin in the mean kinetic parameter values. Using sample controlled thermal analysis in char oxidation studies, on the other hand, proved to

be very complex and time consuming in comparison with the novel thermogravimetric analysis approach. Nonetheless, it was noted that a step-ramp oxidation method may be implemented, which is much simpler than current sample thermal analysis techniques in deriving accurate kinetic parameters. The main findings from this work can be summarised as follows:

1. A modified Coats-Redfern (1964) function was found to be the simplest and most accurate approximate function to the temperature integral of the Arrhenius equation, in order to simulate the air oxidation of most coal chars within the kinetic controlled regime.

2. An optimum-heating rate was clearly defined, which is not dependent on the type of char, particle size, nor the selected kinetic analysis. It is suggested that this optimum-heating rate depends on the thermogravimetric analyser instrument, possibly due to the geometry of the furnace and hence due to induced convection currents inside the furnace. Hence, this optimum-heating rate may vary from one make to the other. For the Setaram TG92, this optimum was observed at a range of heating between 25 - 35 °C min^{-1}.

3. At this identified optimum-heating rate range, the kinetic parameters corresponded to those derived by existing techniques, with the highest degree of accuracy. Hence, this technique is a powerful tool by being both fast and accurate.

4. The level of accuracy resulting from the optimum-heating rate analysis allows for a clear and simple correlation between the kinetic parameters and structural properties of the char.

5. The step ramp method is an improvement to current sample controlled thermal analysis techniques, in that the kinetic parameters are estimated in a simpler manner. However, this method is more complex and unstable than the optimum heating rate analysis. In fact, step-ramp oxidation is strongly affected by mass-transfer effects, so that accurate kinetic parameters can only be derived by close monitoring of the weight loss during each isothermal step.

8.2 Future Work

1. The optimum-heating rate analysis could be incorporated into routine coal characterisation techniques performed in industry; especially with regard to the BCURA coal bank, where various types of coals are characterised and dispatched with precise specification data.

2. A generalised relationship between the activation parameters and the properties of the char could be developed. For this purpose, more coal samples need to be tested for their structural properties, especially with regard to ash composition, and then analysed by means of the optimum-heating rate analysis. In this way, it would be possible to predict and understand structural changes of the char during combustion under kinetic controlled regime.

3. It would be interesting to correlate the kinetic parameters of different chars with their performance in industry. Performance indices may include process efficiency, slagging, fouling, or NOx emissions. An effective relationship would be useful in predicting and comparing the performance of different coals, as well as preparing coal blends.

References

1. Achar, N. N. N., G. W. Brindley and J. H. Sharp (1966). International Clay Conference, Jerusalem
2. Ahmed, S. and M. H. Back (1985). The role of the surface complex in the kinetics of the reaction of oxygen with carbon. Carbon 23(5): 513-524.
3. Alonso, M. J. G., D. Alvarez, A. G. Borrego, R. Menendez and G. Marban (2001a). Systematic effects of coal rank and type on the kinetics of coal pyrolysis. Energy & Fuels 15(2): 413-428.
4. Alonso, M. J. G., A. G. Borrego, D. Alvarez and A. Menendez (2001b). "A reactivity study of chars obtained at different temperatures in relation to their petrographic characteristics." Fuel Processing Technology 69(3): 257-272.
5. Alvarez, T., A. B. Fuertes, J. J. Pis and P. Ehrburger (1995). Influence of coal oxidation upon char gasification reactivity. Fuel 74(5): 729-735.
6. Arenillas, A., F. Rubiera, J. J. Pis, J. M. Jones and A. Williams (1999). The effect of the textural properties of bituminous coal chars on NO emissions. Fuel 78 (14), 1779-1785.
7. Arenillas, A., C. Pevida, F. Rubiera and J. J. Pis (2003). Comparison between the reactivity of coal and synthetic coal models. Fuel 82(15-17): 2001-2006.
8. Arenillas, A., F. Rubiera, C. Pevida, C. O. Ania and J. J. Pis (2004a). Relationship between structure and reactivity of carbonaceous materials. Journal of Thermal Analysis and Calorimetry 76(2): 593-602.
9. Arenillas, A., C. Pevida, F. Rubiera, R. Garcia and J. J. Pis (2004b). Characterisation of model compounds and a synthetic coal by TG/MS/FTIR to represent the pyrolysis behaviour of coal. Journal of Analytical and Applied Pyrolysis 71 (2), 747-763.
10. ASTM D 388 (1966, revised 1984). Classification of coals, American Society for Testing Materials.
11. ASTM D 2798 (1999). Standard Test Method for Microscopical Determination of the Reflectance of Vitrinite in a Polished Specimen of Coal, ASTM International.
12. ASTM D 3172-75 (1989). Proximate analysis of coal and coke, American Society for Testing Materials.
13. ASTM D 3176-79 (1989). Ultimate analysis of coal and coke, American Society for Testing Materials.

14. ASTM D 5341 (1999). Standard test method for measuring coke reactivity index (CRI) and coke strength after reaction (CSR), ASTM International.

15. Atkins, P. W. and J. de Paula, Eds. (2002). Atkins' Physical chemistry. 7th ed. Oxford, Oxford University Press.

16. Banin, V., R. Moors and B. Veefkind (1997). Kinetic study of high-pressure pulverized coal char combustion: Experiments and modelling. Fuel 76(10): 945-949.

17. Berkowitz, N. (1994). An introduction to coal technology. San diego, Academic Press, Inc.

18. Bhatia, S. K. and D. D. Perlmutter (1980). Random pore model for fluid-solid reactions: I. Isothermal, kinetic control. Aiche Journal 26(3): 379-385.

19. BP statistical review of world energy (2005). BP statistical review of world energy june 2005. B. p.l.c. London.

20. Brown, M. E., D. Dollimore and A. K. Galwey (1980). Reactions in the solid state. Amsterdam, Elsevier.

21. Brown, M. E. (1997). Steps in a minefield - Some kinetic aspects of thermal analysis. Journal of Thermal Analysis 49(1): 17-32.

22. Brown, M. E. (2001). Introduction to thermal analysis: Techniques and applications, 2nd. London, Kluwer Academic.

23. Brown, M. E. and A. K. Galwey (2002). The significance of "compensation effects" appearing in data published in "computational aspects of kinetic analysis": ICTAC project, 2000. Thermochimica Acta 387 (2), 173-183.

24. Brunauer, S., P. H. Emmet and E. Teller (1938). Adsorption of gases in multimolecular layers. Journal of American Chemistry Society 60, 309.

25. BS 1016-104 (1998). Methods for analysis and testing of coal and coke: Proximate analysis, British Standards Institution.

26. BS 1016-106 (1996). Methods for analysis and testing of coal and coke: Ultimate analysis of coal, British Standards Institution.

27. BS 1016-108.6 (1992). Methods for analysis and testing of coal and coke: Tests special to coke. Determination of critical air blast value, British Standards Institution.

28. BS 4262 (1984). Method of specifying the technical quality of coke for use in blast furnaces, British Standards Institution.

29. BS 4359-1 (1996). Determination of the specific surface area of powders - Part 1: BET method of gas adsorption for solids (including porous materials).

30. Budrugeac, P. and E. Segal (2004). On the nonlinear isoconversional procedures to evaluate the activation energy of nonisothermal reactions in solids. International Journal of Chemical Kinetics 36 (2), 87-93.

31. Carpenter, A. M. (1988). Coal classification. London, IEA Coal Research.

32. Carpenter, A. M. and N. M. Skorupska (1993). Coal combustion analysis and testing. London, IEA Coal Research.

33. Chan, M.-L., J. M. Jones, M. Pourkashanian and A. Williams (1999). The oxidative reactivity of coal chars in relation to their structure. Fuel 78 (13), 1539-1552.

34. Ceylan, K., H. Karaca and Y. Onal (1999). Thermogravimetric analysis of pretreated Turkish lignites. Fuel 78(9): 1109-1116.

35. Chan, M.-L., J. M. Jones, M. Pourkashanian and A. Williams (1999). The oxidative reactivity of coal chars in relation to their structure. Fuel 78(13): 1539-1552.

36. Chen, D., X. Gao and D. Dollimore (1993). "A Generalized Form of the Kissinger Equation." Thermochimica Acta 215: 109-117.

37. Chen, F., O. T. Sorensen, G. Meng and D. Peng (1998). Thermal decomposition of BaC2O4 center dot 0.5H(2)O studied by stepwise isothermal analysis and non-isothermal thermogravimetry. Journal of Thermal Analysis and Calorimetry 53(2): 397-410.

38. Chen, Q., R. He, X. C. Xu, Z. G. Liang and C. H. Chen (2004). Experimental study on pore structure and apparent kinetic parameters of char combustion in kinetics-controlled regime. Energy & Fuels 18(5): 1562-1568.

39. Coats, A. W. and J. P. Redfern (1964). Kinetic parameters from thermogravimetric data. Nature 201, 68-69.

40. Criado, J. M. and L. A. Perez-Maqueda (2005). Sample controlled thermal analysis and kinetics. Journal of Thermal Analysis and Calorimetry 80(1): 27-33.

41. de la Puente, G., E. Fuente and J. J. Pis (2000). Reactivity of pyrolysis chars related to precursor coal chemistry. Journal of Analytical and Applied Pyrolysis 53(1): 81-93.

42. Doyle, C. D. (1962). Estimating isothermal life from thermogravimetric data. Jounal of Applied Polymer Science 6, 639-642.

43. DTI UK energy in brief july (2005). A national statistics publication. Department of Trade and Industry: The stationery office. Norwich.

44. Dubinin, M. M. and L. V. Radushkevich (1947). Proceedings of the Academy of Science of the USSR 55, 331.

45. Dubinin, M. M. (1975). Physical adsorption of gases and vapors in micropores. New York, Academic Press.

46. Dubinin, M. M. and H. F. Stoeckli (1980). Homogeneous and Heterogeneous Micropore Structures in Carbonaceous Adsorbents. Journal of Colloid and Interface Science 75 (1), 34-42.

47. Dutta, S. and C. Y. Wen (1977). Reacticvity of coal and char.2. In oxygen - nitrogen atmosphere. Industrial and Engineering Chemistry Process Desing and Development 16(1): 31 - 37.

48. European Commission (20/09/05). Pulverised fuel combustion: Future RTD needs. Europa: www.europa.eu.int. Brussels.

49. Feng, B. and S. K. Bhatia (2000). Determination of activation energy distributions for chemisorption of oxygen on carbon: an improved approach. Chemical Engineering Science 55(24): 6187-6196.

50. Feng, B., A. Jensen, S. K. Bhatia and K. Dam-Johansen (2003). Activation energy distribution of thermal annealing of a bituminous coal. Energy & Fuels 17 (2), 399-404.

51. Feng, B. and S. K. Bhatia (2003). Variation of the pore structure of coal chars during gasification. Carbon 41(3): 507-523.

52. Field, M. A. (1969). Rate of combustion of size-graded fractions of char from a low-rank coal between 1 200[deg]K and 2 000[deg]K*1. Combustion and Flame 13 (3), 237-252.

53. Flynn, J. H. and L. A. Wall (1966). General treatment of the thermogravimetry of polymers. Journal of Research of the National Bureau of Standards - A. Physics and Chemistry 70A (6), 487-523.

54. Flynn, J. H. (1997). The 'temperature integral' - Its use and abuse. Thermochimica Acta 300 (1-2), 83-92.

55. Fogler, H. S. (1999). Elements of chemical reaction engineering. New Jersey, Prentice-hall International Inc.

56. Freeman, H. L. and B. Carroll (1958). The application of thermoanalytical techniques to reaction kinetics. The thermogravimetric evaluation of the kinetics of the decomposition of calcium oxalate monohydrate. Journal of Physical Chemistry 62, 394-397.

57. Friedman, H. L. (1964). Journal of Polymer Science 6, 1177.

58. Gadiou, R., Y. Bouzidi and G. Prado (2002). The devolatilisation of millimetre sized coal particles at high heating rate: the influence of pressure on the structure and reactivity of the char. Fuel 81(16): 2121-2130.

59. Gale, T. K., C. H. Bartholomew and T. H. Fletcher (1996). Effects of pyrolysis heating rate on intrinsic reactivities of coal chars. Energy & Fuels 10(3): 766-775.

60. Galwey, A. K. (2003a). What is meant by the term 'variable activation energy' when applied in the kinetic analyses of solid state decompositions (crystolysis reactions)? Thermochimica Acta 397(1-2): 249-268.

61. Galwey, A. K. (2003b). Perennial problems and promising prospects in the kinetic analysis of nonisothermal rate data. Thermochimica Acta 407(1-2): 93-103.

62. Gibbins, J. R. and J. Williamson (1993). 7th International conference on coal science, Banff, Canada.

63. Gopalakrishnan, R. and C. H. Bartholomew (1996). Effects of CaO, high-temperature treatment, carbon structure, and coal rank on intrinsic char oxidation rates. Energy & Fuels 10(3): 689-695.

64. Gorbachev, V. M. (1975). Solution of Exponential Integral in Nonisothermal Kinetics for Linear Heating. Journal of Thermal Analysis 8 (2), 349-350.

65. Gotor, F. J., Perez-Maqueda, L.A., Ortega, A., Criado, J.M. (1998). Kinetic Analysis of Solid State Reactions by Means of Stepwise Isothermal Analysis (SIA) and Constant Rate Thermal Analysis (CRTA) A comparative study. Journal of Thermal Analysis and Calorimetry 53(2): 389-396.

66. Gotor, F. J., J. M. Criado, J. Malek and N. Koga (2000). Kinetic analysis of solid-state reactions: The universality of master plots for analyzing isothermal and nonisothermal experiments. Journal of Physical Chemistry A 104 (46), 10777-10782.

67. Haji-Sulaiman, M. Z. and M. K. Aroua (1997). Activation energy for the oxidation of Malaysian coal chars. Journal of the Institute of Energy 70: 52-56.

68. Hampartsoumian, E., W. Nimmo, P. Rosenberg, E. Thomsen and A. Williams (1998). Evaluation of the chemical properties of coals and their maceral group constituents in relation to combustion reactivity using multi-variate analyses. Fuel 77(7): 735-748.

69. Hatakeyama, T. and L. Zhenhai (1998). Handbook of thermal analysis. Chichester, Wiley.

70. Hayhurst, A. N. and M. S. Parmar (1998). Does solid carbon burn in oxygen to give the gaseous intermediate CO or produce CO2 directly? Some experiments in a hot bed of sand fluidized by air. Chemical Engineering Science 53(3): 427-438.

71. Haykiri-Acma, H., A. Ersoy-Mericboyu and S. Kucukbayrak (2002). Combustion reactivity of different rank coals. Energy Conversion and Management 43(4): 459-465.

72. He, R., J. Sato, Q. Chen and C. Chen (2002). Thermogravimetric analysis of char combustion. Combustion Science and Technology 174(4): 1-18.

73. Hecker, W. C., P. M. Madsen, M. R. Sherman, J. W. Allen, R. J. Sawaya and T. H. Fletcher (2003). High-pressure intrinsic oxidation kinetics of two coal chars. Energy & Fuels 17(2): 427-432.

74. Herbig, C. and A. Jess (2002). Determination of reactivity and ignition behaviour of solid fuels based on combustion experiments under static and continuous flow conditions. Fuel 81 (18), 2387-2395.

75. His Majesty's Stationary Office (1946). DSIR Survey Paper No 58: Coal classification. London, Department of Scientific and Industrial Research.

76. Hu, Y. Q., H. Nikzat, M. Nawata, N. Kobayashi and M. Hasatani (2001). The characteristics of coal-char oxidation under high partial pressure of oxygen. Fuel 80(14): 2111-2116.

77. Hustad, J. E., D. Vareide and O. K. Sonju (1991). Burning rates of coke particles in the freeboard above a fluidized bed reactor. Combustion and Flame 85(1-2): 232-240.

78. Hutson, N. D. and R. T. Yang (1997). Theoretical basis for the Dubinin-Radushkevitch (D-R) adsorption isotherm equation. Adsorption-Journal of the International Adsorption Society 3 (3), 189-195.

79. Ichihara, S. (1994). Thermal analysis fundamentals and applications. Tokyo, Realize.

80. Ishida, M., C. Y. Wen and T. Shirai (1971). Comparison of zone-reaction model and unreacted-core shrinking model in solid--gas reactions--II non-isothermal analysis. Chemical Engineering Science 26(7): 1043-1048.

81. Itay, M., C. R. Hill and D. Glasser (1989). A Study of the Low-Temperature Oxidation of Coal. Fuel Processing Technology 21(2): 81-97.

82. Kajitani, S., S. Hara and H. Matsuda (2002). Gasification rate analysis of coal char with a pressurized drop tube furnace. Fuel 81(5): 539-546.

83. Karr Jr., C. (1978). Analytical methods for coal and coal products. New York, Academic Press Inc.

84. Karsner, G. G. and D. D. Perlmutter (1982). Model for Coal Oxidation-Kinetics .2. An Effectiveness Factor Interpretation. Fuel 61(1): 35-43.

85. Karsner, G. G. and D. D. Perlmutter (1982a). Model for Coal Oxidation-Kinetics .1. Reaction under Chemical Control. Fuel 61(1): 29-34.

86. Katsikas, L. and I. G. Popovic (2003). Improvement to the Flynn-Wall method of determining apparent activation energies of the thermal degradation of polymers. Journal of Physical Chemistry B 107 (30), 7522-7525.

87. Kim, S., E.-S. Jang, D.-H. Shin and K.-H. Lee (2004). Using peak properties of a DTG curve to estimate the kinetic parameters of the pyrolysis reaction: application to high density polyethylene. Polymer Degradation and Stability 85 (2), 799-805.

88. Kissinger, H. E. (1957). Reaction kinetics in differential thermal analysis. Analytical Chemistry 29 (11), 1702-1706.

89. Krishnaswamy, S., S. Bhat, R. D. Gunn and P. K. Agarwal (1996a). Low-temperature oxidation of coal .1. A single-particle reaction-diffusion model. Fuel 75(3): 333-343.

90. Krishnaswamy, S., R. D. Gunn and P. K. Agarwal (1996b). Low-temperature oxidation of coal .2. An experimental and modelling investigation using a fixed-bed isothermal flow reactor. Fuel 75(3): 344-352.

91. Laidler, K. J. (1984). The Development of the Arrhenius Equation. Journal of Chemical Education 61(6): 494-498.

92. Laidler, K. J., J. M. Meiser and B. C. Sanctuary (2003). Chemical kinetics I: the basic ideas. Physical chemistry, Houghton Mifflin Company: 361-388.

93. Lester, E. and M. Cloke (1999). The characterisation of coals and their respective chars formed at 1300[deg]C in a drop tube furnace. Fuel 78(14): 1645-1658.

94. Levenspiel, O. (1972). Chemical reaction engineering. New York, Wiley.

95. Li, C. and T. C. Brown (2001). Carbon oxidation kinetics from evolved carbon oxide analysis during temperature-programmed oxidation. Carbon 39(5): 725-732.

96. Li, C. R. and T. B. Tang (1999). A new method for analysing non-isothermal thermoanalytical data from solid-state reactions. Thermochimica Acta 325 (1), 43-46.

97. Liu, G., P. Benyon, K. E. Benfell, G. W. Bryant, A. G. Tate, R. K. Boyd, D. J. Harris and T. F. Wall (2000). The porous structure of bituminous coal chars and its influence on combustion and gasification under chemically controlled conditions. Fuel 79(6): 617-626.

98. Lizzio, A. A., A. Piotrowski and L. R. Radovic (1988). Effect of Oxygen-Chemisorption on Char Gasification Reactivity Profiles Obtained by Thermogravimetric Analysis. Fuel 67(12): 1691-1695.

99. Lopez-Fonseca, R., I. Landa, M. A. Gutierrez-Ortiz and J. R. Gonzalez-Velasco (2005). "Non-isothermal analysis of the kinetics of the combustion of carbonaceous materials." Journal of Thermal Analysis and Calorimetry 80(1): 65-69.

100. Lu, L. M., C. H. Kong, V. Sahajwalla and D. Harris (2002). Char structural ordering during pyrolysis and combustion and its influence on char reactivity. Fuel 81(9): 1215-1225.

101. Luo, C., T. Watanabe, M. Nakamura, S. Uemiya and T. Kojima (2001). Development of FBR measurement of char reactivity to carbon dioxide at elevated temperatures. Fuel 80(2): 233-243.

102. Mackenzie, R. C. (1970). Differential thermal analysis. London, Academic Press Inc.

103. Madarasz, J., G. Pokol, S. Keki and M. T. Beck (1994). Comparative Thermogravimetric Study of the Air Oxidation of Different Carbons. Carbon 32 (5), 1023-1024.

104. Madhusudanan, P. M., K. Krishnan and K. N. Ninan (1986). New Approximation for the P(X) Function in the Evaluation of Nonisothermal Kinetic Data. Thermochimica Acta 97, 189-201.

105. Magasiner, N., C. Van Alphen, M. B. Inkson and B. J. Misplon (2002). Characterising fuels for biomass - coal-fired cogeneration. International Sugar Journal 104(1242): 251.

106. Mamleev, V., S. Bourbigot, M. Le Bras and J. Lefebvre (2004). "Three model-free methods for calculation of activation energy in TG." Journal of Thermal Analysis and Calorimetry 78(3): 1009-1027.

107. Mothè Filho, H. F., Gonçalves, M. L. A., Mothè, C. G. (2002). "Study of kinetic parameters of reject / clay / composites by thermal analysis." Journal of Thermal Analysis and Calorimetry 67: 381-389.

108. Olofson, J. (1980). Mathematical modelling of fluidised bed combustors. London.

109. Orfao, J. J. M. and F. G. Martins (2002). Kinetic analysis of thermogravimetric data obtained under linear temperature programming - a method based on calculations of the temperature integral by interpolation. Thermochimica Acta 390 (1-2), 195-211.

110. Ortega, A. (2002). The kinetics of solid-state reactions toward consensus, Part 2: Fitting kinetics data in dynamic conventional thermal analysis. International Journal of Chemical Kinetics 34(3): 193-208.

111. Ozawa, T. (1965). A new method of analyzing thermogravimetric data. Bulletin of chemical Society of Japan 38, 1881-1886.

112. Ozawa, T. (2000). Temperature control modes in thermal analysis. Pure and Applied Chemistry 72(11): 2083-2099.

113. Ozawa, T. (2001). Temperature control modes in thermal analysis. Journal of Thermal Analysis and Calorimetry 64(1): 109-126.

114. Paterson, W. L. (1971). Computation of Exponential Trap Population Integral of Glow Curve Theory. Journal of Computational Physics 7 (1), 187-&.

115. Paulik, F. and J. Paulik (1971). "Quasi-isothermal" thermogravimetry. Analytica Chimica Acta 56(2): 328-331.

116. Paulik, F. and J. Paulik (1973). Simultaneous thermogravimetric and thermo-gastitrimetric investigations under quasi-isothermal and quasi-isobaric conditions. Analytica Chimica Acta 67(2): 437-443.

117. Peralta, D., N. P. Paterson, D. R. Dugwell and R. Kandiyoti (2001). Development of a Reactivity Test for Coal-Blend Combustion: The Laboratory-Scale Suspension-Firing Reactor. Energy & Fuels 16(2): 404-411.

118. Perez-Maqueda, L. A., A. Ortega and J. M. Criado (1996). The use of master plots for discriminating the kinetic model of solid state reactions from a single constant-rate thermal analysis (CRTA) experiment. Thermochimica Acta 277: 165-173.

119. Perry, R. H. and D. W. Green, Eds. (1997). Perry's chemical engineer's handbook. 7th edition, McGraw-Hill.

120. Pinheiro, G. F. M., V. L. Lourenco and K. Iha (2002). Influence of the heating rate in the thermal decomposition of HMX. Journal of Thermal Analysis and Calorimetry 67(2): 445-452.

121. Rafsanjani, H. H., E. Jamshidi and M. Rostam-Abadi (2002). A new mathematical solution for predicting char activation reactions. Carbon 40(8): 1167-1171.

122. Ranish, J. M. and P. L. Walker (1993). High-Pressure Studies of the Carbon-Oxygen Reaction. Carbon 31(1): 135-141.

123. Rouquerol, J. (1973). Critical examination of several problems typically found in the kinetic study of thermal decomposition under vacuum. Journal of Thermal Analysis 5: 203 - 216.

124. Rouquerol, F., J. Rouquerol and K. Sing (1999). Adsorption by powders and porous solids: principles, methodology and applications. London, Academic press.

125. Russell, N. V., T. J. Beeley, C. K. Man, J. R. Gibbins and J. Williamson (1998). Development of TG measurements of intrinsic char combustion reactivity for industrial and research purposes. Fuel Processing Technology 57(2): 113-130.

126. Salatino, P., O. Senneca and S. Masi (1998). Gasification of a coal char by oxygen and carbon dioxide. Carbon 36(4): 443-452.

127. Salvador, S., J. M. Commandre and B. R. Stanmore (2003). Reaction rates for the oxidation of highly sulphurised petroleum cokes: the influence of thermogravimetric conditions and some coke properties. Fuel 82(6): 715-720.

128. Sampath, B. S., P. A. Ramachandran and R. Hughes (1975). Modelling of non-catalytic gas--solid reactions--I. Transient analysis of the particle--pellet model. Chemical Engineering Science 30(1): 125-134.

129. Sampath, R., D. J. Maloney and J. W. Zondlo (1998). Evaluation of thermophysical and thermochemical heat requirements dor coals at combustion level heat fluxes. 27 th International Symposium on Combustion, Boulder, Colorado.

130. Sbirrazzuoli, N., Y. Girault and L. Elegant (1995). Simulations for Evaluation of Kinetic Methods in Differential Scanning Calorimetry .1. Application to Single-Peak Methods - Freeman-Carroll, Ellerstein, Achar-Brindley-Sharp and Multiple Linear-Regression Methods. Thermochimica Acta 260, 147-164.

131. Senneca, O., P. Russo, P. Salatino and S. Masi (1997). The relevance of thermal annealing to the evolution of coal char gasification reactivity. Carbon 35(1): 141-151.

132. Senum, G. I. and R. T. Yang (1977). Rational approximations of the integral of the Arrhenius function. Journal of Thermal Analysis 11, 445-447.

133. Serageldin, M. A. and W.-P. Pan (1982). Coal decomposition: Effects of heating rate and furnace atmosphere. 32nd Canadian Chemical Engineering Conference, Vancouver, Canada.

134. Serageldin, M. A., Wei-Ping Pan (1984). Coal analysis using thermogravimetry. Thermochimica Acta 76: 145-160.

135. Sewry, J. D. and M. E. Brown (2002). "Model-free" kinetic analysis? Thermochimica Acta 390 (1-2), 217-225.

136. Shemet, V. Z., A. P. Pomytkin and V. S. Neshpor (1993). High-Temperature Oxidation Behavior of Carbon Materials in Air. Carbon 31(1): 1-6.

137. Sima-Ella, E., G. Yuan and T. Mays (2005). A simple kinetic analysis to determine the intrinsic reactivity of coal chars. Fuel 84 (14-15), 1920-1925.

138. Sima-Ella, E. and T. J. Mays (2005a). Analysis of the oxidation reactivity of carbonaceous materials using thermogravimetric analysis. Journal of Thermal Analysis and Calorimetry 80 (1), 109-113.

139. Sima-Ella, E. and T. Mays (2005b). Oxidation reactivity of coal chars: a simple kinetic analysis. 7th World Congress of Chemical Engineering, Glasgow, UK, CD ROM.

140. Simon, P. (2004). Isoconversional methods - Fundamentals, meaning and application. Journal of Thermal Analysis and Calorimetry 76 (1), 123-132.

141. Slaoui, S. and T. Bounahmidi (2004). Experimental study and modelling of coke combustion kinetics. Comptes Rendus Chimie 7 (5), 547-557.

142. Smith, I. W. (1978). The intrinsic reactivity of carbons to oxygen*1. Fuel 57 (7), 409-414.

143. Smith, I. W. (1982). The combustion rates of coal chars: a review. Nineteenth symposium (International) on combustion, Pittsburgh.

144. Smoot, D. L. and P. J. Smith (1985). Coal combustion and gasification. New York, Plenum Press.

145. Sohn, H. Y. and J. Szekely (1972). A structural model for gas-solid reactions with a moving boundary--III : A general dimensionless representation of the irreversible reaction between a porous solid and a reactant gas. Chemical Engineering Science 27(4): 763-778.

146. Sorensen, L. H., J. Saastamoinen and J. E. Hustad (1996). Evaluation of char reactivity data by different shrinking-core models. Fuel 75(11): 1294-1300.

147. Sorensen, O. T. (1978). Thermogravimetric studies of non-stoichiometric cerium oxides under isothermal and quasi-isothermal conditions. Journal of Thermal Analysis 13: 429-437.

148. Sorensen, O. T. (1992). Thermogravimetric and dilatometric studies using stepwise isothermal analysis and related techniques. Journal of Thermal Analysis 38(1-2): 213-228.

149. Sorensen, O. T. (1999). RCTA techniques used in studies of solid state reactions in inorganic compounds. Journal of Thermal Analysis 56: 17-26.

150. Sorensen, O. T. (2003a). Workshop on Sample Controlled Thermal Analysis. Journal of Thermal Analysis and Calorimetry 72(3): 1077-1079.

151. Sorensen, O. T. (2003b). SCTA and ceramics. Journal of Thermal Analysis and Calorimetry 72(3): 1093-1095.

152. Sorensen, O. T. (2003c). Stepwise and forced stepwise isothermal analysis. Journal of Thermal Analysis and Calorimetry 72 (3), 1075-1076.

153. Sotirchos, S. V., Amundson, N. R. (1984b). Part II: Transient analysis of a shrinking particle. Aiche Journal 30(4): 549-556.

154. Speight, J. G. (1983). The chemistry and technology of coal. New York, Marcel Dekker.

155. Standard Association of Australia (1987). AS 2096: Classification and coding systems for Australian coals.

156. Starink, M. J. (1996). A new method for the derivation of activation energies from experiments performed at constant heating rate. Thermochimica Acta 288 (1-2), 97-104.

157. Starink, M. J. (2003). The determination of activation energy from linear heating rate experiments: a comparison of the accuracy of isoconversion methods. Thermochimica Acta 404 (1-2), 163-176.

158. Tang, L. G., R. P. Gupta, C. D. Sheng and T. F. Wall (2005). The estimation of char reactivity from coal reflectogram. Fuel 84(2-3): 127-134.

159. Tang, W. J., Y. W. Liu, H. Zhang and C. X. Wang (2003). New approximate formula for Arrhenius temperature integral. Thermochimica Acta 408 (1-2), 39-43.

160. Thomas, J. M. and W. J. Thomas (1967). Introduction to the principles of heterogeneous catalysis. London, Academic Press.

161. Ulloa, C., A. G. Borrego, S. Helle, A. L. Gordon and X. Garcia (2005). Char characterization and DTF assays as tools to predict burnout of coal blends in power plants. Fuel 84 (2-3), 247-257.

162. United Nations Publications (1988). ECE/Coal/115: International Codification System for Medium and High Rank Coals, Economic Commission for Europe.

163. Van Krevelen, D. W. (1993). Coal: typology, physics, chemistry, constitution. Amsterdam, Elsevier.

164. Varhegyi, G., P. Szabo, E. Jakab and F. Till (2001). "Least squares criteria for the kinetic evaluation of thermoanalytical experiments. Examples from a char reactivity study." Journal of Analytical and Applied Pyrolysis 57(2): 203-222.

165. Vyazovkin, S. V. and A. I. Lesnikovich (1989). On the Methods of Solving the Inverse Problem of Solid-Phase Reaction-Kinetics .1. Methods Based on Discrimination. Journal of Thermal Analysis 35 (7), 2169-2188.

166. Vyazovkin, S. and D. Dollimore (1996). Linear and nonlinear procedures in isoconversional computations of the activation energy of nonisothermal reactions in solids. Journal of Chemical Information and Computer Sciences 36 (1), 42-45.

167. Vyazovkin, S. (2001a). Two types of uncertainty in the values of activation energy. Journal of Thermal Analysis and Calorimetry 64(2): 829-835.

168. Vyazovkin, S. (2001b). Modification of the integral isoconversional method to account for variation in the activation energy. Journal of Computational Chemistry 22 (2), 178-183.

169. Vyazovkin, S. and N. Sbirrazzuoli (2003). Isoconversional analysis of calorimetric data on nonisothermal crystallization of a polymer melt. Journal of Physical Chemistry B 107 (3), 882-888.

170. Walker Jr, P. L., Rusinko, F. , Austin, L. G. (1959). Gas reactions of carbon, Academic Press.

171. Wang, H., B. Z. Dlugogorski and E. M. Kennedy (1999). Theoretical analysis of reaction regimes in low-temperature oxidation of coal. Fuel 78(9): 1073-1081.

172. Wang, H. H., B. Z. Dlugogorski and E. M. Kennedy (2002a). Thermal decomposition of solid oxygenated complexes formed by coal oxidation at low temperatures. Fuel 81(15): 1913-1923.

173. Wang, H. H., B. Z. Dlugogorski and E. M. Kennedy (2003a). Pathways for production of CO2 and CO in low-temperature oxidation of coal. Energy & Fuels 17(1): 150-158.

174. Wang, H. H., B. Z. Dlugogorski and E. M. Kennedy (2003b). Analysis of the mechanism of the low-temperature oxidation of coal. Combustion and Flame 134(1-2): 107-117.

175. Wang, H. H., B. Z. Dlugogorski and E. M. Kennedy (2003c). Coal oxidation at low temperatures: oxygen consumption, oxidation products, reaction mechanism and kinetic modelling. Progress in Energy and Combustion Science 29(6): 487-513.

176. Wayne, F., Wells, Douglas Smoot, L. (1991). Relation between reactivity and structure for coals and chars. Fuel 70: 454-458.

177. Wen, C. Y. and E. Stanley Lee (1979). Coal conversion technology, Addison-Wesley Publishing Company.

178. Wendlandt, W. M. (1964). Thermal methods of analysis, Interscience.

179. Williams, A., R. Backreedy, R. Habib, J. M. Jones and M. Pourkashanian (2002). Modelling coal combustion: the current position. Fuel 81 (5), 605-618.

180. Zhou, D. L., E. A. Schmitt, G. G. Z. Zhang, D. Law, C. A. Wight, S. Vyazovkin and D. J. W. Grant (2003). Model-free treatment of the dehydration kinetics of nedocromil sodium trihydrate. Journal of Pharmaceutical Sciences 92 (7), 1367-1376.

181. Zimbardi, F. (2000). Evaluation of reaction order and activation energy of char combustion by shift technique. Combustion Science and Technology 156: 251-269.

182. Zolin, A., A. Jensen, L. S. Pedersen, K. Dam-Johansen and P. Torslev (1998). A comparison of coal char reactivity determined from thermogravimetric and laminar flow reactor experiments. Energy & Fuels 12(2): 268-276.

183. Zolin, A., A. D. Jensen, P. A. Jensen and K. Dam-Johansen (2002). Experimental study of char thermal deactivation. Fuel 81(8): 1065-1075.

184. Zsáko, J. (1968). Kinetic analysis of thermogravimetric data. Journal of Physical Chemistry 72 (7), 2406-2411.

185. Zsáko, J., E. Kekedy and C. Varhelyi (1971). Kinetic analysis of thermogravimetric data IV: Influence of heating rate and sample weight on thermal decomposition. 3rd ICTAC, Davos.

Appendix A:

Paper presented at the 7th World Congress of Chemical Engineering, Glasgow (10th-14th July 2005)

OXIDATION REACTIVITY OF COAL CHARS: A SIMPLE KINETIC ANALYSIS

Edwige Sima-Ella, Tim Mays*
Department of Chemical Engineering, University of Bath, Bath BA2 7AY, United Kingdom
*Tel.: + 44 (0) 1225 386528; Fax: + 44 (0) 1225 385713; E-mail address: t.j.mays@bath.ac.uk

Abstract

The intrinsic reactivity in air of three ranks of coals as anthracite, bituminous and subbituminous, was investigated using a new thermogravimetric technique. The conventional single heating rate measurement is enhanced by identifying an optimum-heating rate at which mass transfer limitations are reduced, and true kinetic data are derived. This analysis is presented using the simplest approximation of the temperature integral from the Arrhenius equation. An optimum-heating rate of 25 °C min^{-1} was observed for all the different type of coals, producing reactivity data that correspond to those proposed in the literature for similar materials. Furthermore, these results were compared with values derived from using an existing "isoconversional" analysis approach. They showed good agreement. It is therefore suggested that such an improved thermogravimetric analysis is relatively simple and sufficiently accurate for applications in coal characterisation.

Keywords: Coal characterisation; Intrinsic reactivity; Kinetic analysis.

Introduction

A better understanding of coal combustion is becoming increasingly essential, especially, in pulverised fuel for power generating plants, and through the tuyères of the blast furnace in the steel-making industry. Adequate coal characterisation is required for the design and operating conditions of these systems. One key property of the coal is the intrinsic kinetic parameters of the char. These parameters describe the dynamics of the combustion reactions. Thus, they may be used as an indicator to predict and compare the performance of different coals and coal blends. Reactivity data of various coal chars in air is extensively discussed in the literature (Smith 1982; Smoot and Smith 1985). However, many researchers have considered the overall reactivity as opposed to the intrinsic char reactivity (Field 1969; Herbig and Jess 2002; Peralta et al 2002; Feng et al 2003). The main reason behind this approach is that, intrinsic kinetic data are related to the structure of the material, and therefore not easily measurable. In spite of that, Smith (1978) calculated the intrinsic reactivity in oxygen of various types of carbons. He estimated the different properties of the particle in terms of characteristic particle size, density, specific surface area and pore diameter. Similarly, Chan et al (1999) have studied the oxidative intrinsic reactivity of coal chars by examining the changes in surface area and porosity.

This approach is somewhat tedious, and may be bypassed by carrying out experiments in the chemical control regime, so that intrinsic rates are directly measured. Russell et al (1998)

suggested direct measurement of intrinsic reactivity by performing thermogravimetric analysis (TGA) experiments at low temperature (< 1000 °C); where, reaction is not influenced by transport of gaseous reactants from the bulk gas to the particle surface. In the TGA, the char in the furnace is subjected to a controlled temperature programme. Experiments are ideally carried out non-isothermally, at a constant heating rate. This way, it is possible to obtain kinetic parameters in one single experimental run, and at the same time achieve complete char conversion in a short period of time (approximately < 2 hours). These types of experiments are usually performed at an arbitrary heating rate. This is not such a reliable technique for estimating the activation energy as heating rate influences the shape of the thermogravimetric curve. In fact, the ignition temperature on a TG curve is shifted as the heating rate increases. Hence, activation energy values vary with heating rate. Wendlandt (1964) and Zsakó (1971) suggested that kinetic parameters derived from thermogravimetric curves largely depend on procedural variables. These variables either relate to the instrument: heating rate, geometry of crucible; or to the sample (e.g. sample weight, particle size). Nonetheless, heating rate is probably the most influential as sample temperature strongly correlates with char reactivity. This phenomenon may be explained by thermal effects induced on the sample at the different heating rates. It is believed that heating rate influences the reaction of a compound in a rather complex manner. In some cases, recrystallization may occur followed by a melting process at low heating rates, whereas, superheating may take place at higher heating rates. It is likely, therefore, that there exists a heating rate at which these thermal effects are minimised, and accurate activation parameters are obtained. The literature has recommended heating rates of 5 or 10 °C min^{-1} (Ichihara 1994). Others, have suggested 15 °C min^{-1} (Russell et al 1998). Many researchers have followed these guidelines (Lester et al 1999; Peralta et al 2002). Zolin et al (2002), on the other hand, averaged reactivity values from two different heating rates. In any case, they have failed to verify that their chosen heating rate was the best option. Because of this instability in the determination of kinetic parameters from single heating rate experiments, modern thermal analyses (Vyazovkin 1989, 1990; Brown 2001;) encourage the use of isoconversional methods. These methods combine multiple heating rates, which minimise the thermal interferences occurring from single heating rate measurements.

In this work, the intrinsic reactivity in air of three types of coal chars is estimated at several heating rates. A statistical best-fit criterion is devised to assess the optimum-heating rate at which true kinetic parameters are attained. These parameters are then compared with those obtained by an existing isoconversional analysis. This work emphasises the fact that single heating rate measurement on TGA may be used in a simpler and accurate manner, with the advantage of being faster than the conventional isoconversional analysis.

Kinetic analysis

1.1 Model equation for char oxidation reactivity

The oxidation of char in air may be regarded as the heterogeneous carbon-oxygen reaction. This reaction has often been described as a first order global kinetic reaction model (Smith 1972; Olofson 1980; Van Krevelen 1993), especially in the kinetic control regime. In a more recent review, Hurt and Calo (2001) suggested strong evidence of first order reaction in the similar temperature range. The reaction rate is, therefore, expressed as:

$$\frac{d\alpha}{dt} = k(1-\alpha) \qquad (1)$$

where α is the carbon weight conversion of the char on a dry ash free basis; and k the rate constant defined by an Arrhenius equation:

$$k(T) = A\exp\left(-E/RT\right) \tag{2}$$

where T is the absolute temperature (K) and R is the universal gas law constant (R = 8.314 J mol^{-1} K^{-1}). In non-isothermal conditions, the temperature is changed at a constant rate $\beta = dT/dt$. Combining Eq. (1) and (2):

$$\frac{d\alpha}{dT} = \frac{A(1-\alpha)}{\beta}\exp\left(-E/RT\right) \tag{3}$$

Integrating the above yields:

$$\ln(1-\alpha) = -\frac{A.}{\beta}\int_{T_0}^{T}\exp(-E/RT) \tag{4}$$

Since there is no oxidation ($\alpha = 0$) up to T_0, (ignition temperature of the char), the limits of the integral are changed to $\int_0^T \exp(-E/RT)$, and the function $p(x)$ is introduced, so that:

$$p(x) = \int_x^{\infty}\frac{e^{-x}}{x^2}dx \tag{5}$$

where $x = E/RT$, Eq. (4) is changed to:

$$\ln(1-\alpha) = -\frac{A.E}{\beta.R}p(x) \tag{6}$$

The function $p(x)$ is not analytically solvable. The only way this function may be integrated, consequently, is by means of approximations. Several of these approximations have been derived using either: (i) numerical values of $p(x)$, (ii) series of approximations for $p(x)$ or (iii) approximation to obtain a function that can be integrated (Brown 2001, Starink 2003). For the purpose of this work, a simple and highly accurate approximation to $p(x)$ was selected. Coats and Redfern (1964) derived this approximation by evaluating the integral in Eq.(5) using an asymptotic expansion also discussed by Zsakó and Zivkovic (1984). Only the first two terms of this expression were retained:

$$p(x) \approx \frac{e^{-x}}{x^2} \tag{7}$$

Incorporating this approximation into Eq. (6) leads to the following linear form

$$\ln\left[\frac{-\ln(1-\alpha)}{T^2}\right] = \ln\left(\frac{A.R}{\beta.E}\right) - \frac{E}{RT} \tag{8}$$

At a specific heating rate, the values of A and E are respectively obtained from the intercept and slope of the plot of ln [(-ln (1- α) /T^2] *versus* (1 / T)

Experimental methods.

1.2 Materials and preparation

Three different coals and an activated carbon were studied in this investigation. These coals are generally used in pulverised fuel combustion for power generation; consisting of, an

anthracite from China (Heze), a bituminous coal from England (Kellingley) and a subbituminous coal from the USA (PRB). The activated carbon is a steam activated carbon derived from bituminous coal, commercially available as BPL (Calgon 1998). Proximate analyses of these materials are shown in Table 1. The activated carbon was selected as a suitable model for various coal chars, since it is highly homogeneous.

The coal chars were produced in a Carbolated CIF 15/75 tube furnace with flowing nitrogen gas (99.99% purity) at 0.5 bara. The temperature in the furnace was raised from 20 °C to 1000 °C at 2 °C min^{-1}, and 8 hours dwell to ensure complete charring. The activated carbon did not require pre charring; however, it was heated at 10 °C min^{-1} to 400 °C (temperature at which oxidation initiates) and held at that temperature for 15 minutes to ensure the BPL carbon was totally dry before the oxidation analysis.

1.3 Oxidation reactivity measurements

Oxidation analyses were carried out using a Setaram TG 92 thermogravimetric analyser (TGA) operating at atmospheric pressure. Approximately 50 mg sample was placed, each time, into an alumina crucible and introduced into the furnace of the TGA in flowing dry air (16ml [STP] min^{-1}). Experimental runs proceeded at the following heating rates 5, 10, 20, 30 and 50 °C min^{-1} from 20 to a maximum temperature, T_{max}. This maximum temperature was determined as the limit for kinetic control regime. An Arrhenius plot, was derived for each material at 5 °C min^{-1} and this maximum temperature was deduced. These temperatures are summarised in Table 1. The sample weight was continuously recorded by PC data acquisition, which also registers the temperature measured by a thermocouple placed under the crucible. Each experiment was corrected for buoyancy and selected runs were repeated two or three times showing good repeatability. All weight change data are reported and analysed on a dry, ash-free basis.

Table 1. Proximate analyses for all coal samples

Samples	Class of coal (ASTM 1984)	Maximum temperature (T_{max}°C)	Moisture (%)	Ash level (%)	Volatile matter (%)	Fixed carbon (%)
BPL carbon	Bituminous (derived)	600	2.0	8.0	0.0	90.0
Heze (China)	Anthracite	580	8.0	29.2	9.3	53.5
Kellingley (UK)	Bituminous	570	3.9	16.8	30.2	49.1
PRB (USA)	Subbituminous	565	21.8	5.6	34.1	38.5

Results and discussion

1.4 Single heating rate: oxidation reactivity parameters

The thermogravimetric profiles obtained at 5 and 50 °C min^{-1} heating rates are shown in Fig. 1 as thick lines. The recorded weight during the oxidation phase has been converted into weight loss *(1-α)*. From these experimental data, the values of E and A were obtained by applying Eq. (8). For convenience, only values of E are shown in Table 2. That is, activation energy is more important as it affects the temperature sensitivity of the reaction rate, whereas the pre-exponential factor is related to the structure of the material (Vyazovkin 2001).

As can be seen from Fig. 1, the reaction is shifted to a higher temperature with increasing heating rates for all materials. Similarly, the fractional conversion of carbon is reduced when the heating rate is increased. BPL, for instance, has undergone almost 40 % conversion at 5 °C min^{-1} at 600 °C; whereas, only 2 % of the carbon has reacted at 50 °C min^{-1}. This systematic change is

more pronounced for the coal chars: conversion changes from more than 70 % at 5 °C min^{-1} to merely 5 % carbon conversion at 50 °C min^{-1}. These differences in conversion with heating rates affect the values of the reactivity parameters. As can be seen in Table 2 in the case of BPL carbon, a difference of 50 kJ mol^{-1} would arise in the value of *E*, by using a 5 °C min^{-1} heating rate rather than a 20 °C min^{-1}. For the coal chars the spread in *E-values* is smaller, although, still larger than 15 kJ mol^{-1}. It is therefore believed that the single heating rate method is not an accurate way of estimating these activation parameters.

1.5 Optimum heating rate analysis

In order to identify the true set of kinetic parameters, an optimum-heating rate has to be established. Using the obtained values of E and A, a conversion, α_{calc}, is calculated from the exponential form of Eq. (6) as follows:

$$(1-\alpha_{calc}) = \exp\left[-\frac{ART^2}{\beta.E}\exp\left(-E/RT\right)\right] \qquad (9)$$

From the above equation, a thermogravimetric profile of weight loss is predicted alongside the experimental one. These simulated curves are shown, as thin lines, in Fig. 1 for heating rates of 5 and 50 °C min^{-1}. Although, the simulated profiles do not exactly fit the experimental ones, this inconsistency varies with the heating rate. In other words, a standard error (RMS) in the conversion α, at each heating rate, may be calculated to quantify this difference. This error is evaluated along the same temperature interval (from initial temperature to T_{max}), and the same time interval (for the first 15 minutes after ignition – the time necessary for the 50 °C min^{-1} oxidation curve to reach maximum temperature). These two comparison criteria have an effect on the calculation of the RMS in terms of number of observations (n data points), thus the reason for equally considering both of them. An average standard error is computed as follows

$$\sigma(\%) = \left[\frac{1}{2}\sqrt{\frac{\sum_{i=T_i}^{n=T_{max}}\left(\alpha_{i,calc}-\alpha_{i,exp}\right)^2}{n}} + \frac{1}{2}\sqrt{\frac{\sum_{i=t_0}^{n=t_{15\,min}}\left(\alpha_{i,calc}-\alpha_{i,exp}\right)^2}{n}}\right]\times 100 \qquad (10)$$

The minimum standard error is used to identify the heating rate at which a prediction corresponds with experimental data, so that true kinetic data may be detected. As shown in Fig.2, there always exists a minimum standard error for the range of heating rates examined. This minimum is observed at a heating rate of 30 °C min^{-1}. However, it is not possible to confirm that the minimum error is reached at exactly this heating rate in the 20 - 50 °C min^{-1} range; in fact, the minimum error may occur just before or just after 30 °C min^{-1}. In order to verify this, a series of experiments will need to be carried out in the 20 - 50 °C min^{-1} range. In practice, however, the optimum heating rate may be selected sufficiently close to 30 °C min^{-1}, where the standard error is already very small. In addition, a lower heating rate value is preferred, in order to minimise the effect of gas diffusion limitations and large temperature gradient across the sample. In view of this, 25 °C min^{-1} is most probably the optimum-heating rate. The kinetic parameters at this heating rate are calculated by interpolation and listed in Table 3.

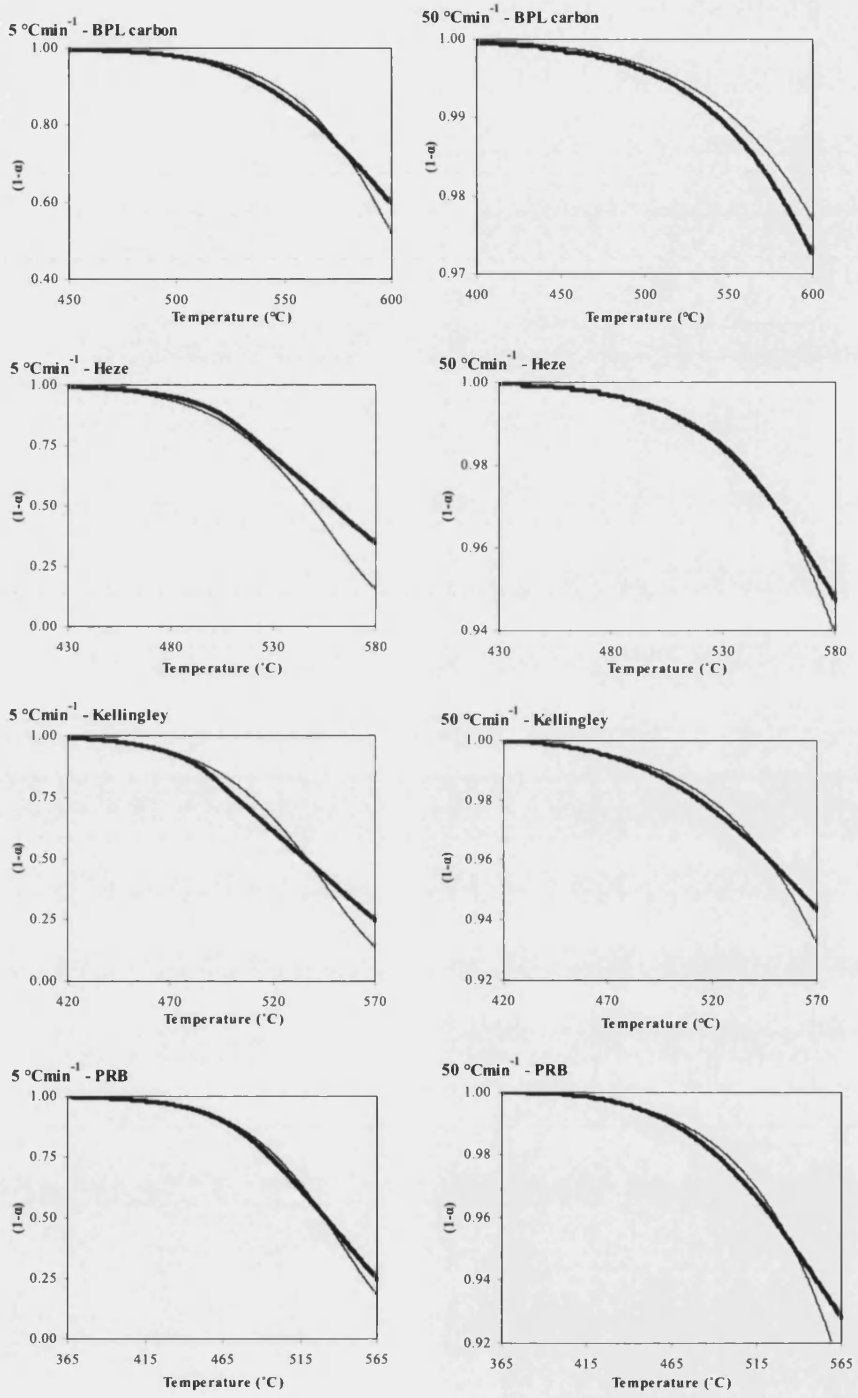

Figure 1. Comparison of the experimental weight loss curves (—) with their corresponding simulated ones (—) for the oxidation in air of different coal chars at 5 and 50 °Cmin^{-1}.

Table 2. Activation energy values (kJ mol^{-1} ± the standard error) for the coal chars at different heating rates

Heating rate, °C min^{-1}	BPL carbon	Heze	Kellingley	PRB
5	190.6 ± 1.3	163.2 ± 0.4	154.6 ± 1.2	127.3 ± 1.3
10	171.8 ± 1.3	154.6 ± 0.1	153.2 ± 1.2	119.6 ± 0.5
20	135.9 ± 0.9	152.6 ± 0.8	133.8 ± 0.1	110.1 ± 0.8
30	122.8 ± 1.0	147.2 ± 1.0	129.6 ± 0.3	110.0 ± 1.0
50	92.6 ± 0.6	145.4 ± 1.0	127.2 ± 1.9	104.3 ± 1.4

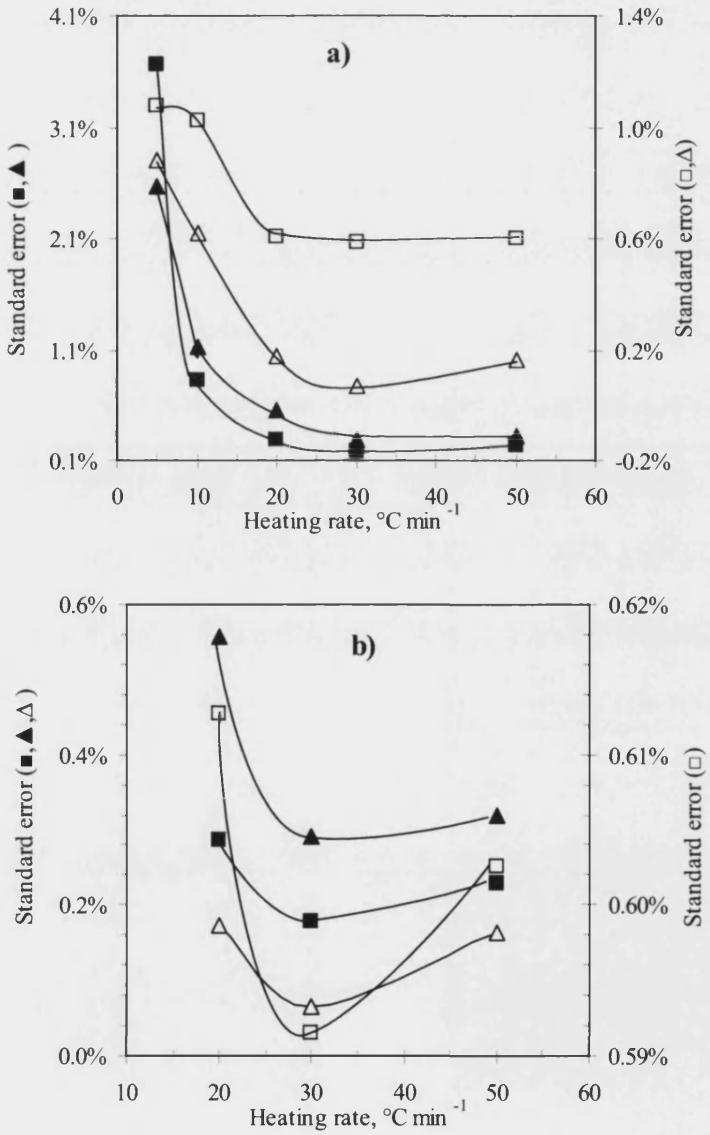

Figure 2. Standard error in the fit of TGA data for BPL (Δ) Heze (■), Kellingley (▲) and PRB (□) at a) - five different heating rates and b)- enlarged view.

1.6 Comparison with activation energy values by the Ozawa method

The Ozawa method also known as the Ozawa-Flynn-Wall method (OFW) (Ozawa 1965; Flynn and Wall 1966) is a widely used analytical technique for evaluating the apparent activation energy of a material. This analysis is an isoconversional technique, applicable to processes with constant activation energy. For the same conversion α, the Ozawa method expression is as follows:

$$[\ln \beta] vs \left[1.052 E/RT_{\alpha} \right] \quad \textbf{(11)}$$

where T_{α} is the temperature at the specific fractional conversion.

The above equation incorporates the *p(x)* function of Doyle's approximate expression (Doyle 1962), which only applies to conversion $\alpha < 20\%$. The activation energy is evaluated from the slope of the plot of ln β *versus* $(1/T_{\alpha})$. In this study, a 5% conversion was selected as the maximum conversion attained under kinetic control region for all the coal chars. The Ozawa plots for all these chars are shown in Fig. 3. They all present a good fit, suggesting that activation energy is constant up to 5% conversion. A summary of these activation energy value, estimated at 95% confidence interval, is shown in Table 3. As presented in this table, these values are in statistical agreement with those derived using the optimum-analysis approach. The latter, nonetheless, provides values with a narrower bound interval. It is therefore suggested that this newer kinetic analysis approach is sufficiently simple and highly accurate for determining the intrinsic oxidation reactivity of coal chars.

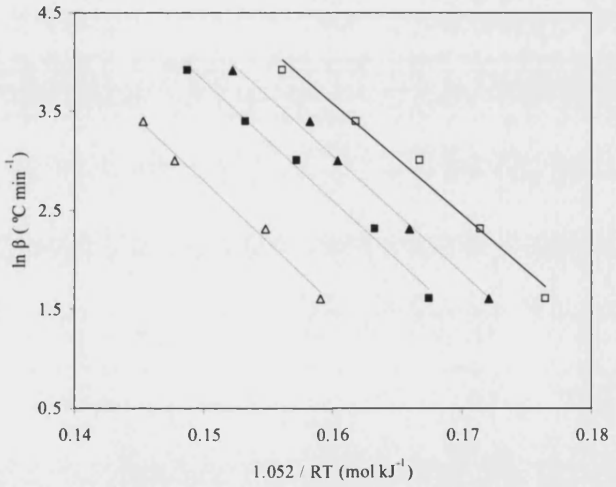

Figure 3. Ozawa method for the determination of activation energy during the oxidation of the coal chars at 5 % carbon conversion: BPL (Δ) Heze (■), Kellingley (▲) and PRB (□)

Table 3. Comparison of activation energy values (± the standard error, kJ mol^{-1}) by the optimum-analysis method and the OFW method

Coal samples	E - values at 25 °C min^{-1} (kJ mol^{-1})	E - values by the OFW method (kJ mol^{-1})
BPL carbon	129.4 ± 1.3	123.4 ± 39.2
Heze	149.9 ± 1.3	124.8 ± 36.2
Kellingley	131.7 ± 0.3	119.5 ± 19.9
PRB	110.0 ± 1.3	112.8 ± 27.6

Conclusions

Experimental TGA investigation of the optimum-heating rate on the intrinsic reactivity in air of three ranks of coals was performed in the temperature range 300 – 600 °C. The kinetic control regimes for the oxidation of the different chars were pre-established by studying their Arrhenius plots at a very slow heating rate. The reaction was modelled as a first order kinetic, and a non-isothermal TGA method was applied to derive both the activation energy and the pre-exponential factor. For the three types of coal chars, a constant optimum-heating rate was observed at 25 °C min^{-1}. It is therefore suggested that this optimum-heating rate is an instrumental factor, and therefore might only vary with the TG equipment used. At this heating rate, activation energy values coincided with those derived by the Ozawa isoconversional method. Isoconversional methods assess the value of activation energy alone, and not the pre-exponential factor; whereas, the proposed alternative kinetic analysis allows for both parameters to be estimated simultaneously. In addition, the optimum-heating rate analysis presents a higher degree of accuracy at 95 % confidence interval than the isoconversional method. Furthermore, these activation energy values are in line with those presented in the literature for similar materials (Smith 1978; Russell et al 1998; Zolin 2002). It appears, therefore, that once this optimum-heating rate has been established for a particular TG apparatus, accurate intrinsic reactivity parameters may be evaluated at a single heating rate measurement. This alternative kinetic analysis is simple and sufficiently accurate; therefore, presents a great potential in coal combustion and pyrolysis where adequate and fast char characterisation is essential.

Acknowledgement

The authors gratefully acknowledge financial support in the form of a research grant by the British Coal Utilisation Research Association (Contract number B 56), United Kingdom.

References

1. ASTM, American Society for Testing Materials D388. (1984). Classification of coals.
2. Brown, M. E. (2001). Introduction to thermal analysis: Techniques and applications. London, Kluwer Academic.
3. Calgon Carbon Corporation (1998). Product bulletin: BPL 4x10 granular activated carbon. Pittsburgh.
4. Chan, M.-L., J. M. Jones, et al. (1999). Fuel **78**(13): 1539-1552.

5. Coats, A. W. and Redfern, J. P. (1964). Nature **201**: 68-69.
6. Doyle, C. D. (1962). Jounal of Applied Polymer Science **6**: 639-642.
7. Feng, B., Jensen, A., et al. (2003). Energy & Fuels **17**(2): 399-404.
8. Field, M. A. (1969). Combustion and Flame **13**(3): 237-252.
9. Flynn, J. H., Wall, L. A. (1966). Journal of Research of the National Bureau of Standards - A. Physics and Chemistry **70A**(6): 487-523.
10. Hatakeyama, T., Zhenhai, L. (1998). Handbook of thermal analysis. Chichester, Wiley.
11. Herbig, C. and A. Jess (2002). Fuel **81**(18): 2387-2395.
12. Hurt, R. H. and J. M. Calo (2001). Combustion and Flame **125**(3): 1138-1149.
13. Ichihara, S. (1994). Thermal analysis fundamentals and applications. 3rd ed. Tokyo, Realize.
14. Lester, E. and Cloke, M. (1999). Fuel **78**(14): 1645-1658.
15. Olofson, J. (1980). Mathematical modelling of fluidised bed combustors. London.
16. Ozawa, T. (1965). Bulletin of chemical Society of Japan **38**: 1881-1886.
17. Peralta, D., Paterson, N.P., et al. (2001). Energy & Fuels **16**(2): 404-411.
18. Russell, N. V., Beeley, T.J., et al. (1998). Fuel Processing Technology **57**: 113-130.
19. Smith, I. W. (1978). Fuel **57**(7): 409-414.
20. Smith, I. W. (1982). Nineteenth symposium (International) on combustion. The Combustion Institute. Pittsburgh.
21. Smith, I. W. and Tyler, R. J. (1972). Fuel **51**(4): 312-321.
22. Smoot, L. D. and Smith, P.J. (1985). Coal combustion and gasification. Plenum Press.
23. Starink, M. J. (2003). Thermochimica Acta **404**(1-2): 163-176.
24. Van Krevelen, D. W. (1993). Coal: typology, physics, chemistry, constitution. Elsevier.
25. Vyazovkin, S. (2001). Journal of Computational Chemistry **22**(2): 178-183.
26. Vyazovkin, S. V. and Lesnikovich, A. I. (1989). Journal of Thermal Analysis **35**(7): 2169-2188.
27. Vyazovkin, S. V. and Lesnikovich, A. I. (1990). Journal of Thermal Analysis **36**(2): 599-615.
28. Wendlandt, W. M. (1964). Thermal methods of analysis. Interscience.
29. Zolin, A., Jensen, A. D. et al. (2002). Fuel **81**(8): 1065-1075.
30. Zsako, J., et al (1971). 3rd International Conference on Thermal analysis, Davos, Switzerland.
31. Zsako, J. and Zivkovic, Z. D. (1984). Thermal analysis. Beograd, University of Beograd.

Appendix B:

MATLAB Program for the calculation of p(x)-function

Numerical calculation of the p(x)-function by the trapezoidal rule:

$$p(x) = \int_0^x \frac{e^{-x}}{x^2} dx$$

```
function y = integrate (initial, final, step)
%       example:
%       result = integrate (0.001, 1, 0.001)
%       this gives the integral of the y function using increments of 0.001
r = initial:step:final;

x=exp(-r)./(r^2);
y=abs(x(2:end)+x(1:end-1)))*step/2;
y=sum(y(:));
plot(r,x)
```

Appendix C:

Examples of Particle size estimation using SEM

a)

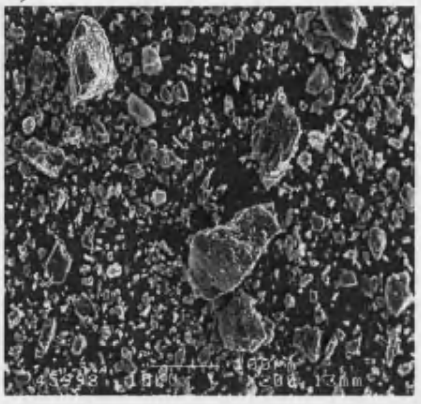

b)

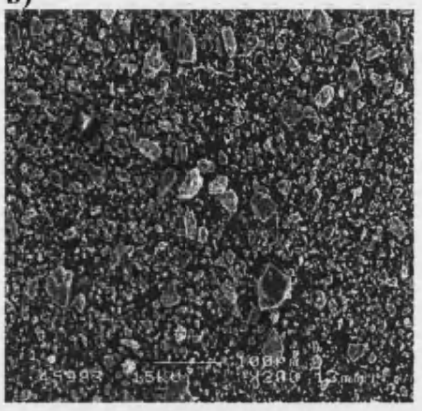

Figure B1: Particle size distribution using SEM at 200X magnification on a sample of: a) Pha Lai char and; b) BPL crushed.

a)

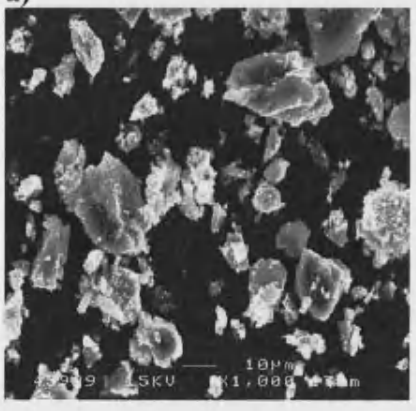

b)

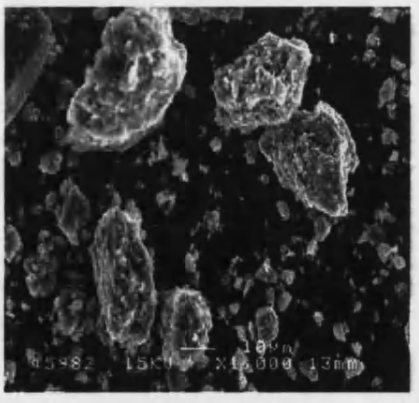

Figure B2: Particle size distribution using SEM at 1000X magnification on a sample of: a) Pha Lai char and; b) BPL crushed.

Appendix D:

Step-ramp analysis of the various coal chars

Table C4: Weight loss (wt %) and mean activation energy values resulting from different step-ramp temperature programmes during the air oxidation of BPL crushed. Shaded area corresponds to the chemical control zone. Actual activation energy value derived from optimum-heating rate analysis is 124 ± 6 kJ mol $^{-1}$

Temperatures (°C)	# 1	# 2	# 3	# 4
400	0.13	0.20	0.15	-
425	0.42	0.42	-	0.18
450	0.71	0.64	0.64	-
475	1.06	1.10	-	0.45
500	1.80	1.75	0.95	-
525	3.54	3.35	-	1.17
550	6.12	5.92	2.93	-
575	10.45	9.96	-	2.99
600	15.01	13.21	5.87	5.02
E (400-600 °C), kJ mol^{-1}	149 ± 8	150 ± 10	144 ± 6	150 ± 12
E (shaded area), kJ mol^{-1}	145 ± 14	137 ± 15	85 ± 0	122 ± 0

Table C5: Weight loss (wt %) and mean activation energy values resulting from the different step-ramp temperature programmes during the air oxidation of Pha Lai. Shaded area corresponds to the chemical control zone. Actual activation energy value derived from optimum-heating rate analysis is 157 ± 2 kJ mol $^{-1}$

Temperatures (°C)	# 1	# 2	# 3	# 4
400	0.49	0.14	0.59	0.37
425	1.22	0.50	-	-
450	1.91	0.90	2.51	1.72
475	3.22	1.74	-	-
500	6.28	2.78	4.90	3.80
525	12.85	4.69	-	-
550	18.45	7.96	14.63	9.91
570	25.27	12.59	29.34	18.99
E (400-570 °C), kJ mol^{-1}	138 ± 9	136 ± 8	126 ± 13	132 ± 14
E (shaded area), kJ mol^{-1}	161 ± 2	157 ± 3	156 ± 2	151 ± 8

Table C6: Weight loss (wt %) and mean activation energy values resulting from the different step-ramp temperature programmes during the air oxidation of Chang Cun char. Shaded area corresponds to the chemical control zone. Actual activation energy value derived from optimum-heating rate analysis is 147 ± 3 kJ mol $^{-1}$

Temperatures (°C)	# 1	# 2	# 3	# 4
375	-	-	-	0.11
390	0.40	0.50	0.33	-
415	1.05	0.72	-	-
425	-	-	-	0.59
440	1.60	1.14	0.76	-
465	2.80	2.17	-	-
475	-	-	-	2.03
490	4.82	4.66	1.68	-
515	7.25	8.04	-	-
525	-	-	-	4.68
540	10.70	13.10	4.90	7.59
E (365-540 °C), kJ mol^{-1}	145 ± 12	149 ± 10	138 ± 6	134 ± 9
E (shaded area), kJ mol^{-1}	150 ± 6	151 ± 3	170 ± 0	148 ± 6

Table C7: Weight loss (wt %) and mean activation energy values resulting from the different step-ramp temperature programmes during the air oxidation of Kellingley char. Shaded area corresponds to the chemical control zone. Actual activation energy value derived from optimum-heating rate analysis is 142 ± 2 kJ mol $^{-1}$

Temperatures (°C)	# 1	# 2	# 3	# 4
375	-	0.19	-	0.15
400	0.32	0.75	0.80	-
425	0.65	1.27	-	1.61
450	1.35	2.54	4.63	-
475	2.88	5.59	-	4.16
500	6.45	9.63	9.28	-
525	-	15.89	-	11.53
540	11.01	23.01	18.10	-
E (375-540 °C), kJ mol^{-1}	120 ± 9	134 ± 12	114 ± 14	134 ± 16
E (shaded area), kJ mol^{-1}	146 ± 2	144 ± 6	126 ± 0	130 ± 19

Table C8: Weight loss (wt %) and mean activation energy values resulting from the different step-ramp temperature programmes during the air oxidation of Columbian. Shaded area corresponds to the chemical control zone. Actual activation energy value derived from optimum-heating rate analysis is 138 ± 4 kJ mol $^{-1}$

Temperatures (°C)	# 1	# 2	# 3	# 4
370	0.13	0.13	-	0.09
395	0.35	0.33	0.27	-
420	0.54	0.51	-	0.56
445	1.02	0.80	0.66	-
470	1.97	1.47	-	1.90
495	3.46	2.50	1.75	-
520	5.74	4.14	-	4.22
545	9.45	7.01	4.41	-
570	14.30	10.87	7.38	7.28
E (375-570 °C), kJ mol^{-1}	136 ± 12	134 ± 10	136 ± 16	138 ± 24
E (shaded area), kJ mol^{-1}	134 ± 3	133 ± 3	137 ± 0	140 ± 0

Table C9: Weight loss (wt %) and mean activation energy values resulting from the different step-ramp temperature programmes during the air oxidation of PRB. Shaded area corresponds to the chemical control zone. Actual activation energy value derived from optimum-heating rate analysis 109 ± 1 kJ mol $^{-1}$

Temperatures (°C)	# 1	# 2	# 3	# 4
375	-	4.98	-	-
400	1.13	5.44	1.38	1.03
425	2.72	6.29	-	-
450	3.94	8.13	4.09	2.70
475	6.10	11.88	-	-
500	8.98	15.95	10.17	8.88
525	13.53	22.03	-	-
550	18.53	29.39	20.39	17.54
565	24.60	34.68	-	23.86
E (375-565 °C), kJ mol^{-1}	106 ± 7	75 ± 7	109 ± 16	107 ± 18
E (shaded area), kJ mol^{-1}	109 ± 7	108 ± 7	108 ± 0	105 ± 9

Table C10: Weight loss (wt %) and mean activation energy values resulting from the different step-ramp temperature programmes during the air oxidation of EC2038. Shaded area corresponds to the chemical control zone. Actual activation energy value derived from optimum-heating rate analysis 161 ± 5 kJ mol $^{-1}$

Temperatures (°C)	# 1	# 2	# 3	# 4
400	0.12	0.21	0.09	0.13
425	0.29	0.27	-	-
450	0.44	0.50	0.32	0.31
475	0.79	0.94	-	-
500	1.65	2.17	1.15	0.89
525	4.09	4.62	-	-
550	7.12	7.16	5.58	4.32
565	9.74	10.26	1037	8.88
E (400-565 °C), kJ mol^{-1}	144 ± 8	151 ± 12	135 ± 10	128 ± 9
E (shaded area), kJ mol^{-1}	165 ± 7	160 ± 6	159 ± 4	159 ± 11

Table C11: Weight loss (wt %) and mean activation energy values resulting from the different step-ramp temperature programmes during the air oxidation of EC2106. Shaded area corresponds to the chemical control zone. Actual activation energy value derived from optimum-heating rate analysis 151 ± 1 kJ mol $^{-1}$.

Temperatures (°C)	# 1	# 2	# 3	# 4
410	0.17	0.12	-	-
435	0.32	0.32	0.28	0.26
460	0.61	0.51	-	-
485	0.92	0.92	0.56	1.35
510	1.70	1.96	-	-
535	3.71	3.64	1.55	3.51
560	6.24	5.99	-	-
580	9.85	9.07	4.47	8.35
600	13.35	11.35	6.52	11.70
E (400-600 °C), kJ mol^{-1}	147 ± 7	147 ± 9	133 ± 14	153 ± 12
E (shaded area), kJ mol^{-1}	159 ± 15	157 ± 11	153 ± 7	152 ± 23